EARTHQUAKE-INDUCED LIQUEFACTION AND SUBSIDENCE OF GRANULAR MEDIA

S. NEMAT-NASSER

NORTHWESTERN UNIVERSITY
EVANSTON, ILLINOIS 60201

USGS CONTRACT NO. 14-08-0001-17770
Supported by the EARTHQUAKE HAZARDS REDUCTION PROGRAM

OPEN-FILE NO.81-259

NORTHWESTERN UNIVERSITY

Contract No: 14-08-0001-17770

Final Technical Report

Submitted to

U. S. GEOLOGICAL SURVEY

on

Earthquake-Induced Liquefaction and Subsidence of Granular Media

by

S. Nemat-Nasser
Principal Investigator

Government Technical Officer:	Dr. Gordon W. Greene
Effective Date of Contract:	21 February 1979
Contract Expiration Date:	20 February 1980, extended to 30 September 1980
Amount of Contract:	$65,307.-

November 1980

THE VIEWS AND CONCLUSIONS CONTAINED IN THIS DOCUMENT ARE THOSE OF THE AUTHOR AND SHOULD NOT BE INTERPRETED AS NECESSARILY REPRESENTING THE OFFICIAL POLICIES, EITHER EXPRESSED OR IMPLIED, OF THE U.S. GOVERNMENT.

TABLE OF CONTENTS

PREFACE

The objective of the research has been to understand the behavior of dry or saturated granular materials under cyclic shearing. To this end, two fundamental subjects have been considered. These are:

(1) To understand what happens to granular materials under confining pressure, when subjected to a cyclic shearing, without requiring the detailed behavior in each cycle.

(2) To understand, in terms of statistically described grain behavior, the detailed response in each cycle.

Objective (1) relates to the overall macroscopic failure mechanisms of soils under dynamic loading, whereas Objective (2) seeks to provide a microscopic basis for the detailed understanding of the overall macroscopic responses.

Progress has been made in both of the above-mentioned subject areas. The results are summarized in this report.

The report is organized in the following manner. In Chapter 1, a summary of the basic problem area and results are presented. In Chapter 2, the details of an energy method for the calculation of the void ratio in the case of dry sand, and the pore water pressure in the case of saturated undrained sand, are presented together with a comparison with experimental results. In Chapter 3, a framework is given for the calculation of the stress amplitude in terms of the number of cycles and the strain amplitude, or the strain amplitude in terms of the number of cycles and the stress amplitude, for both dry and saturated samples subjected to cyclic shearing. Chapter 4 examines the flow

of granular materials from a point of view different from that of the preceding chapters. In this chapter the response of granular materials to monotone loading is considered in the context of a plasticity theory which includes dilatancy and pressure sensitivity. Moreover, the questions of densification and liquefaction under cyclic loading are reexamined in the context of dimensional analysis. In Chapter 5, a statistical approach to the behavior of a dry granular mass in simple shear is presented, and the observed initial densification, subsequent dilatancy, and the net densification upon load reversal are given microstructural explanation. Chapter 6 presents the results of a systematic experimental work on densification and liquefaction in simple shearing. These results are rather striking and provide remarkable confirmation of the theory presented in Chapter 5.

Each chapter is written in such a manner that it can be read independently.

CHAPTER 1

SUMMARY OF RESULTS AND RECOMMENDATIONS

1. INTRODUCTION

As mentioned in the preface, the basic subjects of the present work are:

(1) To understand what happens to granular materials under confining pressure, when subjected to a cyclic shearing, without requiring the detailed behavior in each cycle.

(2) To understand, in terms of statistically described grain behavior, the detailed response in each cycle.

Subject (1) can be further subdivided into:

A. Densification of dry sand in cyclic shearing;

B. Liquefaction of saturated undrained sand in cyclic shearing.

In the sequel, these areas will be discussed.

2. Ddensification

Consider strain-controlled cyclic shearing, where the strain is prescribed to be

$$\gamma = \gamma_0 \, \phi(t) \ , \quad -1 \leq \phi(t) \leq +1 \ , \tag{1}$$

where ϕ is a given periodic function. Let τ_M be the stress amplitude when $\gamma = \gamma_0$, and assume that the corresponding value of the relative void ratio* is ρ_M. In our theory we attempt to obtain an expression for τ_M in the following

*The relative void ratio is defined as $\rho = e - e_m$, where e is the void ratio, and e_m is its minimum value.

form:

$$\tau_M = \hat{\tau}(\gamma_0, \rho_M) \ . \tag{2}$$

To this end, we first establish with the aid of an energy consideration, an explicit expression for ρ_M in terms of γ_0 and the number of cycles N; the details are given in Chapter 2, where results are compared with experiments. Then we use symmetry and other arguments in an effort to render the right-hand side of (2) explicit. For example, one notes that

$$\hat{\tau}(-\gamma_0, \rho_M) = -\hat{\tau}(\gamma_0, \rho_M) \ ,$$
$$\frac{\partial \hat{\tau}}{\partial \rho_M} < 0, \quad \hat{\tau}(0, \rho_M) = 0 \ ; \tag{3}$$

the detailed results are given in Chapter 3.

In obtaining explicit relations for the functions and parameters which describe the material response, we require extensive experimental data. However, published experimental results and reports do not include all the necessary information. This has resulted in a hindrance for further development regarding this subject area. To overcome this difficulty, we have completed a series of experiments ourselves; see Chapter 6.

3. LIQUEFACTION

Consider stress-controlled cyclic shearing, where the stress is prescribed to be

$$\tau(t) = \tau_0 \phi(t) \ , \ -1 \leq \phi(t) \leq +1 \ , \tag{4}$$

where ϕ is as in (1). Let γ_M and p_M respectively be the strain amplitude and the normalized* excess pore water pressure. In the present theory we attempt

* If the excess pore water pressure is $\hat{p}$ and the confining pressure is σ_c, then the normalized excess pore water pressure is defined as $p = \hat{p}/\sigma_c$.

to obtain γ_M in the following form.

$$\gamma_M = \hat{\gamma}(\tau_0, p_M) \ . \tag{5}$$

In this case again, we first use an energy consideration to express p_M in terms of τ_0 and the number of cycles N, and then, again using symmetry and other considerations, obtain an explicit form for the right-hand side of (5); these and related calculations are given in detail in Chapters 2 and 3. As is discussed in Chapters 2 and 3, the theory corresponds well with some existing experimental results. However, further progress requires additional coordinated experiments.

4. STATISTICAL CONSIDERATIONS

Since a mass of granular materials consists of a collection of a large number of grains, it is reasonable to expect that by appropriate statistical considerations and the use of the basic laws of mechanics, one should be able to obtain basic equations which characterize the overall macroscopic behavior of the material in terms of the statistics of grain distribution, the coefficient of friction, and other relevant parameters. (For geotechnical applications, the grains can be considered as rigid, since low confining pressures are involved.) While this sounds like a very ambitious objective, some progress has been made. The work completed under the present project is given in Chapter 5. It involves the calculation of the rate of dilatancy or densification in simple shearing, in terms of some energy considerations and simple statistics of microstructural behavior. The results serve to explain the observed volumetric behavior of granular materials in monotone as well as cyclic shearing. In particular, it brings into focus the importance of the granular fabric in relation to the corresponding liquefaction potential.

5. FABRIC AND LIQUEFACTION POTENTIAL

The theory suggests that during a cycle of loading and unloading, the fabric of the granular material is changed. This change may result in a drastic change of the liquefaction potential of the sample. For example, if a drained sample is first subjected to a relatively large shear stress and then the stress is brought to zero, in subsequent cyclic shearing under undrained conditions, the sample may liquefy immediately. Experimental results support this finding, as discussed in Chapter 6. These experimental results are rather striking. For example, in Fig. 3b of Chapter 6, densification under cyclic loading of a virgin sample (the lower figure) is compared with that of a liquefied sample (the upper figure). As is seen, due to liquefaction the fabric is changed, and, even with a smaller void ratio, the preliquefied sample shows much larger densification potential than the virgin sample. Results presented in Chapter 6 clearly show that much remains to be learned on the mechanics of liquefaction. In our laboratory, we have been able to prepare two samples of identical density from the same sand, but with such fabrics that one would liquefy within one cycle while the other one after more than 100 cycles of the same stress shape and amplitude.

Our recommendation is that further scientific experimental and theoretical research is necessary in the area of liquefaction and densification of granular masses in cyclic loading, if we are to develop the technical ability for predicting and preventing ground failures induced by earthquakes.

CHAPTER 2

A UNIFIED APPROACH TO DENSIFICATION AND LIQUEFACTION OF COHESIONLESS SAND IN CYCLIC SHEARING

1. INTRODUCTION

It is known that loose sand (either dry or saturated but drained) undergoes densification (compaction) when subjected to cyclic shearing. This subject has been experimentally treated extensively by a number of investigators who have brought into focus essential features of this phenomenon; see for example, Silver and Seed (1971a,b),* Youd (1970 and 1972), and references cited therein; see also Faccioli and Resendiz (1976) for a review of recent developments. In the case of undrained saturated sand, the tendency for densification leads to an increase in pore water pressure, and therefore a reduction in the shear strength of the sand. A continuous loss of strength of this kind can lead to the phenomenon of liquefaction which has been observed to occur during earthquakes, as well as in laboratory experiments; see for example, Seed and Idriss (1967 and 1969), Seed and Lee (1966), Seed and Peacock (1971), Martin et al. (1975), Faccioli and Resendiz (1976) and references cited therein. In view of the extensive experimental and field investigations by the above-mentioned authors and others, the basic physics of the phenomenon of liquefaction has been fairly well understood. To our knowledge, however, there exists no fundamental theory for either the densification or the liquefaction phenomenon.

In this chapter we shall present a unified theory for the densification and liquefaction of cohesionless sand. The theory is motivated by a consideration

---

* References are listed at the end of this chapter.

of the microstructural (at the grain size level) rearrangement of the sand particles, which takes place during cyclic shearing, and which leads to the densification of dry or saturated but drained sand, and to the liquefaction of saturated undrained sand. We shall apply the results of our theory to several sets of relevant available experimental results, in order to show how effectively the theory accounts quantitatively for the observed behavior.

The theory is based on the observation that the densification of sand involves rearrangements of its grains and hence, an expenditure of a certain amount of energy which increases as the void ratio approaches its minimum value, this minimum of course depending on the grain structure, size distribution, confining pressure, and other relevant parameters. If the saturated sand is undrained and is subjected to a fixed confining pressure, the tendency toward densification induced by cyclic shearing, results in an increase in the pore water pressure, and therefore a decrease in the frictional and contact forces that exist at the interface between adjacent sand particles. Hence the corresponding energy required to decrease the pore volume, decreases with increasing pore water pressure. On the basis of these observations, a differential equation is proposed, which relates the energy loss in cyclic shearing to the consequent change in the void ratio for the dry sand, and to the consequent increase in the pore water pressure in the saturated undrained case. The theory then is applied in its simplest form to predict some of the existing experimental results for both the densification and liquefaction phenomena; the obtained results seem to lend considerable credit to the basic approach.

2. THEORY

Consider a sand sample of volume V which contains a certain amount of solid having the volume V_s. The remaining volume, $V - V_s = V_p$, will be

assumed to be occupied by water for saturated sand ($V_p \equiv V_w$) or be empty for dry sand ($V_p \equiv V_v$). Since we wish to treat the densification and liquefaction phenomena in a unified manner, we define $e = V_p/V_s$, and refer to it as the void ratio, keeping in mind that, for saturated sand, it actually represents the ratio of the volume of the water, V_w, to the volume of the solid, V_s, in a given sample of volume V.

Assume that the sample is subjected to a fixed confining pressure σ_c, and consider its cyclic shearing. To change the void ratio from its current value, e, to e + de, a certain amount of energy must be consumed. We observe that this energy must be a <u>decreasing</u> function of $e - e_m$, where e_m is the minimum void ratio which will depend in general on the size and shape distribution of the sand particles, on the confining pressure, and on other relevant parameters. Moreover, this energy must be a <u>decreasing</u> function of the <u>excess</u> pore water pressure, $p = \bar{p}/\sigma_c$, where $\bar{p}$ is the actual excess pore water pressure. To support these two statements, we observe that the void ratio cannot be decreased below its minimum, e_m, without the expenditure of an "infinite" amount of energy. Hence, more and more energy will be required for densification, as e_m is being approached. When this sample is undrained, the tendency for a reduction in e results in a tendency for increasing p. The increase in the excess pore water pressure p then causes a reduction in the inner particle forces. Thus it becomes easier to rearrange the particles, and therefore cause further increase in the pore water pressure.

To quantify the above observations, let dW be the amount of energy (measured per unit volume of the sample) required to change the void ratio e to e + de, and set

$$dW = -\tilde{\nu}\,\frac{de}{f(1+p)g(e-e_m)}\quad , \tag{1}$$

where, with prime denoting differentiation, we must require that

$$f(1) = 1, \quad f' \geq 0, \quad g(0) = 0, \; g' \geq 0 \; , \tag{2}$$

and where $\tilde{\nu}$ is a positive parameter which may depend on σ_c, but not on the void ratios.

In Eq. (1) e and p are dimensionless quantities, as are the functions f and g. The physical dimensions of $\tilde{\nu}$ and dW must therefore be the same. However, we assume that both $\tilde{\nu}$ and dW are rendered dimensionless with respect to a suitable reference value W_0. As will be seen later on, since we calculate dW on the basis of a dimensionless shear stress $\tau_0 = \hat{\tau}_0/\sigma_c$, it will be properly dimensionless and will represent the energy measured per unit volume per unit confining pressure; see Eq. (11) and Fig. 1. Hence, in all subsequent equations all variables and functions are physically nondimensional (unless otherwise stated explicitly).

The quantity $(e - e_m)$ enters in a natural way in many of our subsequent expressions. It represents the maximum amount of reduction in the void ratio that can be theoretically accomplished (without crushing and changing individual grains); since e is the present value of the void ratio, $(e - e_m)$ represents the relative looseness of the sand (the larger this quantity, the looser the sand). We shall refer to $(e - e_m)$ as the relative void ratio. We observe that in soil mechanics literature the quantity

$$D_r = \frac{e_M - e}{e_M - e_m} \times 100 \; , \tag{3}$$

i.e. the relative density is commonly used to characterize the relative denseness of the sand; in (3) e_M is the maximum void ratio.

For the drained sample, we set p = 0, so that f = 1, and obtain

$$dW = -\tilde{\nu} \frac{de}{g(e - e_m)} \; , \tag{4}$$

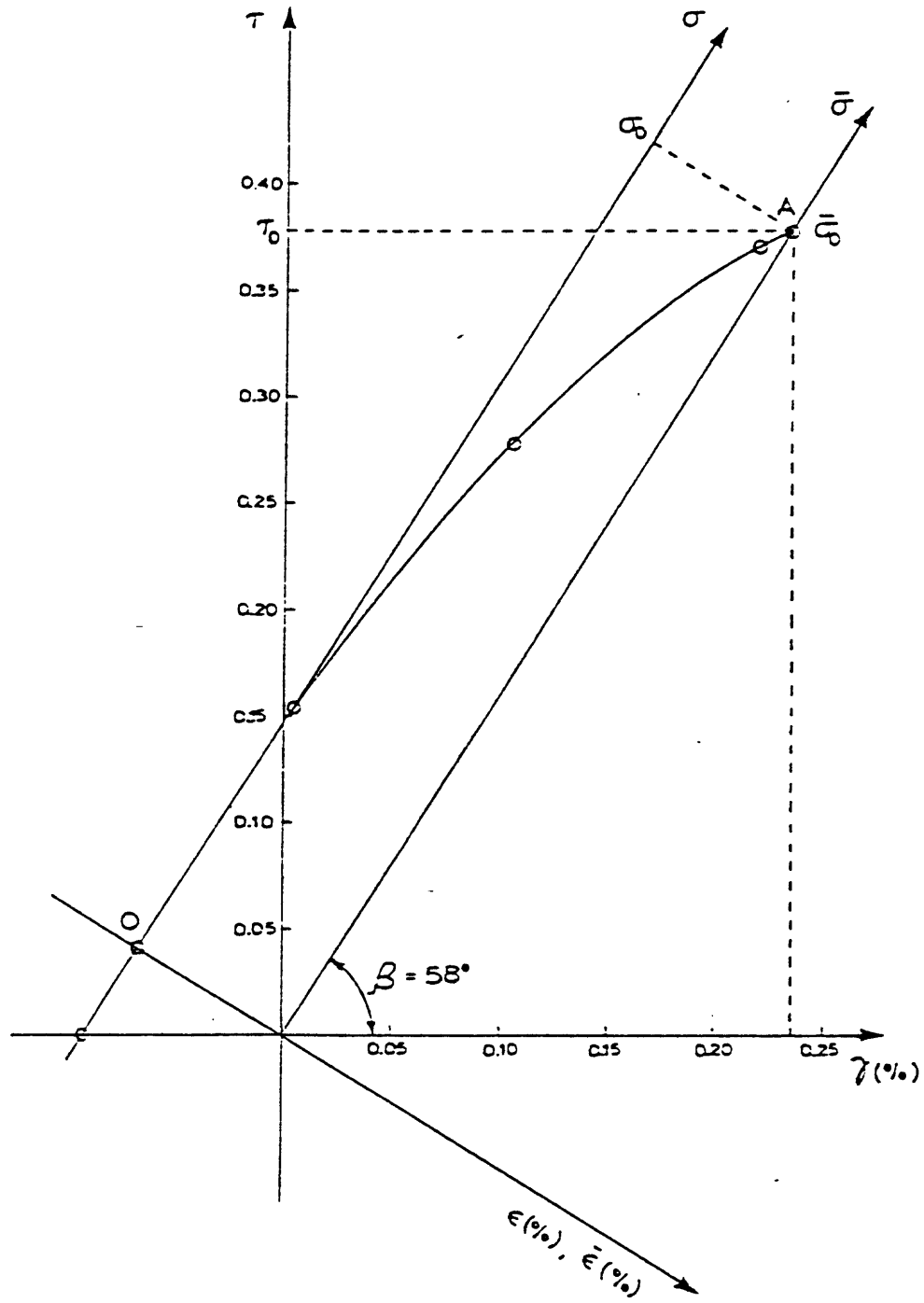

Fig. 1. 1/4 of a typical hysteretic loop (data from Silver and Seed, 1971a).

For the undrained sample, we observe that

$$de = \frac{dV_p}{V_s} = \frac{dV_p}{V_p}\frac{V_p}{V_s} = -\frac{1}{\kappa_w}\left(-\kappa_w \frac{dV_p}{V_p}\right)e = -\frac{e}{\kappa_w}d\bar{p} = -\frac{e\sigma_c}{\kappa_w}dp \ ,$$

so that (1) becomes

$$dW = \nu \frac{edp}{f(1+p)g(e-e_m)} \ , \tag{5}$$

where κ_w is the bulk modulus of the water, $\nu = \frac{\tilde{\nu}\sigma_c}{\kappa_w}$, and $dp = d\bar{p}/\sigma_c$. We now observe that the initiation of liquefaction is defined when the excess pore water pressure equals the confining pressure σ_c, i.e., when $p = 1$. Since in all practical cases, σ_c does not exceed a hundred psi, the corresponding total volumetric pore strain for $p = 1$, which does not exceed $-\sigma_c/\kappa_w$, is negligibly small (usually of the order of 10^{-5}). Hence, for computational convenience, we can set, in Eq. (5), $e = e_0$, the initial void ratio, and arrive at

$$dw = \frac{\nu e_0}{g(e_0 - e_m)} \frac{dp}{f(1+p)} \ , \tag{6}$$

We shall now integrate Eqs. (4) (for densification, and (6) for liquefaction), and arrive at the following general results:

$$\Delta W = -\tilde{\nu} \int_{e_0}^{e} \frac{de'}{g(e' - e_m)} \quad \text{for densification,} \tag{7}$$

$$\Delta W = \frac{\nu e_0}{g(e_0 - e_m)} \int_0^p \frac{dp'}{f(1+p')} \quad \text{for liquefaction,} \tag{8}$$

where ΔW is the total energy consumed for the corresponding change.

In the sequel we shall use elementary forms for functions g and f, obtain explicit results from Eqs. (7) and (8), and compare these results with experimental observations. To this end we need to express more explicitly the energy loss, ΔW, in terms of the number of cycles and the shear stress amplitude (for the stress-controlled test) or the shear strain amplitude (for the strain-controlled test).

Estimate for Energy Loss ΔW

We shall estimate the energy loss ΔW after N cycles of shearing, using the data for hysteretic damping obtained in cyclic shearing of drained cohesionless sand. To this end let A_i be the area enclosed by the hysteretic loop during the i^{th} cycle of shearing, and denote by ΔW_i the corresponding energy that has been actually used in rearranging the grain particles (both A_i and ΔW_i are dimensionless, and are measured per unit volume of the sample and per unit confining pressure). We must have $\Delta W_i = \lambda_i A_i$, where $0 < \lambda_i < 1$, and where λ_i may depend on the number of preceding cycles as well as other parameters. The energy loss ΔW may therefore be expressed as

$$\Delta W = \sum_{i=1}^{N} \Delta W_i = \sum_{i=1}^{N} \lambda_i A_i \ , \tag{9}$$

Figure 1 shows a portion of a typical hysteresis loop obtained experimentally by Silver and Seed (1971a) for cohesionless sand in cyclic shearing. In the ε,σ-coordinates with origin at O, the curve OA may be approximated by the expression

$$\varepsilon = K_i \sigma^{\alpha_i} \ , \tag{10}$$

where the subscript i indicates that the hysteretic loop in the i^{th} cycle of shearing is being considered. Clearly, one may use more elaborate expressions than (10) to represent hysteretic damping. However, our main objective here is only to estimate the total area of the loop, and therefore, Eq. (10) seems to be quite adequate.

The complete hysteretic loop is not quite symmetric with respect to the $\bar{\varepsilon}$- and $\bar{\sigma}$- axis of Fig. 1. However, the deviation from symmetry for cyclic shearing of cohesionless sand, seems to be small enough to permit the assumption of symmetry, which has been implied by many authors; see Silver and

Seed (1971a,b), Hardin and Drnevich (1972), Yoshimi et al. (1977), and references cited therein. If we use the assumption of symmetry, then the area of the hysteretic loop in the i^{th} cycle can be estimated as

$$A_i = 4 \int_0^{\sigma_0} \sigma \, d\varepsilon = 4K_i \frac{\alpha_i}{1 + \alpha_i} \sigma_0^{\alpha_i + 1} .$$

Transferring to the γ,τ-coordinates, noting that ΔW_i is proportional to A_i, and collecting all the resulting coefficients, we obtain

$$\Delta W_i = \hat{h}_i \tau_0^{\alpha_i + 1} , \quad \tau_0 = \hat{\tau}_0 / \sigma_c , \tag{11}$$

where $\hat{\tau}_0$ is the applied shear stress amplitude, and where, for a given sand, the coefficient $\hat{h}_i$ in general depends on the number of preceding cycles, on the confining pressure, on the relative void ratio $e - e_m$, as well as on other relevant parameters. In the above expression it is also implied that the exponent α_i varies from cycle to cycle. Although, in general, this is probably the case, for our purposes here we can replace α_i by an average constant value α, and assuming that the hysteretic loop is completely symmetrical with respect to the $\bar{\varepsilon}$-axis in Fig. 1, assign a positive even value to α; in all our calculations, we have found that $\alpha = 4$ yields results which are compatible with experimental observations in the liquefaction of cohesionless sand.

In view of the above comments, we set $\alpha_i = \alpha$ in Eq. (11), and substitute the result into Eq. (9) to arrive at

$$\Delta W = \sum_{i=1}^{N} \hat{h}_i \tau_0^{\alpha+1} = \hat{h} \tau_0^{\alpha+1} , \quad \hat{h} = \sum_{i=1}^{N} \hat{h}_i . \tag{12}$$

Most results reported for the densification of drained sand in cyclic shearing are for strain-controlled tests, where the amplitude of the applied shearing strain is kept fixed, and the corresponding shearing stress

amplitude is measured as a function of number of cycles for various test conditions. It is observed that as the sample densifies with increasing number of cycles in a strain-controlled test, the corresponding shear stress amplitude increases (slightly) with the number of cycles, causing the hysteretic loop to elongate. Therefore, if we consider for a fixed number of cycles the relation between the stress amplitude and the corresponding strain amplutide, experimental results show that we arrive at a curve similar to QOP in Fig. 2; see, for example, Hardin and Drnevich (1972), and Yoshimi et al. (1977). In Fig. 2 a typical hysteretic loop is shown with dashed curves. The curve QOP is often approximated by the expression

$$\gamma_0 = a\tau_0 + b\tau_0^c \ .$$

This equation permits us to express the energy loss ΔW in terms of the strain amplitude γ_0 for strain-controlled tests using Eq. (12) which corresponds to the stress-controlled test. However, as it stands, the above equation is too difficult to solve for τ_0, and obtain a simple expression. In view of the approximations involved, we feel justified to use the following much simpler relation:

$$\gamma_0 = A\tau_0^\beta \ , \tag{13}$$

where, since curve QOP is centrally symmetric, we assign a positive odd value to β; in all our calculations for densification in cyclic shearing we have found that $\beta = 5$ yields results which are compatible with experimental observations. Based on the experimental results, we observe that the coefficient A in Eq. (13) must be a decreasing function of the number of cycles and of the relative density (i.e. A must decrease with decreasing relative void ratio $e - e_m$). These conclusions are intuitively reasonable, because if the stress amplitude is kept fixed, then the corresponding strain amplitude must

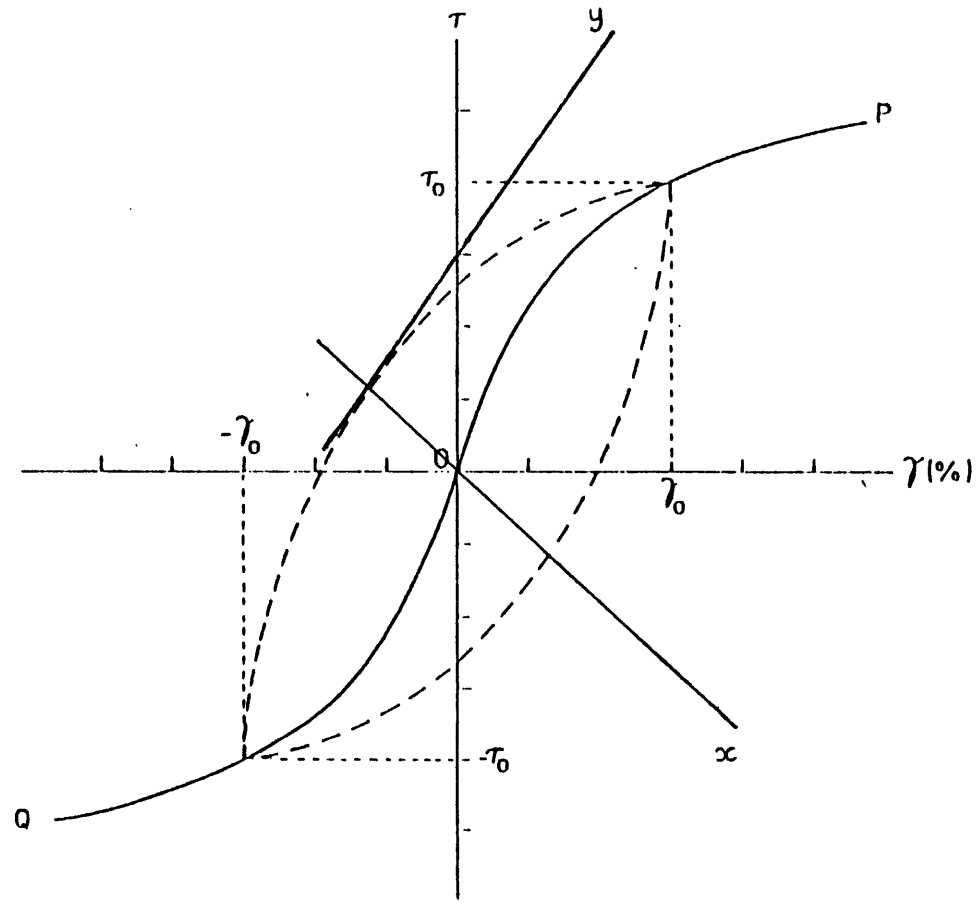

Fig. 2. A typical maximum shear stress - shear strain curve in cyclic shearing (from Hardin and Drnevich (1972)).

decrease with the number of cycles (which causes further densification). Moreover, if we start out with smaller initial values of $e - e_m$ (i.e., with denser sands), for the same stress amplitude and after the same number of cycles, we must obtain smaller strain amplitude. Hence, A must decrease with decreasing $(e_0 - e_m)$.

If we now substitute from Eq. (13) into Eq. (12), we arrive at

$$\Delta W = \hat{k}\gamma_0^{\frac{\alpha+1}{\beta}} \quad . \tag{14}$$

We shall use Eqs. (12) and (14) in conjunction with (7) and (8) in all our subsequent calculations. As was mentioned before, because of the symmetry requirements, α will be assigned a positive even value, and β will be assigned a positive odd value. In fact, as stated earlier, we shall set $\alpha = 4$, and $\beta = 5$. The coefficients $\hat{h}$ in Eq. (12) and $\hat{k}$ in Eq. (14) for a given sand, in general, depend on the number of cycles, on the confining pressure, and on the initial value of the relative void ratio $e - e_m$ (or the relative density D_r), as well as on other relevant parameters. Both $\hat{h}$ and $\hat{k}$ must be monotonically increasing function of the number of cycles N.

When the stress amplitude (in stress-controlled tests) or the strain amplitude (in strain-controlled tests) is relatively large, a substantial rearrangement of the sand particles takes place during each cycle of shearing. In this case, the energy loss in each cycle is quite large and essentially independent of the previous cycles. On the other hand, when the amplitude of shearing is very small (for example, strain amplitudes of much less than 0.1%), the rearrangement of sand particles within each cycle will be very small, but during each cycle the particles tend to arrange themselves into more stable positions. After a large number of cycles which will be required to cause any substantial changes, there will be less subsequent rearrangement of the

particles, and therefore the energy loss tends to decrease with the number of cycles (which is large) for very small strain amplitude shearing.

In view of the above comments, we may assume, for relatively large stress amplitude in the stress-controlled test, that the coefficient $\hat{h}$ in Eq. (12) is approximately proportional to the number of cycles, and hence use the following expression:

$$\Delta W = hN\tau_0^{\alpha+1} , \tag{15}$$

where h is viewed as an average quantity. Similarly, when we deal with relatively large strain amplitudes (say, strain amplitudes much greater than 0.1%), we may approximate Eq. (14) by

$$\Delta W = k_1 N \gamma_0^{\frac{\alpha+1}{\beta}} , \text{ for large strain amplitude.} \tag{16}$$

For very small strain amplitude shearing, we have examined experimental results reported by Silver and Seed (1971a,b) and also given to us by Professor Silver and Dr. Youd in private communications, and have observed that the area of the hysteretic loop seems to decrease as $1/\sqrt{N}$, with the number of cycles. With this observation we have found that if we take $\hat{k}$ to be proportional to $\sqrt{N}$, (which is obtained by integrating $dN/\sqrt{N}$) then we can fit very nicely all the densification data reported by Youd (1972, 1977) for strain amplitudes $\leq$ 0.1%. Hence, we shall set

$$\Delta W = k_2 \sqrt{N} \gamma_0^{\frac{\alpha+1}{\beta}} , \text{ for small strain amplitude.} \tag{17}$$

For future use we rewrite Eqs. (7) and (8) in the following form:

$$\hat{k}\gamma_0^{\frac{\alpha+1}{\beta}} = -\hat{\nu} \int_{e_0}^{e} \frac{de'}{g(e' - e_m)} \quad \text{for densification} , \tag{18}$$

$$\hat{h}\tau_0^{\alpha+1} = \frac{\nu e_0}{g(e_0 - e_m)} \int_0^{p} \frac{dp'}{f(1 + p')} \quad \text{for liquefaction} , \tag{19}$$

where a strain-controlled cyclic shearing is assumed for the densification test, and a stress-controlled one for the liquefaction experiment.

In connection with Eqs. (18) and (19) one point must be carefully noted. The left-hand sides in these equations represent the work performed, whereas the right-hand sides denote the work required for the corresponding test. Moreover, whereas the effect of the initial relative void ratio $e_0 - e_m$ is explicitly included in the function g in the right-hand sides of (18) and (19), and therefore, parameter $\tilde{\nu}$ in (18) and ν in (19) should no longer be regarded as functions of $e_0 - e_m$, the same is not true for parameters $\hat{k}$ and $\hat{h}$ in the corresponding left-hand sides. As we mentioned above, both $\hat{k}$ and $\hat{h}$ in general depend on $e_0 - e_m$, as well as on the confining pressure σ_c and the number of cycles N. In fact, it is reasonable to expect that $\hat{h}$ and $\hat{k}$ should increase with increasing confining pressure, and with decreasing initial value of the relative void ratio, $e_0 - e_m$; because, in cyclic shearing, more energy must be supplied in order to rearrange the sand particles under a larger confining pressure, and also when a denser sand is used. However, experimental results suggest that $\hat{h}$, for example, is rather insensitive to the variations of the initial value of D_r (or $e_0 - e_m$), if the sand is not relatively too dense. In all the experimental results that we have examined (for liquefaction), we have found that h in Eq. (15) can be taken to be independent of D_r (or $e_0 - e_m$) for relative densities less than about 70%. When D_r exceeds 80%, a strongly nonlinear relation between h and D_r becomes necessary in order to correlate experimental results with the theory. This suggests that a different deformation pattern may be taking place for dense sands as compared with those with moderate values of D_r. For D_r's exceeding 80%, h seems to take on larger values, although in this range little experimental results are available to justify even a tentative conclusion.

We finally point out that in calculating the energy loss ΔW, say, Eq. (12), we have ignored the work corresponding to volumetric changes, i.e. we have only included the work due to shearing. This is because the work due to volumetric changes is, in general, several orders of magnitude smaller than that pertaining to the shear deformation. For example, for the undrained saturated sample, the volumetric strain for confining pressures of about 10 psi, is of the order of 10^{-5}, and therefore the corresponding work per unit volume per unit confining pressure is of the same order of magnitude. On the other hand, the area of the hysteretic loop in Fig. 1, which is also the dimensionless work per unit volume per unit confining pressure, is of the order of 10^{-3}, and therefore the total work in, say, 10 cycles, would be of the order of 10^{-2}. In a similar way, it can easily be estimated that the work done by the confining pressure on the drained sample during compaction is at least 2 orders of magnitude smaller than the work involved in the inelastic shearing of the specimen. This is indeed the case for all available experimental results that we have examined or used in this paper. However, in very special circumstances and under very large confining pressures, the work due to volumetric changes may become significant, and accordingly it may have to be included in the theory.

3. Ddensification

Experimental Observations

Youd (1972) has summarized the essential features involved in the compaction of sand by repeated shear straining, and has presented extensive experimental results which confirm previous findings of Silver and Seed (1971a,b). It is observed that the compaction increases with the shear strain amplitude, with the number of cycles, and with the initial void ratio. It is, however,

independent of the frequency in the range of 10 to 100 or even more cycles per minute.

Application of the Theory

The simplest version of the theory is obtained if we set, in Eq. (18),

$$g(e - e_m) \equiv (e - e_m)^n , \quad n \geq 1 \tag{20}$$

Then we obtain, upon integration,

$$\Delta W = \begin{cases} \tilde{\nu} \ell n \left(\frac{e_0 - e_m}{e - e_m}\right) & \text{for } n = 1, \\ \frac{\tilde{\nu}}{n-1} \left[(e-e_m)^{1-n} - (e_0 - e_m)^{1-n}\right] & \text{for } n > 1. \end{cases} \tag{21}$$

Solving (21) for the void ratio e, we obtain

$$e = \begin{cases} e_m + (e_0 - e_m)\exp\left[-\frac{\Delta W}{\tilde{\nu}}\right] & \text{for } n = 1 , \\ e_m + \left[(e_0 - e_m)^{1-n} + \frac{n-1}{\tilde{\nu}}\Delta W\right]^{\frac{1}{1-n}} & \text{for } n > 1 . \end{cases} \tag{22}$$

Equations (22) show that the void ratio decreases monotonically, approaching asymptotically the minimum value e_m, as the energy input per unit volume of the sand, ΔW, in cyclic shearing becomes very large. We have found that Eq. $(22)_1$, namely n = 1, does not correspond to any of the observed experimental results. Hence we have concluded that n must be greater than 1. As a first approximation, our basic theory now yields

$$e = e_m + \left[(e_0 - e_m)^{1-n} + \hat{k}\gamma_0^{\frac{\alpha+1}{\beta}}\right]^{\frac{1}{1-n}} , \tag{23}$$

where a strain-controlled cyclic shearing with amplitude γ_0 is assumed, Eq. (14) is used, and since the function $\hat{k}$ is not as yet determined, we have absorbed it into the parameter $(n-1)/\tilde{\nu}$.

We shall now compare Eq. (23) with rather extensive experimental results reported by Youd (1972).

Comparison with Experimental Results

In a series of experiments reported by Youd (1972), standard gradation Ottawa sands were densified in a Norwegian Geotechnical Institute type simple shear apparatus under repeated cycles of shear strains. Strains from 0.1% to 9% were applied under normal stresses ranging from 100 psf (4.8 kN/m^2) to 4,000 psf (192 kN/m^2) with the number of strain cycles ranging from 1 to 150,000. In Fig. 3 the solid curves represent Youd's results, where the initial void ratio e_0 is reported to be within the range 0.543 to 0.548, the vertical pressure to be 1,000 psf, and the minimum void ratio attained, to be about 0.412.

To compare Eq. (23) with the experimental results, we distinguish small strain results ($\gamma_0 \leq 0.1\%$) from those for large strain amplitudes ($\gamma_0 > 0.1\%$). In the first case we use Eq. (17) and in the second case Eq. (16). With $\alpha = 4$ and $\beta = 5$, Eq. (23) then yields

$$e = \begin{cases} e_m + [(e_0 - e_m)^{1-n} + k_2\sqrt{N}\gamma_0]^{\frac{1}{1-n}}, & \text{for small strain amplitudes,} \\ e_m + [(e_0 - e_m)^{1-n} + k_1 N\gamma_0]^{\frac{1}{1-n}}, & \text{for large strain amplitudes.} \end{cases} \quad (24)$$

We now set $e_0 = 0.545$, $e_m = 0.412$, and observe that our theoretical results are rather insensitive to the exact values of the parameters k_1, k_2, and n, as long as these parameters are within a specific range. In fact, as far as the experimental data in Fig. 3 are concerned, we may choose $500 < k_1 < 1500$, $6500 < k_2 < 7500$ and $3 < n < 4$. As a specific case, we set $k_1 = 1000$, $k_2 = 7000$, and $n = 3.5$. Equations (24) then reduce to

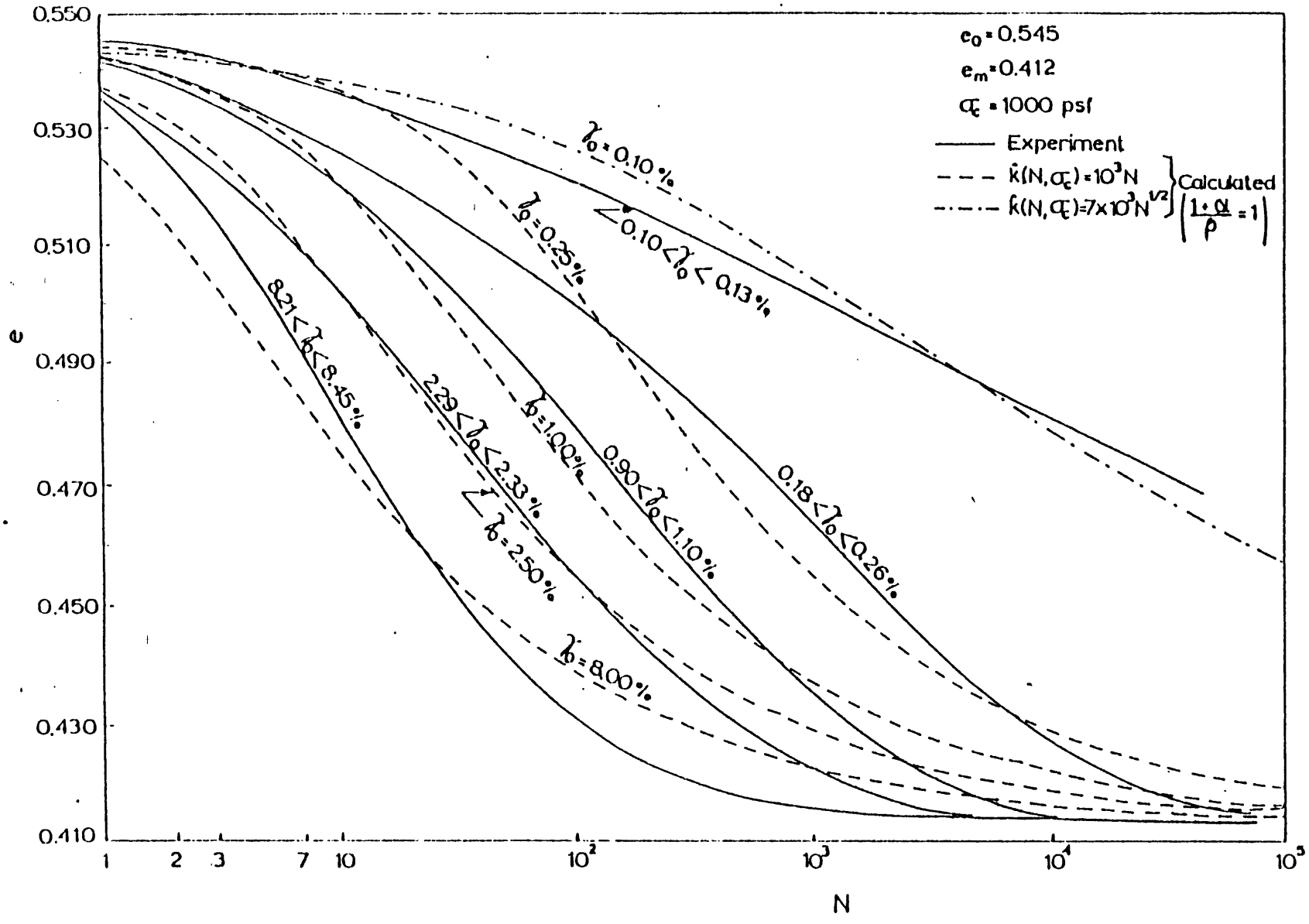

Fig. 3. Void ratio e versus number of cycles in cyclic shearing of dry sand (data from Youd, 1972).

$$e = \begin{cases} 0.412 + [155 + 7000\sqrt{N}\gamma_0]^{-2/5} & \text{, for small strain amplitudes,} \\ 0.412 + [155 + 1000N\gamma_0]^{-2/5} & \text{, for large strain amplitudes.} \end{cases} \quad (25)$$

The dotted lines in Fig. 3 are graphs of Eq. (25) for the indicated values of γ_0. We see that over the range of 0.1 to 8% strain amplitudes, and for 1 to 100,000 cycles, our theoretical results adequately fit the experiments, although we have introduced rather rough estimates for some of the essential quantities, such as the energy loss per cycle and its variation with the number of cycles. Also it should be pointed out that Eq. (20) is the simplest elementary form that can be attributed to the function g, and that, guided by experimental observation, one may be able to define the form of this function more accurately. In fact, it may be possible to obtain the general property of this function on the basis of microstructural rearrangements which take place in the cyclic shearing of a given sand. But this will require careful observation and extensive experimentation. Notwithstanding all this, Eq. (25) seems to give the trend of the general behavior rather well over a wide range of strain amplitudes and the number of cycles. In fact, for N = 1, the theoretical results suggest some inaccuracy for the experimental results, especially for the lowest curve corresponding to a large strain amplitude. As is seen, an increase in strain amplitude from about 1% (the middle solid curve) to a little more than 2% (second solid curve from below), a large drop in void ratio occurs after one cycle of shearing. A similar drop is observed when the strain amplitude is changed from 0.1% to about 0.2% (upper two solid curves). However, when the strain amplitude is changed from a little over 2% to a little over 8%, no such drop is recorded in the experimental data. Equations (25), on the other hand, predict that the void ratio

will change from approximately 0.538 for $\gamma_0 = 2.26\%$ to 0.524 for $\gamma_0 = 8.33\%$, which seems reasonable.

Dr. Youd has provided us with additional experimental results with a lower strain amplitude range. These results are shown in Fig. 4 by means of various geometrical marks. The data are for $e_0 = 0.584$, $e_m = 0.428$, and $\sigma_c = 400$ psf. In this case if we set $k_1 = 300$, $k_2 = 4500$, and as before $n = 3.5$, we obtain

$$e = \begin{cases} 0.428 + [104 + 4500\sqrt{N\gamma_0}]^{-2/5}, & \text{for small strain amplitude,} \\ 0.428 + [104 + 300N\gamma_0]^{-2/5}, & \text{for large strain amplitude.} \end{cases} \quad (26)$$

In Fig. 4 the dashed curves (small strain amplitude) and the solid curves (large strain amplitude) compare the theoretical predictions of Eq. (26) with the experimental results. Comparing Eqs. (25) and (26), observe that the coefficients k_1 and k_2 increase with increasing confining pressure σ_c, as has been pointed out before.

It should be noted that the experimental shear strain amplitudes reported in Figs. 3 and 4 are average quantities as the shear strain was not uniform throughout the thickness of the sample. This has been illustrated in Fig. 1 of Youd's paper (1972) which gives the profile of the edge of the deformed sample at the position of maximum shear deformation, for $\gamma_0 = 4.7$, 5, and 5.1% shear strain amplitudes, and after 1, 50, and 1,000 cycles, respectively.* Therefore, one may expect a somewhat nonhomogeneous densification of the experimental sample, whereas the theoretical results are based on the assumption of homogeneous densification.

---

* The additional information has been provided by Dr. Youd in a private communication.

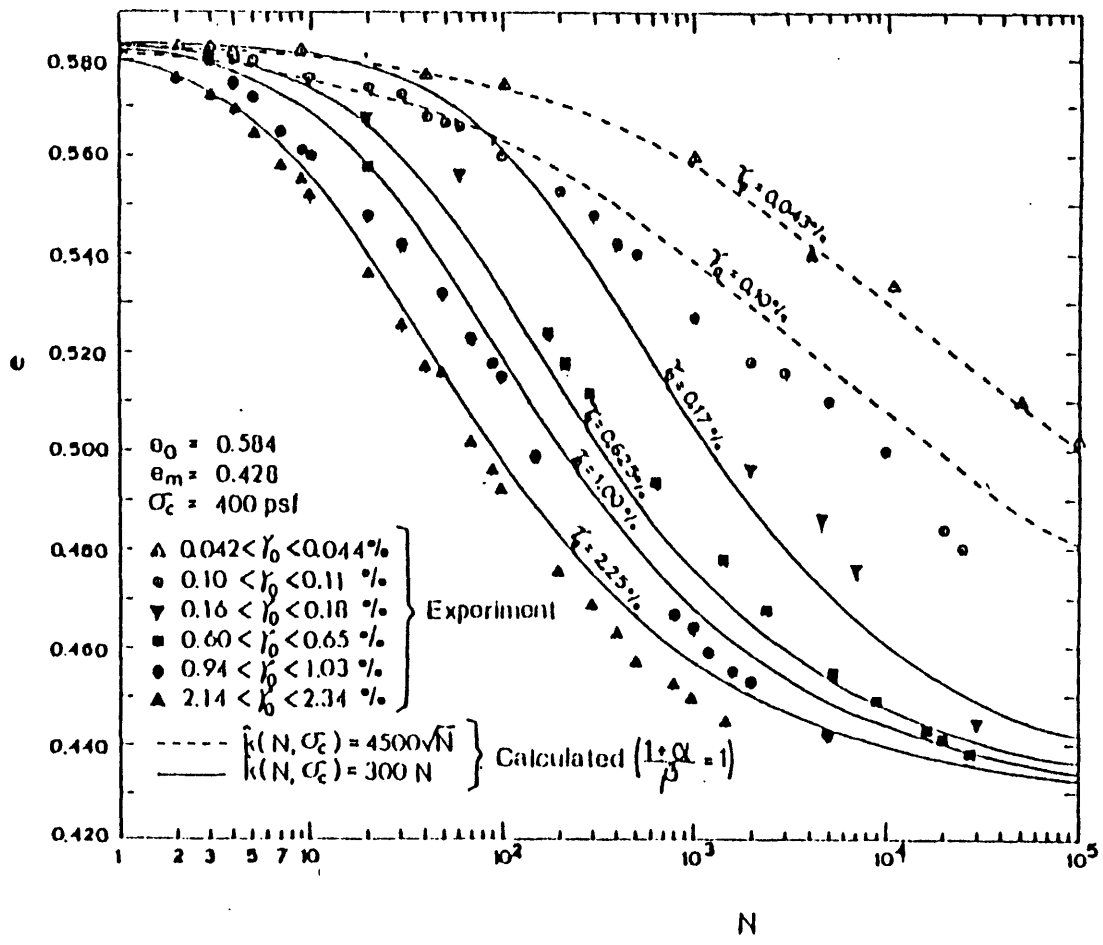

Fig. 4. Void ratio e versus number of cycles in cyclic shearing of dry sand (data from Youd, 1977).

4. LIQUEFACTION

Experimental Observations

In a comprehensive report, DeAlba, Chan, and Seed (1975) cite experimental work in the liquefaction of saturated cohesionless sand, and present extensive results on a series of experiments conducted at the University of California at Berkeley, with the aid of a large shaking table, on rather large samples. The material used was Monterey number 0 sand with minimum void ratio, $e_m = 0.564$, and reported maximum void ratio, $e_M = 0.852$. Experiments were performed on samples with 54, 68, 82, and 90% relative densities, at about 8 psi confining pressures,* and cyclic shearing with various fixed shear stress amplitudes. The pore water pressure build-up as a function of the number of cycles, the number of cycles to initial liquefaction for given shear stress amplitudes, and other relevant experimental results are reported by DeAlba et al. (1975), and the corresponding data are analyzed and corrected for the effect of the apparatus on the test results.

Here we shall apply our theory to these results, in order to test the validity of our approach. Although we have made rough estimates in order to render our results explicit, we have found an amazing correlation between our theoretical predictions and the experimental results. In addition to the experimental data from DeAlba et al. (1975), we shall also compare our results with experiments reported by Yoshimi and Oh-Oka (1975), and by Peacock and Seed (1968).

Application of the Theory

The simplest theory corresponds to the following elementary forms for the functions f and g in Eq. (8):

* One experiment is reported for $\sigma_c = 4.53$ psi by DeAlba et al. (1975).

$$f(1 + p) \equiv (1 + p)^r \qquad r > 0,$$

$$g(e_0 - e_m) \equiv (e_0 - e_m)^n, \qquad n > 0 \ . \tag{27}$$

Since the value of n has been set in the densification analysis at 3.5, we shall use the same value here.* Our calculations have revealed that r must be greater than 1, and that actually it ranges between 2 and 3. Therefore, we shall take $r \approx 2.5$ in the sequel.

Upon substitution into (19) and integration, we obtain, in view of the discussion preceding Eq. (15),

$$hN\tau_0^{1+\alpha} = \frac{\hat{\nu} e_0}{(e_0 - e_m)^n} [(1 - (1 + p)^{1-r}] \ , \tag{28}$$

where we have set $\hat{\nu} = \nu/(r-1)$.

Comparison with Experiments for Sand with Relative Densities Less than 70%

For a given sand with a given grain size and shape distribution, we expect that $\hat{\hat{\nu}} = \hat{\nu}/h$ should depend on the confining pressure and on the initial value of the relative density. Since we identify the liquefaction initiation with a state at which the pore water pressure equals the confining pressure, i.e. when p = 1, we can immediately test the validity of (28), by setting p = 1, $N = N_\ell$ (namely, the number of cycles to liquefaction), and obtain

$$N_\ell \tau_0^{1+\alpha} \frac{(e_0 - e_m)^n}{e_0} = \hat{\hat{\nu}}(1 - 2^{1-r}) \equiv \eta \ . \tag{29}$$

We now set $\alpha = 4$, $n = 3.5$, and $r = 2.5$ in Eq. (29), and observe that the effect of the initial relative density D_r, and the confining pressure σ_c is included in the parameter η. As discussed before (see comments which followed

* Note that the function g is the same as that used for the densification; see Eq. (20).

Eq. (19)), h and therefore η appear to be rather insensitive to the variation in the initial relative density D_r for D_r less than about 70%; there may be a lower limit for this insensitivity, but we have no experimental result to make any assessment in this regard. Table 1 gives results obtained from Eq. (20) on the basis of data reported by DeAlba et al. (1975), page 96, Fig. 5.1. We see that the value of η is indeed a constant (within experimental error) for relative densities 54% and 68%. In fact, we shall set

$$\eta = 0.87 \times 10^{-6} \text{ or } \hat{\nu} = 1.35 \times 10^{-6} , \tag{30}$$

for this sand with relative densities less than 70%. With these values, (28) becomes

$$N\tau_0^5 = \frac{1.35 \times 10^{-6} e_0}{(e_0 - e_m)^{3.5}}[1 - (1 + p)^{-1.5}] \tag{31}$$

which relates the number of cycles for a given τ_0 to the corresponding pore water pressure. There are no free constants in this equation. Hence it can be tested for its validity against experimental results presented by DeAlba et al. (1975). Figures 5 and 6 represent such a comparison for sand at 54% relative density, where the solid lines correspond to Eq. (31) and the marks with various geometries are the corresponding experimental results. Note that the experimental points associated with the middle curve in Fig. 5 is reported by DeAlba et al. (1975) to correspond to 4.5 psi confining pressure, whereas all other experimental data are for 8 psi confining pressure.

Without changing any parameters in Eq. (31), but only substituting for the corresponding value e_0, for sand with relative density of 68% (i.e. $e_0 = 0.656$), we have compared the results of this equation with the corresponding experimental observations in Figs. 7 and 8. We observe that although we have employed the most elementary forms for the functions g and f, our results are in rather good agreement with experiments over a wide range of stress amplitudes

Table 1

$e_0 - e_m$	σ_c (psi)	N_ℓ	τ_0	$\eta \times 10^6$ (*)
0.132 (D_r = 54%)	8.07	8	0.155	0.859
	8.03	3.25	0.185	0.846
	4.53	12.5	0.144	0.929
	8.02	16	0.135	0.861
	8.14	63	0.104	0.920
0.092 (D_r = 68%)	8.09	15	0.171	0.790
	7.99	4	0.230	0.927
	8.08	53	0.134	0.824
	8.06	6	0.211	0.903

(*) $$\eta = \frac{(e_0 - e_m)^{3.5}}{e_0} N_\ell \tau_0^5 \text{ with } e_m = 0.564,\ e_M = 0.852$$

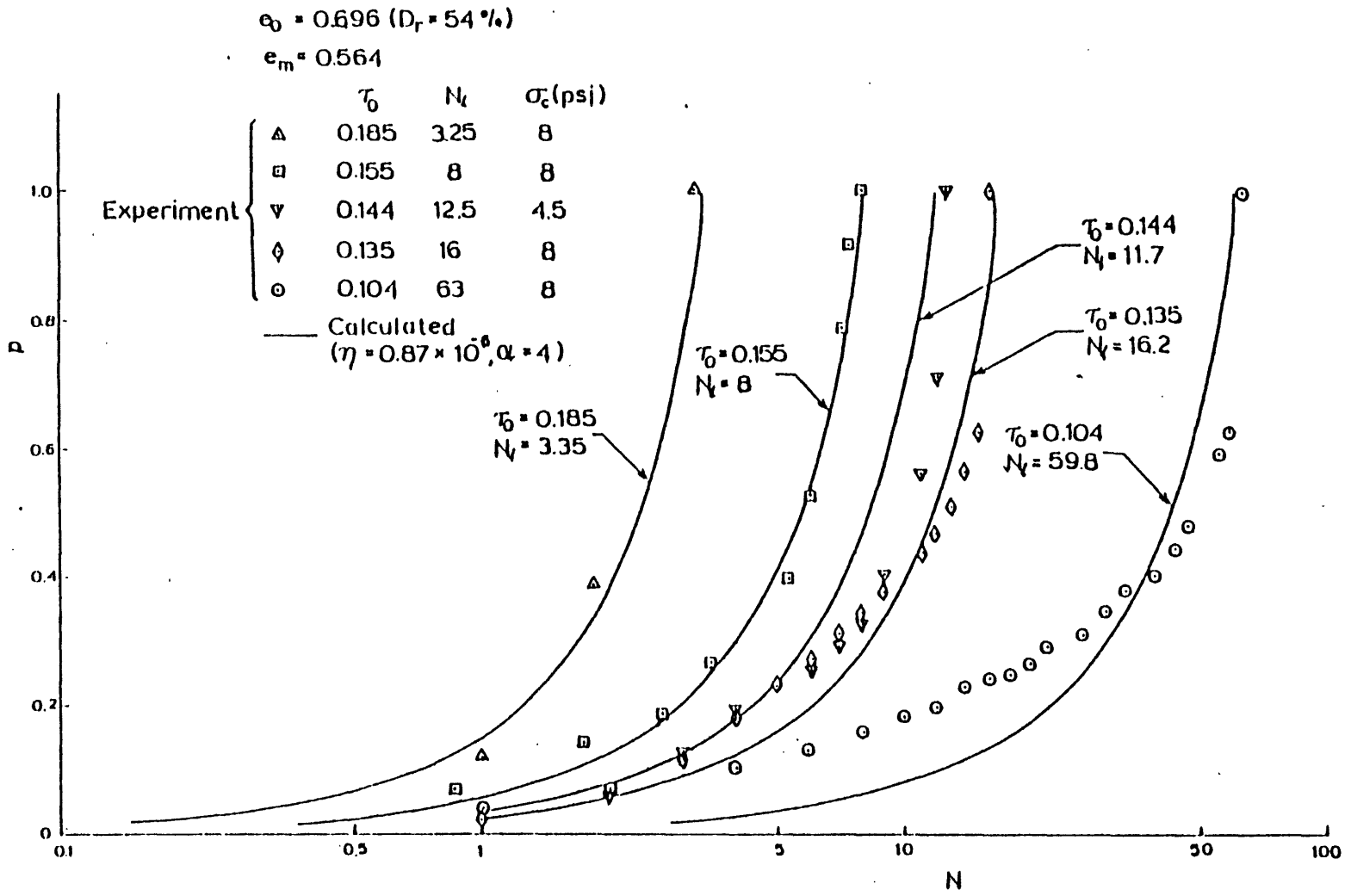

Fig. 5. Normalized excess pore water pressure p versus number of cycles in cyclic shearing of undrained saturated sand (data from DeAlba et al., 1975).

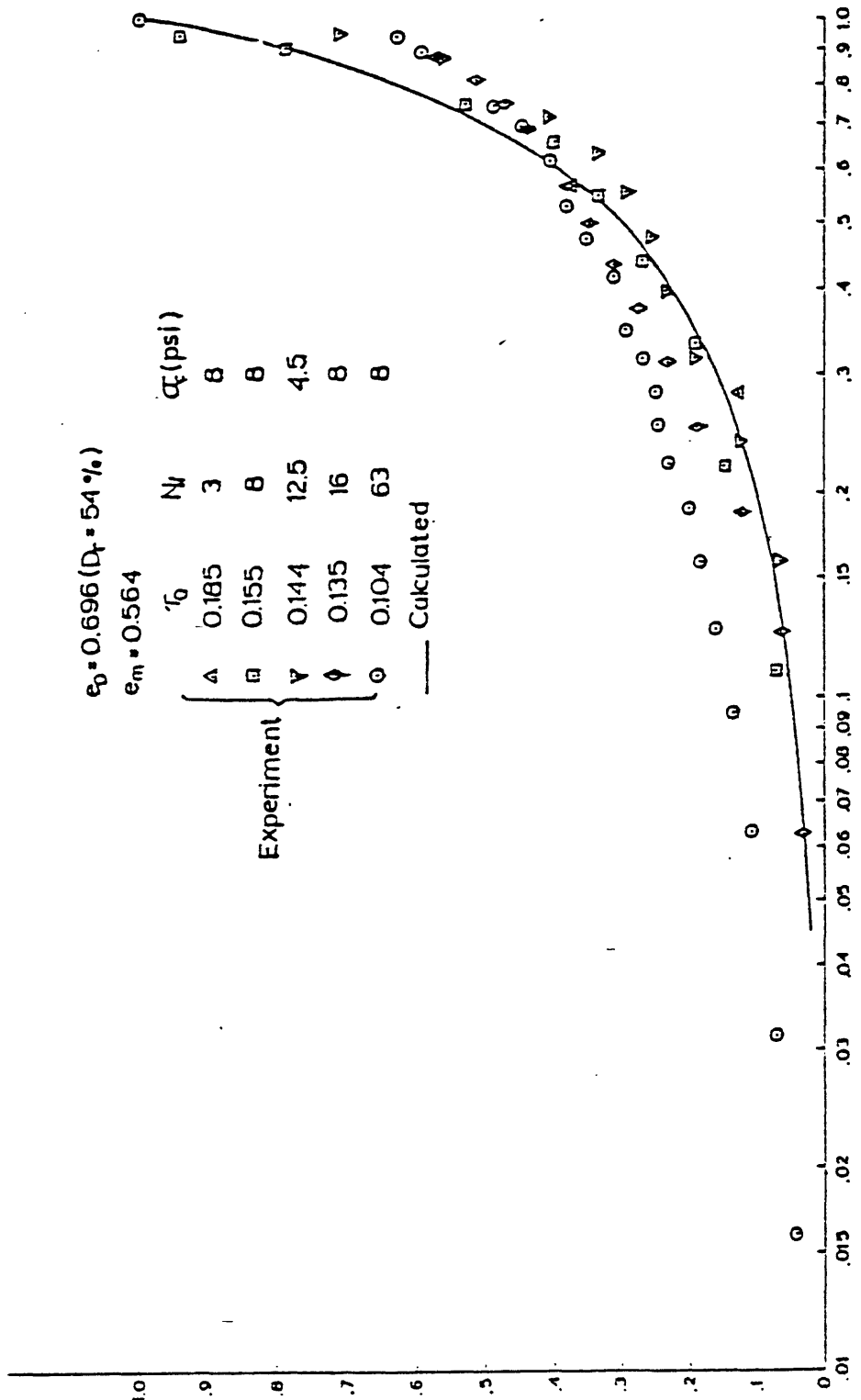

Fig. 6. Normalized excess pore water pressure p versus normalized number of cycles in cyclic shearing of undrained saturated sand (data from DeAlba et al., 1975).

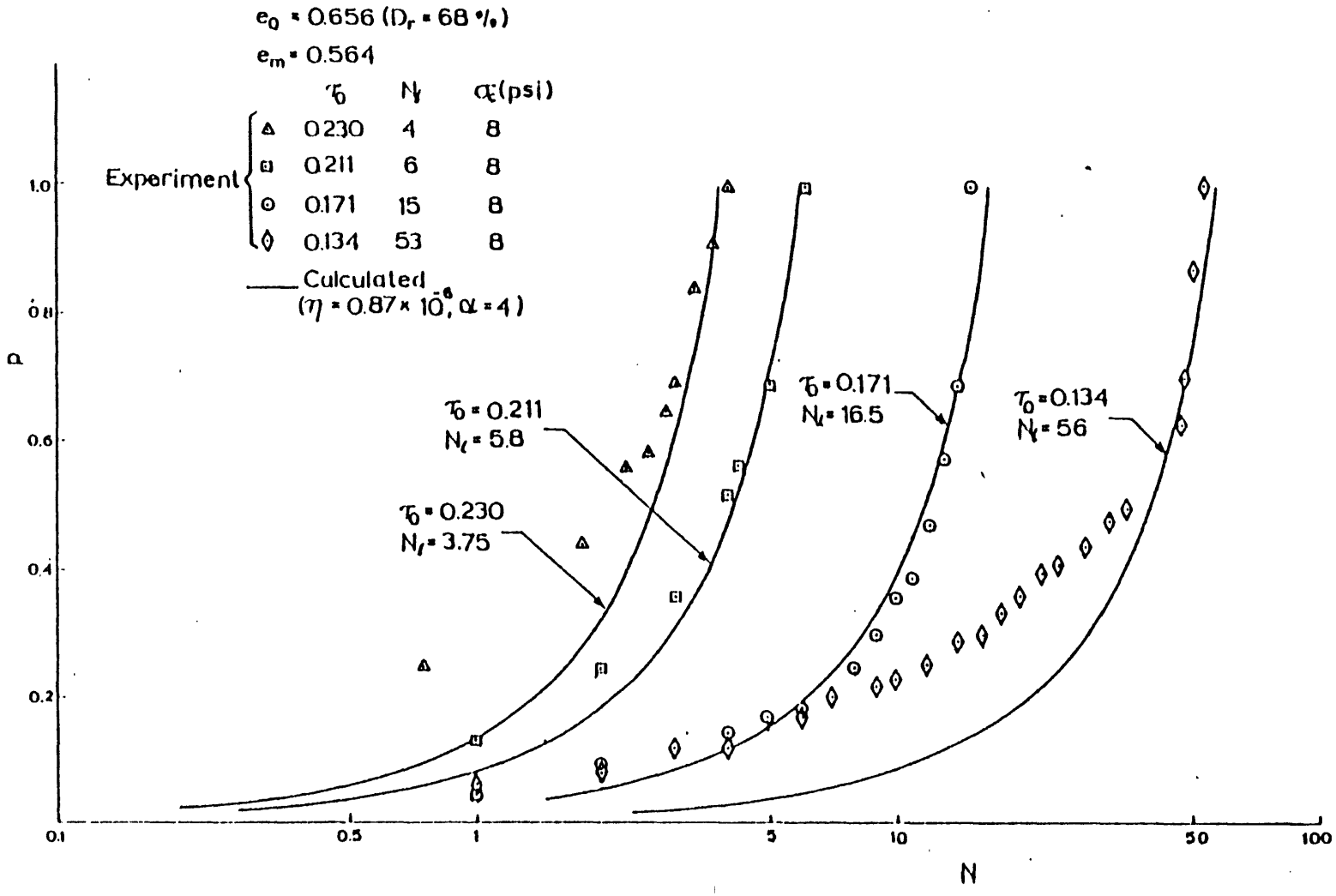

Fig. 7. Normalized excess pore water pressure p versus number of cycles in cyclic shearing of undrained saturated sand (data from DeAlba et al., 1975).

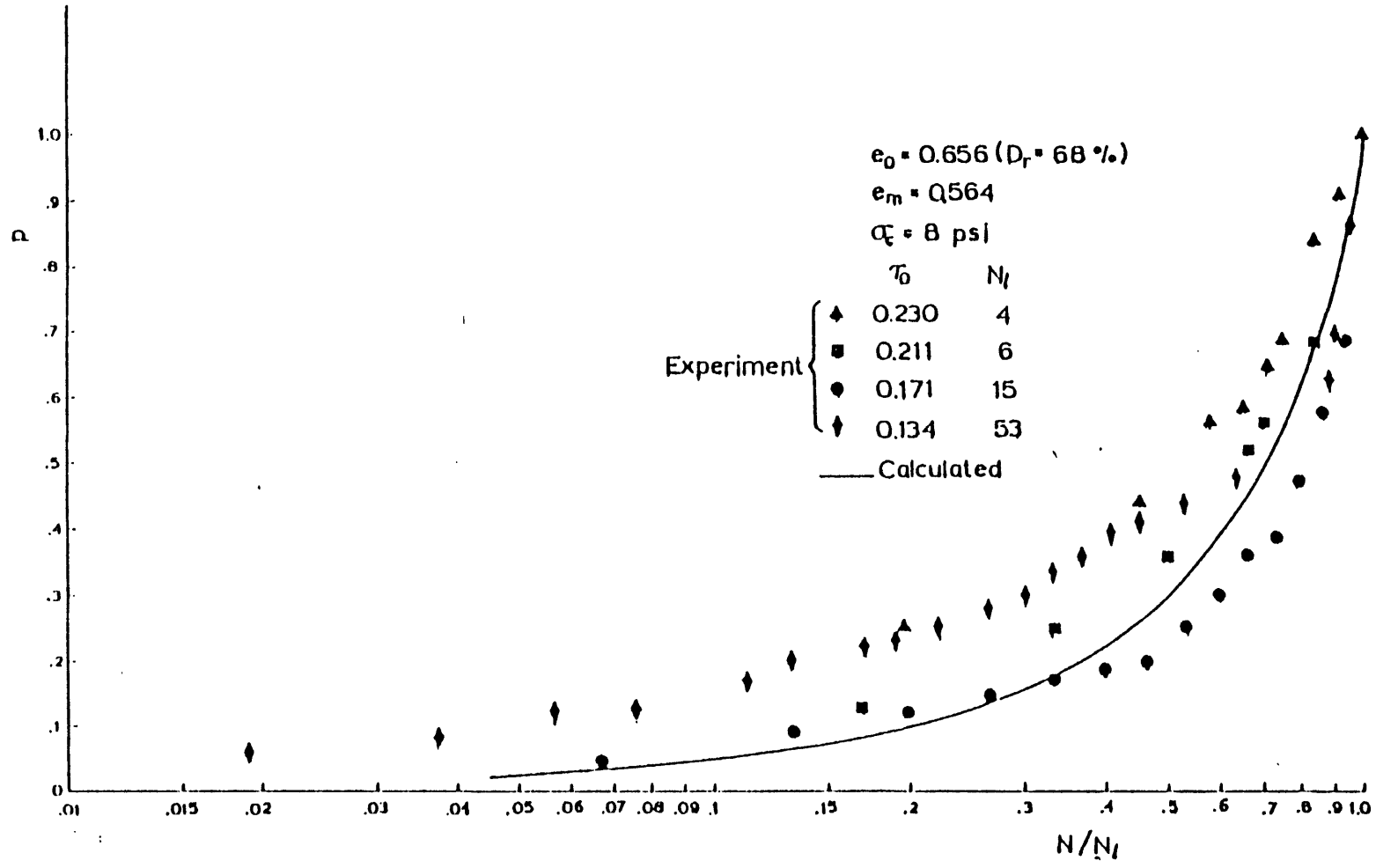

Fig. 8. Normalized excess pore water pressure p versus normalized number of cycles in cyclic shearing of undrained saturated sand (data from DeAlba et al., 1975).

and the number of shearing cycles. It is however possible to improve on fitting the experimental results in Figs. 5-8 by choosing less elementary forms for functions g and f. Lacking substantial experimental data, we have felt that this is unnecessary and premature at this time.

We set p = 1 for liquefaction, and from (31) obtain

$$N_\ell \tau_0^5 (e_0 - e_m)^{3.5}/e_0 = 0.87 \times 10^{-6} \ . \tag{32}$$

The two lower curves in Fig. 9 are plots of Eq. (32). The geometrical marks are the corresponding experimental results. The correlation between experiment and theory is indeed remarkable.

Comparison with Experiments for Relatively Dense Sands

As the relative density increases (the initial void ratio e_0 approaches e_m), Eq. (28) shows that more and more energy will be required to increase the pore water pressure by a fixed amount. This is in accord with experimental observations. If we set p = 1 (liquefaction initiation) and in view of Eq. (3), we can rewrite Eq. (28) as

$$\hat{\tau}_0 = \left\{\frac{n[e_M - d_r(e_M - e_m)]}{N_\ell (e_M - e_m)^n (1 - d_r)^n}\right\}^{\frac{1}{1+\alpha}} \sigma_c, \quad d_r = D_r/100 \ , \tag{33}$$

where $\hat{\tau}_0$ is the actual shear stress amplitude, and σ_c is the confining pressure.

For a fixed number of cycles to liquefaction, Eq. (33) shows that the required shear stress amplitude becomes very large as the relative density, D_r, increases, approaching infinity as D_r approaches 100%. It is often very difficult to test accurately for large relative densities. Therefore little data are available in this range. Figure 10 shows experimental results reported by Peacock and Seed (1968). A crude comparison would be obtained if we set, in Eq. (33), $\alpha = 4$ (as we have done so far), $n = 3.5$ (again, as before),

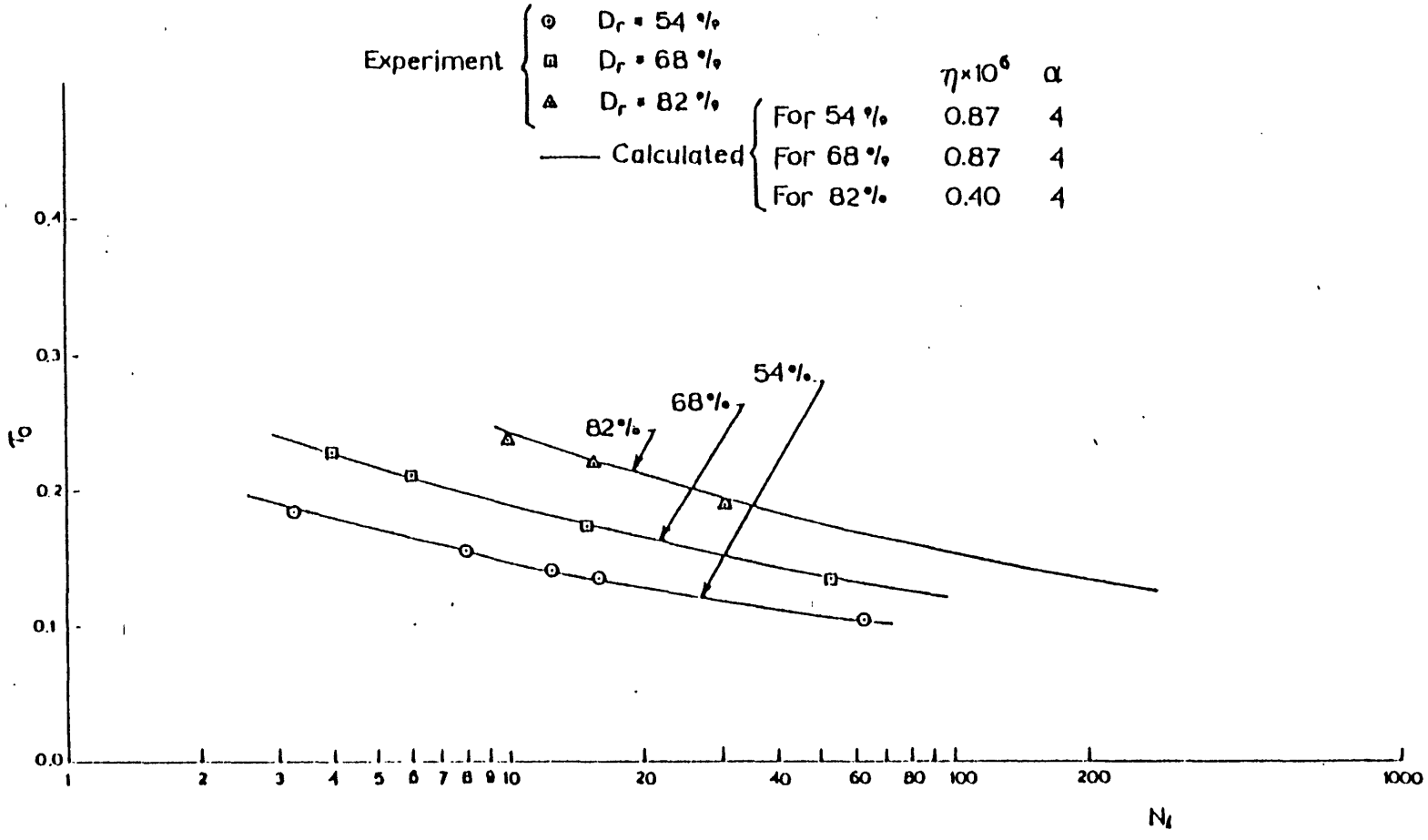

Fig. 9. Normalized shear stress amplitude τ_0 versus number of cycles to liquefaction (data from DeAlba et al., 1975).

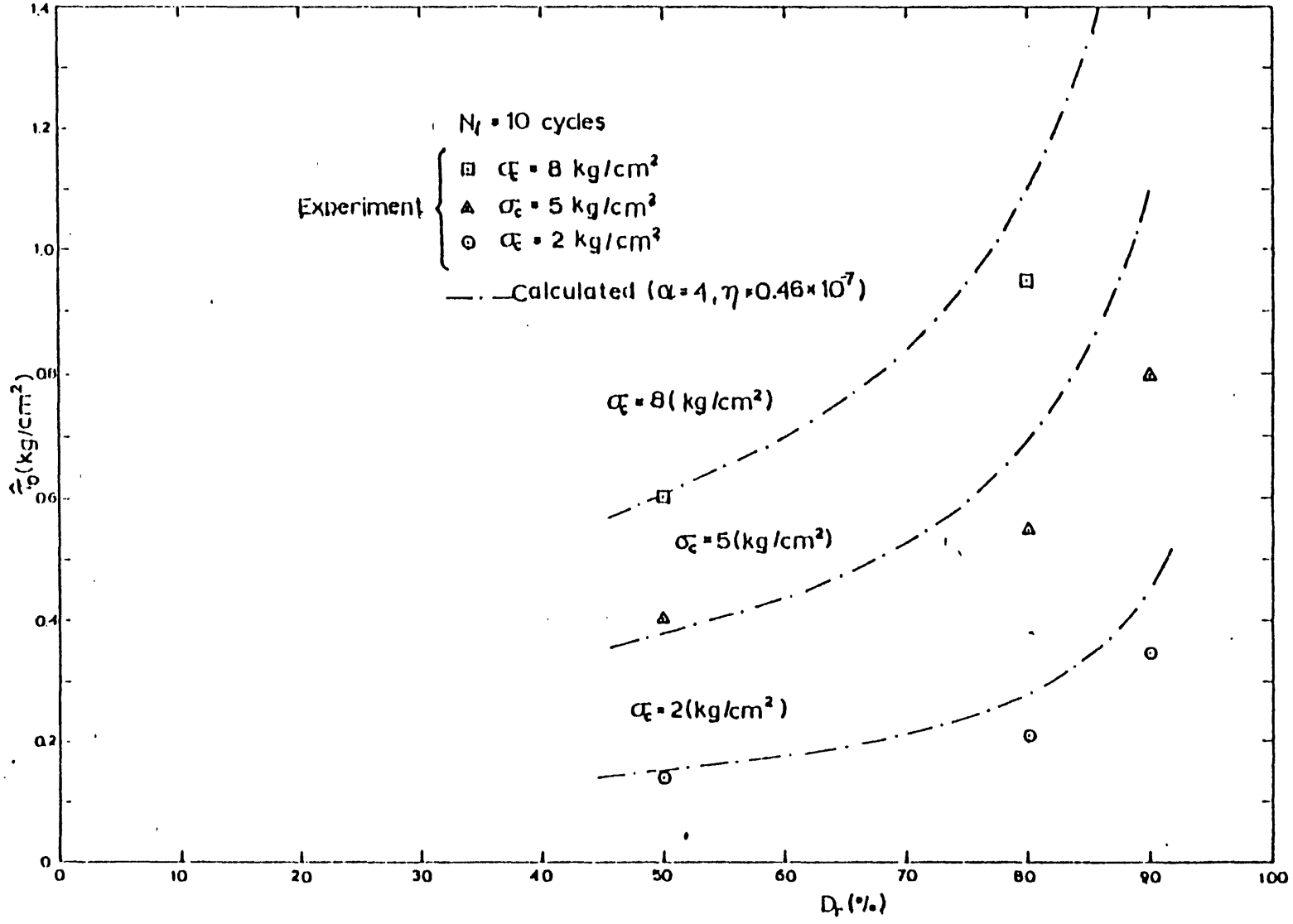

Fig. 10. Variation of shear stress amplitude τ_0 with relative density for indicated confining pressure; number of cycles to liquefaction N_ℓ = 10 (data from Peacock and Seed, 1968).

and choose arbitrarily one experimental point in order to fix the material parameter η; note that since a different material is involved, the corresponding material parameter η will be different from that given by Eq. (30). We have chosen the point with coordinates $\hat{\tau}_0 = 0.6$ kg/cm^2, and $D_r = 50\%$, for $\sigma_c = 8$ kg/cm^2. This substitution into Eq. (33) then yields $\eta \approx 0.46 \times 10^{-7}$. This constant is then used to calculate the dotted curves in Figs. 10 and 11. It is seen that the experimentally reported trend is nicely displayed by the theoretical results. However, the theoretical curve deviates from the experimental points, as the relative density exceeds 80%, and reaches 90%. This indicates that the rather simple approach to estimate ΔW in Eq. (15), with the parameter h kept at a fixed value independently of the value of the initial relative density, may not be good enough for a dense sand, as has been mentioned before. To further stress this point, in Table 2 we have calculated the parameter η in Eq. (29), using the experimental results by DeAlba *et al.* (1975) for $D_r = 82\%$. We see that although η remains essentially constant in this range, it does not have the same value as that for 54 and 68% relative densities; see Table 1. As was discussed in connection with Eq. (15), the value of h in the expression for the work may tend to become larger for D_r exceeding 80%. Since η is inversely proportional to h, its value decreases with increasing D_r, as is seen from Tables 1 and 2. Figures 12 and 13 compare our theoretical results with the corresponding experiments for $D_r = 82\%$. The upper curve in Fig. 9 gives the theoretical curve relating shear stress amplitude to the number of cycles to liquefaction, for $D_r = 82\%$.

Comparison with Other Experiments

In an effort to test the range of the validity of Eq. (28), we have tried to compare its predictions with other experimental results. However,

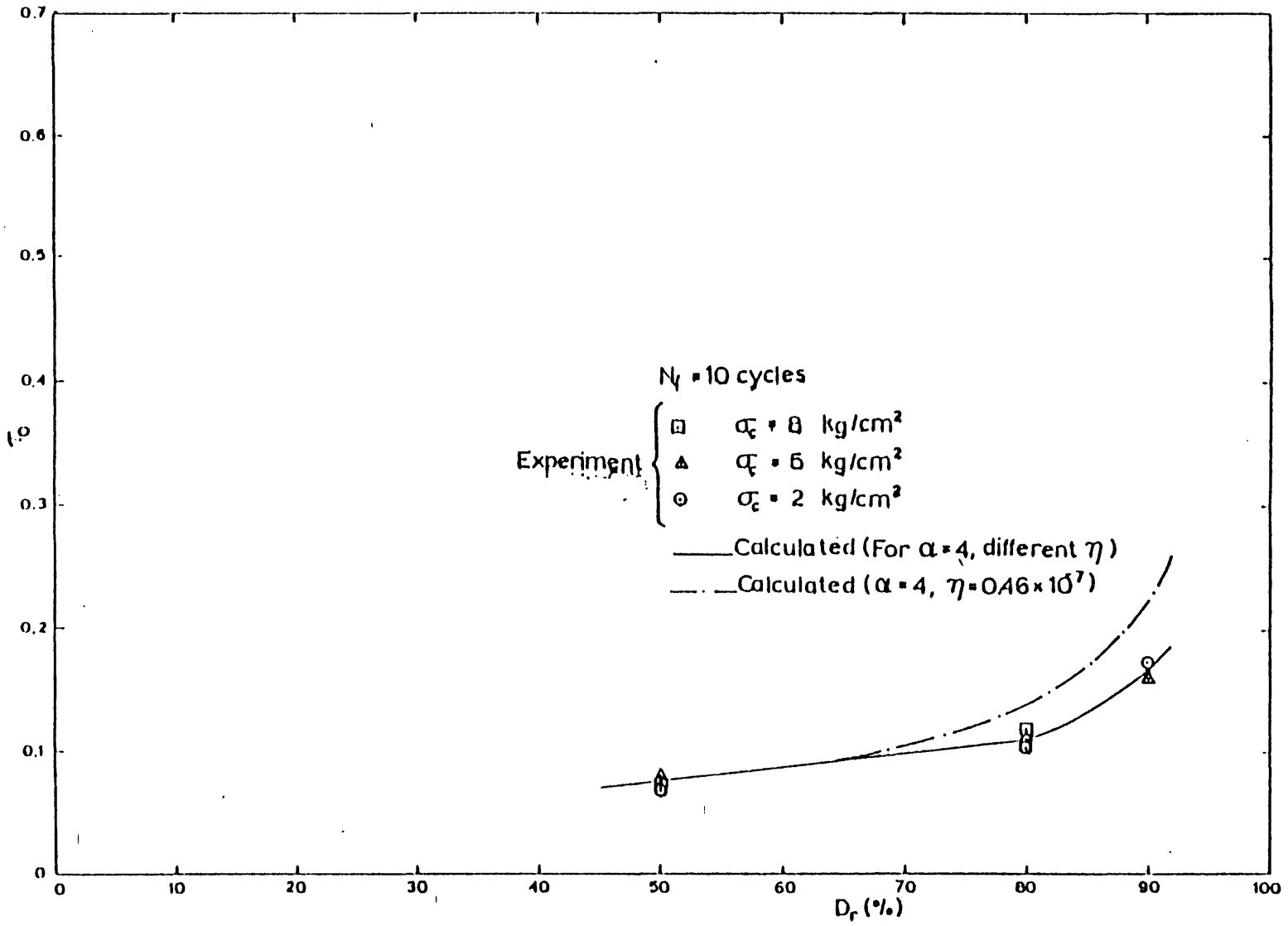

Fig. 11. Variation of normalized shear stress amplitude τ_0 with relative density; number of cycles to liquefaction N_ℓ = 10 (data from Peacock and Seed, 1968).

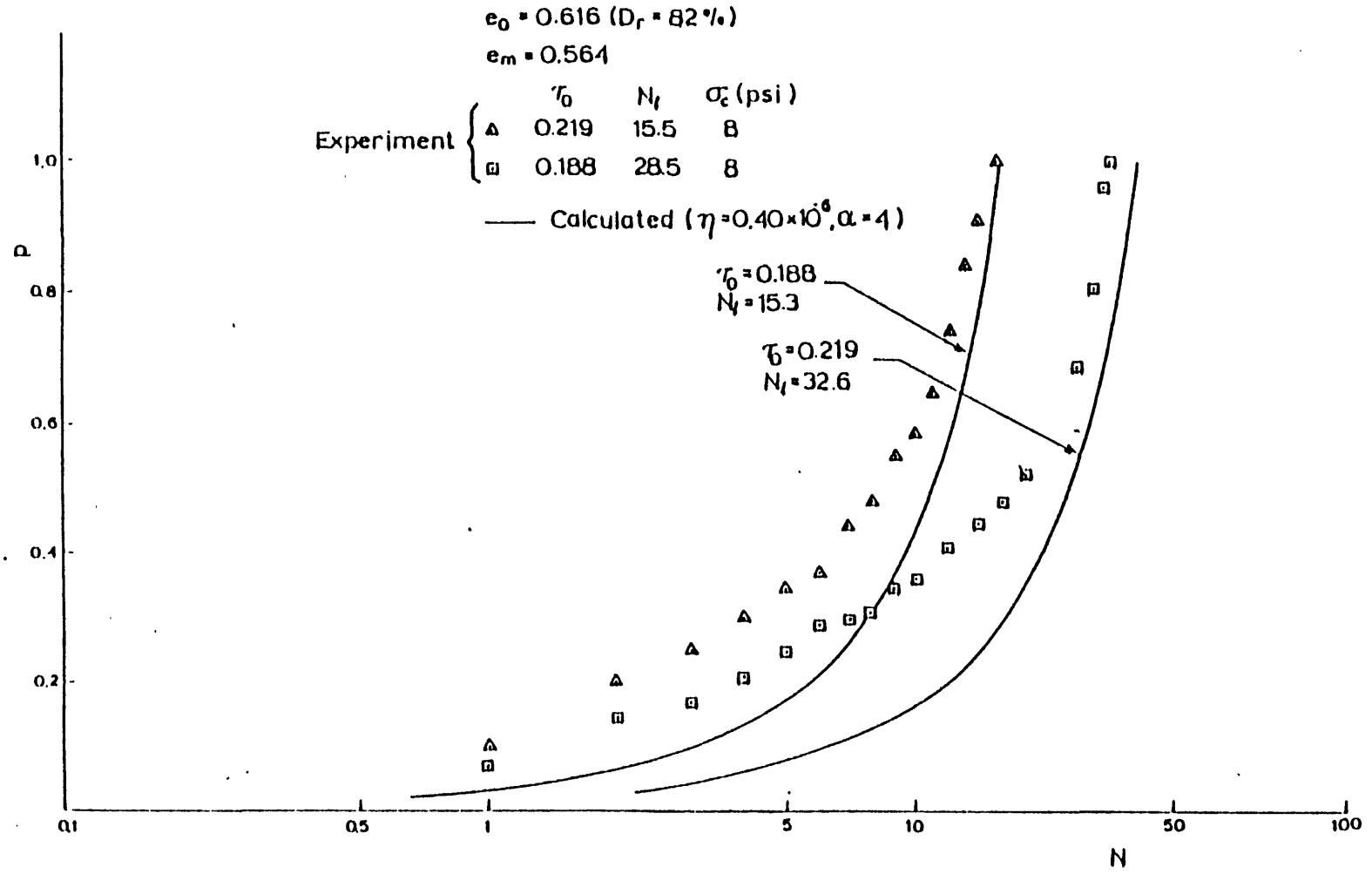

Fig. 12. Normalized excess pore water pressure p versus number of cycles in cyclic shearing of undrained saturated sand (data from DeAlba et al., 1975).

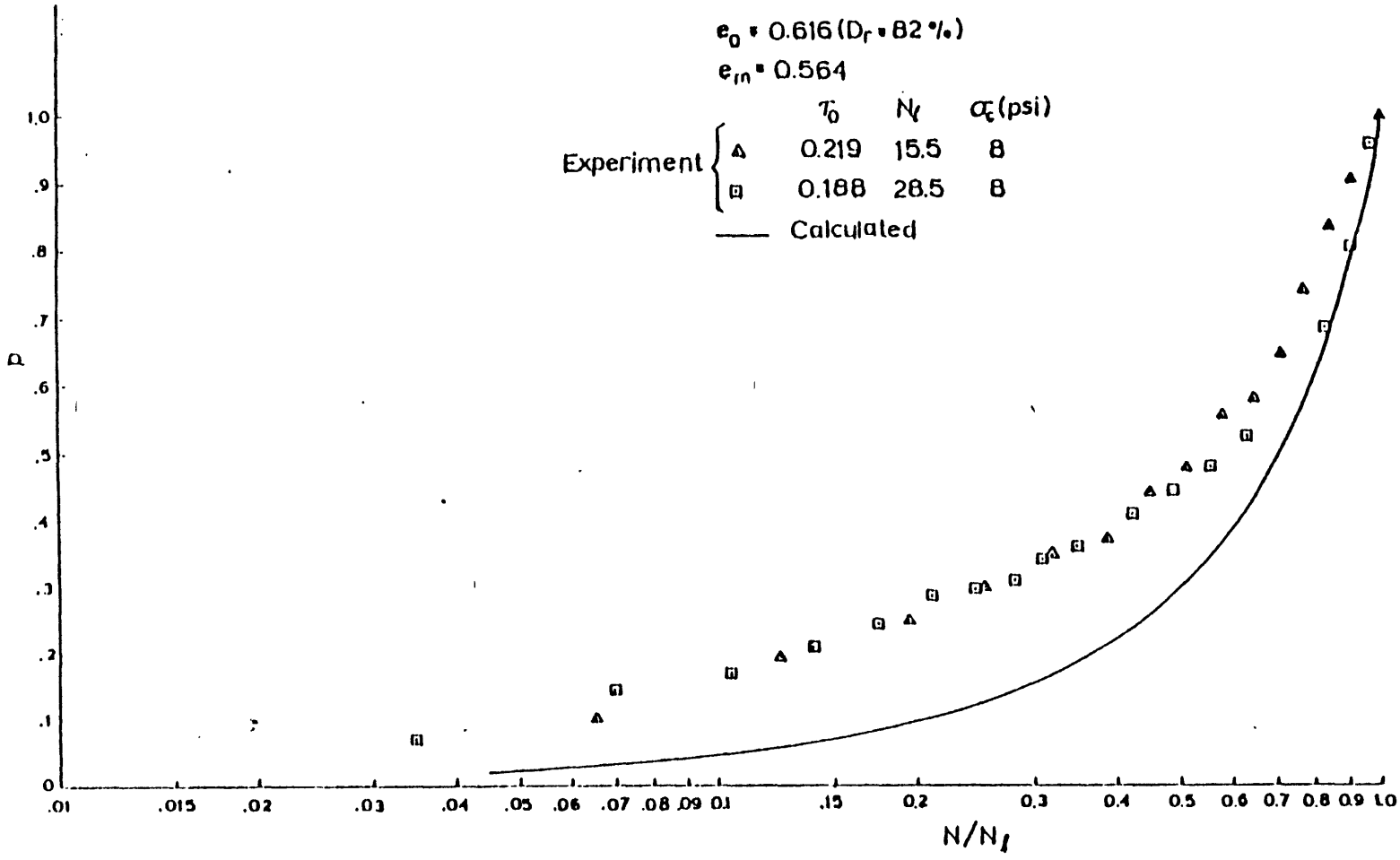

Fig. 13. Normalized excess pore water pressure p versus normalized number of cycles in cyclic shearing of undrained saturated sand (data from DeAlba et al., 1975).

Table 2

$e_0 - e_m$	σ_c (psi)	N_ℓ	τ_0	$\eta \times 10^{6(*)}$
0.052	8.0	10	0.239	0.406
(D_r = 82%)	8.03	28.5	0.188	0.348
	8.08	15.5	0.211	0.406

(*) $$\eta = \frac{(e_0 - e_m)^{3.5}}{e_0} N_\ell \tau_0^5 \text{ with } e_m = 0.564,\ e_M = 0.852$$

many of these results are in the form of small graphs, and some authors do not report all the necessary parameters. Hence it is difficult to make as detailed comparisons with other experimental results, as is done with the data from DeAlba et al. (1975). However, if we accept Eq. (29) as a rough estimate, for a given e_0 and e_m we may write

$$N_\ell \tau_0^5 = \text{constant} \ . \tag{34}$$

In this equation, τ_0 may be interpreted as a dimensionless distortional stress amplitude proportional to $\hat{\tau}_0/\sigma_c$, because if instead of the latter, one uses $m\hat{\tau}_0/\sigma_c$ with a constant m, only the constant in the right-hand side will be changed.

Now we may fix the right-hand side of Eq. (34), by using one experimental point, and then compare the results with other experimental data on the same sand, with the same D_r. Figures 14 and 15 are obtained in this manner, where the corresponding experimental points are taken from Yoshimi and Oh-Oka (1975), and Peacock and Seed (1968), respectively.

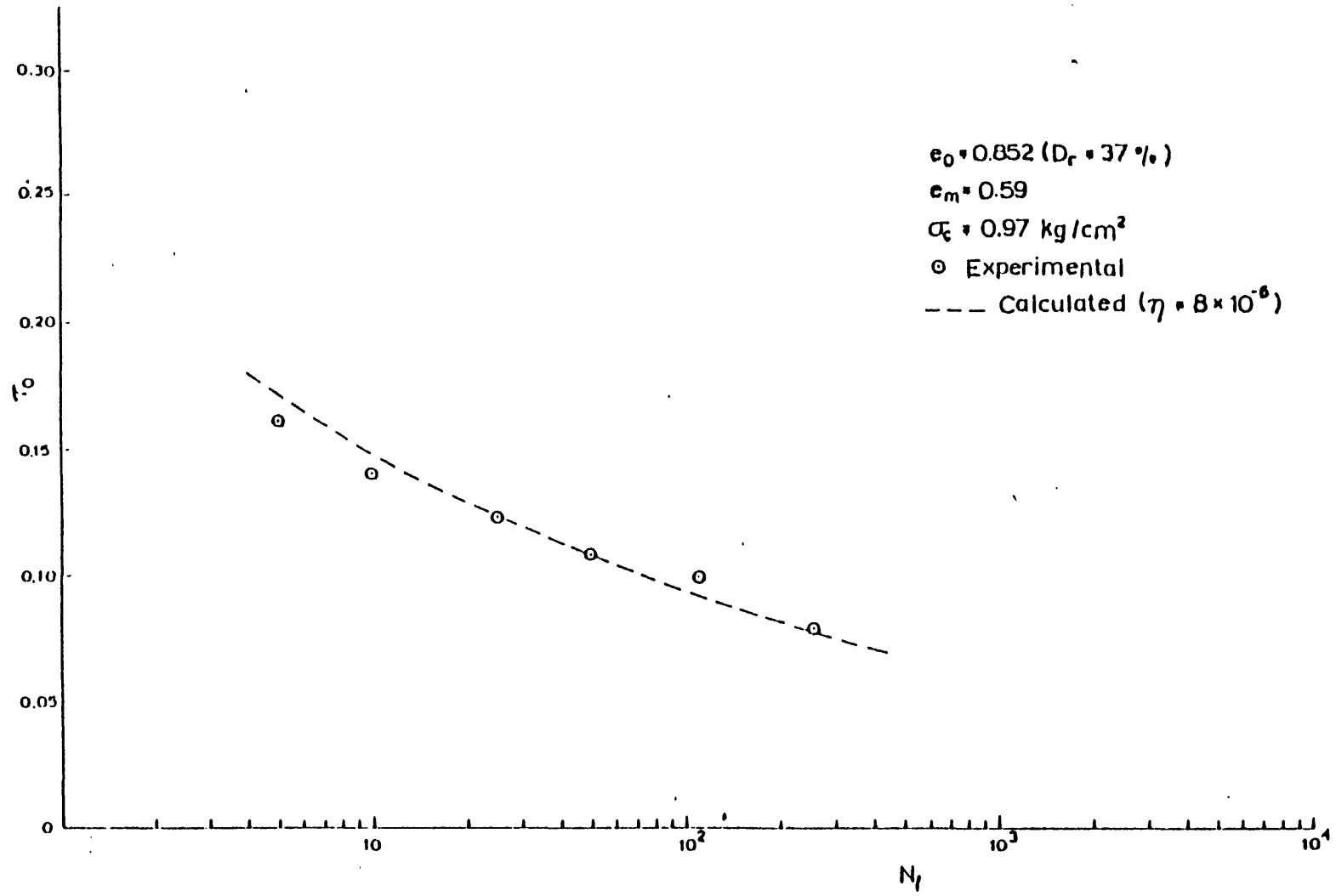

Fig. 14. Normalized shear stress amplitude τ_0 versus number of cycles to liquefaction (data from Yoshimi and Oh-Oka, 1975).

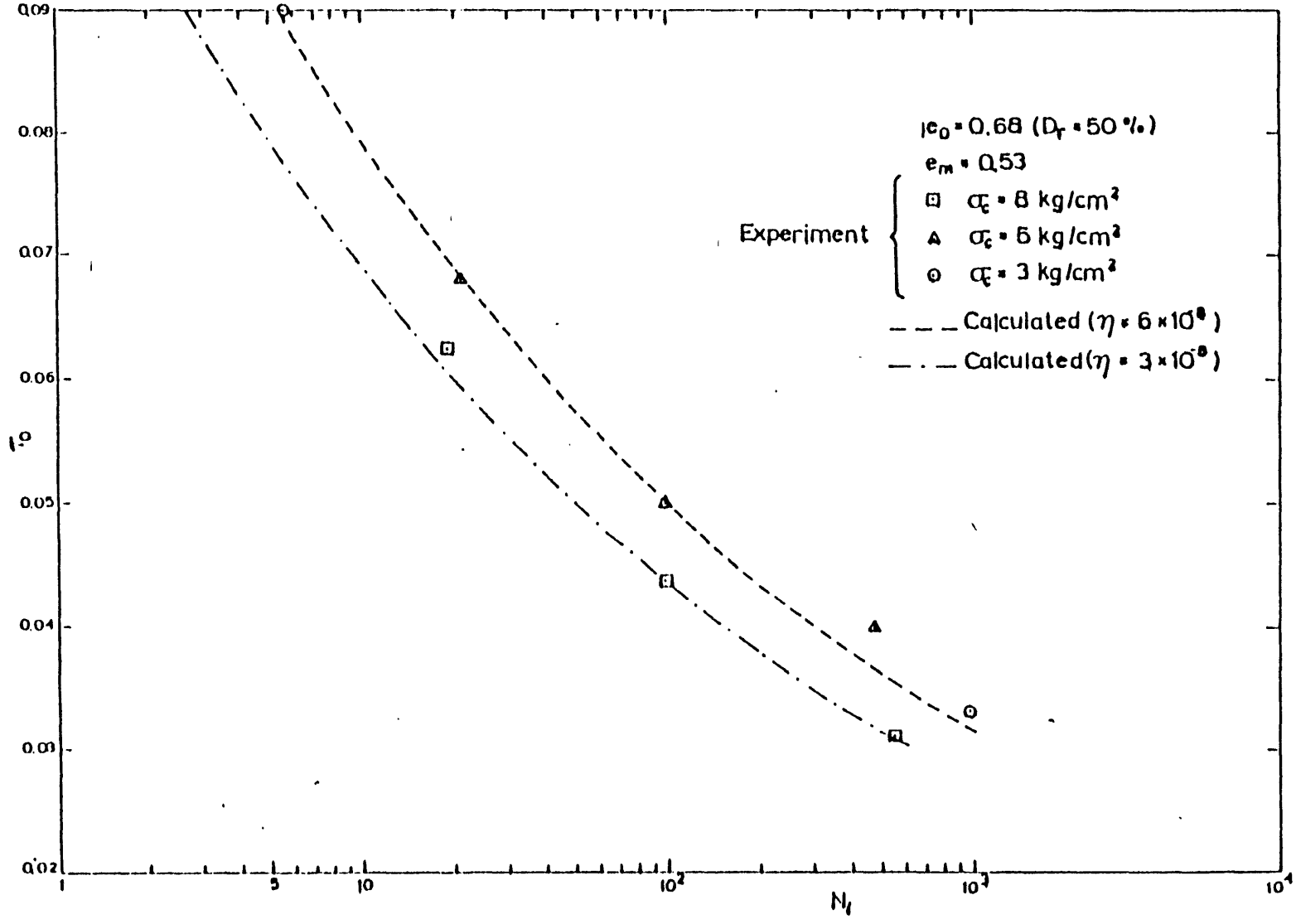

Fig. 15. Normalized shear stress amplitude τ_0 versus number of cycles to liquefaction (data from Peacock and Seed, 1968).

Effect of Confining Pressure

As has been discussed before, we expect parameters h and $\hat{\nu}$ in Eq. (28) to depend on the confining pressure σ_c, which then suggests that η in Eq. (29) should depend on σ_c. Basically, an increase in σ_c tends to increase h, and therefore may decrease η. This is reasonable since, for a fixed value of τ_0, and after a given number of cycles, more work will be supplied under a large confining pressure, and therefore, h in Eq. (15) should be expected to increase with σ_c, if α is kept fixed. In Fig. 16 the results of Eq. (33) are compared with experimental observation by DeAlba et al. (1975) and Peacock and Seed (1968), where the dashed lines are the calculated values. In each case, one experimental point is used to estimate the value of η, and as is seen, the other experimental points fall nicely on the corresponding line, which confirms that, for a constant D_r and σ_c, η is indeed a material constant.

It should be possible to express η as an explicit function of σ_c and D_r, by a microstructural consideration. However, this is a rather difficult task and requires careful study.

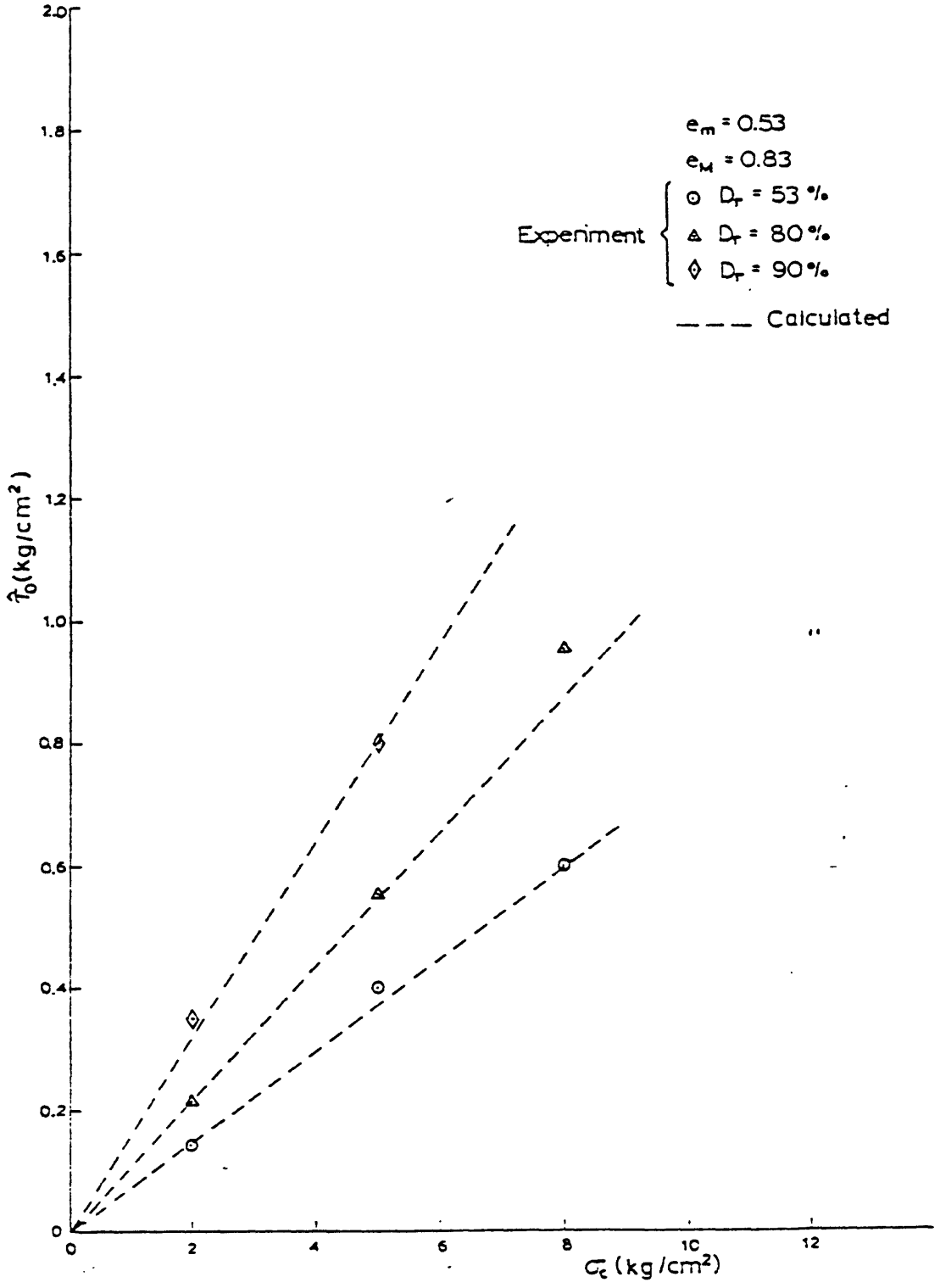

Fig. 16. Variation of shear stress amplitude $\hat{\tau}_0$ with confining pressure; number of cycles to liquefaction $N_\ell = 10$ (data from Peacock and Seed, 1968).

REFERENCES

DeAlba, P. S., Chan, C. K., and Seed, H. B. (1975). Determination of soil liquefaction characteristics by large-scale laboratory tests. NUREG-0027, NRC-6, Shannon and Wilson, Inc., and Agbabian Assoc., Seattle, Washington, Sept. 1976, prepared for the U. S. Nuclear Regulatory Commission under Contract Number AT (04-3)-954; manuscript completed May, 1975; see also ERRC Report 75-14, Univ. Calif. Berkeley, CA.

Faccioli, E., and Resendiz, D. (1976). Soil dynamics: Behavior including liquefaction. Seismic Risk and Engineering Decisions by C. Lomnitz and E. Rosenblueth (eds.), Elsevier Scientific Publ. Co.

Hardin, B. O., and Drnevich, V. P. (1972). Shear modulus and damping in soils: Design equations and curves. Jnl. Soil Mech. Fnd. Div. Am. Soc. Civ. Engrs. 98, SM7, 667-692.

Martin, G. R., Finn, W. D. L., and Seed, H. B. (1975). Fundamentals of liquefaction under cyclic loading. Jnl. Geotech. Eng. Div. Am. Soc. Civ. Engrs. 101, GT5, 423-438.

Peacock, W. H., and Seed, H. B. (1968). Sand liquefaction under cyclic loading simple shear conditions. Jnl. Soil Mech. Fnd. Div. Am. Soc. Civ. Engrs. 94, SM3, 689-708.

Seed, H. B., and Idriss, I. M. (1967). Analysis of soil liquefaction: Niigata earthquake. Jnl. Soil Mech. Fdn. Div. Am. Soc. Civ. Engrs. 93, SM3, 83-108.

Seed, H. B., and Idriss, I. M. (1969). Influence of soil conditions on ground motions during earthquakes. Jnl. Soil Mech. Fdn. Div. Am. Soc. Civ. Engrs. 95, SM1, 99-137.

Seed, H. B., and Lee, K. L. (1966). Liquefaction of saturated sands during cyclic loading. Jnl. Soil Mech. Fdn. Div. Am. Soc. Civ. Engrs. 92, SM6, 105-134.

Seed, H. B., and Peacock, W. H. (1971). Test procedures for measuring soil liquefaction characteristics. Jnl. Soil Mech. Fdn. Div. Am. Soc. Civ. Engrs. 97, SM8, 1099-1119.

Silver, M. L., and Seed, H. B. (1971a). Deformation characteristics of sands under cyclic loading. Jnl. Soil Mech. Fdn. Div. Am. Soc. Civ. Engrs. 97, SM8, 1081-1098.

Silver, M. L., and Seed, H. B. (1971b). Volume changes in sands during cyclic loadings. Jnl. Soil Mech. Fdn. Div. Am. Soc. Civ. Engrs. 97, SM9, 1171-1182.

Yoshimi, Y., and Oh-Oka, H. (1975). Influence of degree of shear stress reversal on the liquefaction potential of saturated sand. Soils and Foundations 15, 3, 27-40.

Yoshimi, Y., Richart, F. E., Prakash, S., Barkan, D. D., and Ilyichev, V. A. (1977). Soil dynamics and its application to foundation engineering. State-of-the-Art Report, ICSMFE IX, Tokyo.

Youd, T. L. (1970). Densification and shear of sand during vibration. Jnl. Soil Mech. Fdn. Div. Am. Soc. Civ. Engrs. 96, SM3, 863-880.

Youd, T. L. (1972). Compaction of sands by repeated shear straining. Jnl. Soil Mech. Fdn. Div. Am. Soc. Civ. Engrs. 98, SM7, 709-725.

Youd, T. L. (1977). Private communication.

CHAPTER 3

A FRAMEWORK FOR PREDICTION OF DENSIFICATION AND LIQUEFACTION OF SAND IN CYCLIC SHEARING

1. INTRODUCTION

In Chapter 2 we have developed an energy approach for the theoretical quantification of densification of loose dry sand and liquefaction of saturated undrained sand (both cohesionless). Employing rather crude estimates for the functions and parameters which enter the theory, it has been shown that the theory includes the essential features of the involved physical phenomena, and therefore can predict rather accurately many existing experimental results. For the verification of the theory we have used data from experimental works by Seed and Lee (1966), Peacock and Seed (1968), Seed and Peacock (1971), Youd (1970 and 1972), Silver and Seed (1971a,b), DeAlba et al. (1975), and Yoshimi and Oh-Oka (1975).

It is the purpose of the present chapter to provide a fundamental thermodynamic framework for the unified theory of densification and liquefaction of cohesionless sands given in Chapter 2, and in this manner to develop the corresponding stress-strain relations for cyclic loadings. In light of such an approach we are able to give a more systematic characterization of the theory, and predict experimental observations in finer detail than before. Moreover, the theory provides guidance for future experimental work in this important area and defines significant parameters which require measurement and monitoring. In Section 2 we introduce the concept of internal variables and define the corresponding evolutionary equations. There we use the relative void ratio, $\rho = e - e_m$ (which is the current value of the void ratio minus its minimum value), for the densification problem, and the normalized

excess pore water pressure, p, for the liquefaction problem, as our corresponding internal variables; i.e. we use only one internal variable in each case. We note that in Chapter 2 an energy concept has been used to obtain explicit relations for the void ratio and the excess pore water pressure in terms of the stress or strain amplitude, the number of cycles in a cyclic shearing, and other relevant parameters. In the present chapter we shall integrate these results into a theromodynamic setting and give a more detailed account of the physical process. These are done in Section 3 for the densification and in Section 4 for the liquefaction phenomena.

2. INTERNAL VARIABLES AND EVOLUTIONARY EQUATIONS

We shall need to treat the strain-controlled and the stress-controlled cases separately. We shall give detailed results for densification, assuming strain-controlled tests, and for liquefaction assuming stress-controlled tests, and then briefly discuss opposite cases.

Densification

Let us assume that a sample of dry loose sand of unit mass is subjected to a cyclic shear straining given by

$$\gamma(t) = \gamma_0 \phi(t), \quad -1 \leq \phi(t) \leq +1. \tag{1}$$

Let τ denote the corresponding shear stress, θ be the temperature, and write for the Helmholtz free energy,*

$$\psi = \hat{\psi}(\gamma, \theta, \rho), \quad \rho \equiv e - e_m, \tag{2}$$

where the relative void ratio, ρ, is viewed as a measure of internal structural rearrangements which take place as a result of cyclic shearing of the

* Note that $\hat{\psi}$ depends parametrically on σ_c, ρ_0, etc.

sample. In this formulation the thermodynamic state is defined by the state variables $\{\gamma,\theta\ ,\rho\}$. The first two variables are assumed controllable externally, whereas the last variable, ρ, measures dissipative internal processes that take place during the loading history and are responsible for the inelastic macroscopic behavior of the sample.

The shear stress is now given by*

$$\tau = \frac{\partial\hat{\psi}}{\partial\gamma} = \hat{\tau}(\gamma,\ \theta,\ \rho). \tag{3}$$

In the sequel we consider an isothermal case, θ = const., and do not display the temperature explicitly. Hence, instead of (2) and (3), we write

$$\psi = \hat{\psi}(\gamma,\ \rho),\ \tau = \frac{\partial\hat{\psi}}{\partial\gamma} = \hat{\tau}(\gamma,\ \rho). \tag{4}$$

Here the stress is expressed as a function of the present value of strain γ, and the present value of the relative void ratio ρ. The effect of the history and inelasticity is included only through the internal variable ρ. If ρ is

---

* In the context of irreversible thermodynamics, see for example, Nemat-Nasser (1975 and 1977), one also defines

$$\eta = -\frac{\partial\hat{\psi}}{\partial\theta}\ ,\ \text{and}\ \Lambda = -\frac{\partial\hat{\psi}}{\partial\rho}\ ,$$

where η is the entropy, and Λ is the thermodynamic force conjugate to the internal variable ρ. The second law requires that

$$\Lambda\dot{\rho} = -\frac{\partial\hat{\psi}}{\partial\rho}\ \dot{\rho} = -\dot{\hat{\psi}}\big|_{\theta,\ =\text{const.}} \geq 0.$$

Moreover, we must have

$$\dot{\eta}\big|_{\gamma,\theta=\text{const.}} = \frac{\partial}{\partial\theta}(\Lambda\dot{\rho}) \geq 0\ .$$

In these equations and in what follows a superposed dot denotes time differentiation. We shall not need to use the above relations in this study.

fixed, then we have the case of elasticity (no dissipation); however, the functional form for $\hat{\psi}$ and $\hat{\tau}$ will parametrically depend on the (fixed) value of ρ.

To complete the formulation, one must establish an evolutionary equation for the internal variable ρ. Therefore in a rather general setting we write,

$$\dot{\rho} = \hat{F}(\gamma, \rho). \tag{5}$$

When the function $\hat{F}$ is known, then for a given strain history, $\gamma = \hat{\gamma}(t)$, one can integrate (5) and obtain ρ as a functional of the strain history. Substitution for ρ in (4) then gives the present value of stress in terms of the present value of strain and the strain history.

The most difficult task in application to real cases is to identify the function $\hat{F}$. The only thermodynamic restriction here is the dissipation inequality,

$$-\frac{\partial \hat{\psi}}{\partial \rho}\hat{F} = -\dot{\hat{\psi}}\Big|_{\gamma=\text{const.}} \geq 0 \tag{6}$$

which states that a change in the internal structure of the material must be accompanied by some energy loss into dissipation.

For cyclic loading in the frequency range of 10 to 100 or even more cycles per minute, experiments show that the densification of dry or saturated but drained sand is essentially independent of the frequency. Therefore, Eq. (5) must be rate-independent. To implement this fact, we observe that any change in ρ involves some restructuring of the sand grains, and any such (micro) restructuring involves a certain amount of energy dissipation. Thus, for $d\rho \neq 0$, we must have some energy dissipation $dW > 0$. We can therefore rewrite Eq. (5),

$$\dot{\rho} = \frac{d\rho}{dW}\frac{dW}{dt} = \hat{F}(\gamma, \rho). \tag{7}$$

Now for a rate-independent process the rate of energy loss must be only a function of state, so that*

$$\frac{dW}{dt} = \hat{W}(\gamma, \rho) \ . \tag{8}$$

Combining Eqs. (7) and (8) we obtain

$$d\rho = \overline{F}(\gamma, \rho)dW, \tag{9}$$

where we have set $\overline{F} = \hat{F}/\hat{W}$.

Comparing Eq. (9) with Eq. (4) of Chapter 2, we observe that the latter is a special case of (9), in the sense that it is assumed that $\overline{F}(\gamma, \rho) \equiv -\frac{1}{\nu}g(\rho)$.

Equation (9) can be used to establish the time-history of ρ, provided that the time-history of γ is known. However, this would require extensive experimental results which do not exist at this time. Hence instead, we shall attempt to establish the change in ρ at the end of, say, N cycles in the cyclic straining of the kind defined by (1). Furthermore, we assume that N is very large, and for calculation, regard it as a continuous variable. Thus, setting $\gamma = \gamma_0$ in (9), rearranging terms, and integrating over N cycles, we obtain

$$\Delta W = \int_{\rho_0}^{\rho} \frac{d\rho'}{\overline{F}(\gamma_0,\rho')} \ , \tag{10}$$

where ΔW is the total amount of energy used in rearranging the particles over N cycles, and the upper limit, ρ, of the integral in the right-hand side, is the value of the relative density at the end of the N^{th} cycle. The energy loss, ΔW, in general, depends on the strain amplitude, γ_0, on the number of cycles, N, as well as parametrically on the initial value of ρ, confining

---

* It should be noted that $\hat{W}$, as well as $\hat{F}$ and $\hat{\psi}$, in general, will depend on the confining pressure σ_c, the initial relative void ratio $\rho_0 = e_0 - e_m$, on the grain size and shape distribution, and other relevant physical parameters.

pressure, σ_c, and other relevant physical parameters. In addition, it is a functional of the form of the periodic straining used, i.e. it depends on the form of the prescribed function $\phi(t)$ in Eq. (1). Before proceeding to obtain an explicit, albeit approximate, expression for the energy loss, it is more convenient to first examine the liquefaction phenomenon, and obtain an expression for the energy loss for the stress-controlled tests.

Liquefaction

Consider now a sample of undrained saturated (macroscopically homogeneous) loose sand subjected to cyclic shearing,

$$\tau(t) = \tau_0 \tilde{\phi}(t), \quad |\tilde{\phi}(t)| \leq 1. \tag{11}$$

The procedure for formulating a thermodynamic setting for liquefaction follows the same line of reasoning as that for densification, except for the following modifications: i) the pore pressure, p, replaces the relative void ratio, ρ, as the internal (uncontrollable) state variable; and ii) since we consider stress-controlled loading, Gibbs' function, $\tilde{\chi}$, replaces the Helmholtz free energy function, $\hat{\psi}$. Accordingly, the state variables are $\{\tau,\theta,p\}$ and since $\chi = \tau\gamma - \psi = \tilde{\chi}(\tau,\theta,p)$, it follows that*

$$\gamma = \frac{\partial \tilde{\chi}}{\partial \tau} = \tilde{\gamma}(\tau,\theta,p). \tag{12}$$

In the sequel, the dependence on θ will not be displayed.

The evolutionary equation for p is given by**

---

* Here the entropy, η, and the thermodynamic variable, λ, conjugate to p, are respectively defined as

$$\eta = \frac{\partial \tilde{\chi}}{\partial \theta} = \tilde{\eta}(\tau,\theta,p), \quad \lambda = \frac{\partial \tilde{\chi}}{\partial p} = \tilde{\lambda}(\tau,\theta,p).$$

However, in what follows these will not be used.

** It should be noted that the function $\tilde{G}$ in general depends parametrically on σ_c, ρ_0, θ = const. (isothermal processes) and other relevant physical parameters.

$$\dot{p} = \tilde{G}(\tau, p). \tag{13}$$

Now, as in the case of densification, we note that the phenomenon of liquefaction in a frequency range of 10 to 100 cycles per minute, is independent of the frequency. Therefore, we may write

$$\dot{p} = \frac{dp}{dW}\frac{dW}{dt} = \tilde{G}(\tau, p) \ , \tag{14}$$

and assume that $\frac{dW}{dt} = \tilde{W}(\tau, p)$ is rate-independent. Thus,

$$dp = \bar{G}(\tau,p)dW, \tag{15}$$

where $\bar{G} \equiv \tilde{G}/\tilde{W}$ is a rate-independent function. Observe that Eq. (5) of Chapter 2 is a special case of (15): it is obtained by setting $\bar{G}(\tau,p) = \frac{1}{\nu e} g(\rho)f(1+p)$ in (15).

Here again, we shall confine attention to a cyclic shearing defined by (11), consider a relatively large number of cycles, and evaluate the pore pressure, p, at the end of each cycle. Then substituting τ_0 for τ in (15), rearranging and integrating over N cycles, we obtain

$$\Delta W = \int_0^p \frac{dp'}{\bar{G}(\tau_0,p')} \ , \tag{16}$$

where ΔW is the energy loss over N cycles, and in general depends on the stress amplitude, τ_0, the number of cycles, N, and other relevant physical parameters.

3. DENSIFICATION ANALYSIS

We shall now sketch how one may obtain in a strain-controlled cyclic shearing of dry or saturated but drained sand, the stress amplitude in terms of the strain amplitude and the number of cycles. To this end we consider a typical cycle, and denote by τ_M the stress amplitude and by ρ_M the value of the relative void ratio at the instant when the strain just attains the value γ_0. From Eq. (4) we then obtain

$$\tau_M = \hat{\tau}(\gamma_0, \rho_M) \ . \tag{17}$$

It is clear that $\hat{\tau}$ must be an odd function of γ_0, and must increase as the void ratio decreases, i.e. we must have

$$\hat{\tau}(-\gamma_0, \rho_M) = -\hat{\tau}(\gamma_0, \rho_M) \ ,$$

$$\frac{\partial \hat{\tau}}{\partial \rho_M} < 0, \ \hat{\tau}(0,\rho_M) = 0 \ . \tag{18}$$

The relative void ratio can be expressed in terms of γ_0 and the number of cycles. To this end we obtain from Eq. (22) of Chapter 2,

$$\rho_M = [\rho_0^{1-n} + \hat{\nu} \ \Delta W]^{\frac{1}{1-n}} \ , \tag{19}$$

where we have set $\rho = \rho_M$, and $\hat{\nu} = (n-1)/\tilde{\nu}$. To compare (19) with experimental results, we rewrite Eqs. (24) of Chapter 2, as

$$\rho_M = [\rho_0^{1-n} + k_1 \dot{N}^{1/2} \gamma_0^{\frac{1+\alpha}{\beta}}]^{\frac{1}{1-n}} \text{ for small strain amplitudes,} \tag{20}$$

and

$$\rho_M = [\rho_0^{1-n} + k_2 N \gamma_0^{\frac{1+\alpha}{\beta}}]^{\frac{1}{1-n}} \quad \text{for large strain amplitudes,} \tag{21}$$

where the coefficient $\tilde{\nu}$ is absorbed in k_1 and k_2. In Chapter 2 we have compared the results obtained from (20) and (21) with experimental observations reported by Youd (1972). Setting $\alpha = 4$, $\beta = 5$, and $n = 3.5$, we obtained good correlation with experiments over a wide range of strain amplitudes and number of cycles.

Substitution from either (20) or (21) into (17) now yields an expression for the stress amplitude which involves the strain amplitude and the number of cycles. Since $\hat{\tau}$ is odd in γ_0, we may consider the following series expansion:

$$\tau_M = \bar{A}_1 \gamma_0 + \bar{A}_3 \gamma_0^3 + \ldots, \tag{22}$$

where the parameters $\bar{A}_1, \bar{A}_3, \ldots$, are functions of ρ_M, and because of $(18)_2$, we must require that

$$\frac{\partial A_i}{\partial \rho_M} < 0, \quad i = 1,3,\ldots . \tag{23}$$

A possible explicit form for τ_M is

$$\tau_M = (A_1\gamma_0 + A_3\gamma_0^3 + \ldots)/(1 + B_1\rho_M + B_2\rho_M^2 + \ldots), \tag{24}$$

where A_1, A_3, ..., and B_1, B_2, ..., are all positive constants which however depend on the confining pressure, σ_c, and on other relevant parameters, but are independent of γ_0, N, and ρ_M. These constants must be evaluated by comparison with experimental results. Unfortunately experimental results suitable for this purpose do not exist at this time. We note that, instead of (24) one may consider

$$\tau_M = (A_1\gamma_0 + A_3\gamma_0^3 + \ldots)/(1 + B\rho_M)^m, \quad m \geq 1 , \tag{25}$$

where m is a constant.

4. LIQUEFACTION ANALYSIS

We shall now attempt to obtain in a stress-controlled test, an expression for the strain amplitude in terms of the number of cycles, and the applied stress amplitude in the liquefaction of saturated undrained cohesionless sand. To this end we consider the Gibbs function χ introduced in Section 3, and observe that if the shear stress τ in Eq. (12) is changed to $-\tau$, the shear strain γ must change to $-\gamma$, and therefore we must have

$$\tilde{\gamma}(-\tau,p) = -\tilde{\gamma}(\tau,p), \tag{26}$$

where the dependence on temperature θ is not displayed. Furthermore, as in the case of densification, we shall assume that the dependency of $\tilde{\gamma}$ on τ and p is separable, and hence

$$\tilde{\chi} = \hat{\chi}_1(\tau)/\hat{\chi}_2(p) \ , \tag{27}$$

and therefore in view of (12) we obtain

$$\tilde{\gamma}(\tau,p) = \frac{\hat{\gamma}_1(\tau)}{\hat{\chi}_2(p)} \ . \tag{28}$$

Consider now the i^{th} cycle in a cyclic shearing with constant (dimensionless) stress amplitude τ_0. To be definite, define the beginning of the i^{th} cycle as the state at which the shear stress τ has just attained the value τ_0 in the preceding cycle, and is being decreased. We denote the value of the shear strain at the completion of the i^{th} cycle by γ_M, and the corresponding value of the excess pore water pressure, by p_M, and we seek to obtain an explicit relation for γ_M in terms of the number of cycles N, the shear stress amplitude τ_0, and other parameters; for a fixed number of cycles, a typical γ_M, τ_0-relation is shown by the solid curve POQ in Fig. 2 of Chapter 2. It should be noted however, that in the stress-controlled cyclic shearing of undrained saturated sand, the shear strain, in general, attains its maximum value somewhat after the shear stress has attained the value τ_0, and has actually decreased below this value. However, for application, γ_M, as defined above, provides an adequate measure of the shear strain build-up.

From Eq. (28) we therefore obtain,

$$\gamma_M = \frac{\hat{\gamma}_1(\tau_0)}{\hat{\chi}_2(p_M)} \ , \tag{29}$$

where we must have

$$\hat{\gamma}_1(-\tau_0) = -\hat{\gamma}_1(\tau_0), \ \hat{\gamma}_1(0) = 0 \ , \tag{30}$$

and since the strain amplitude must increase with increasing excess pore water pressure, we require that $\hat{\chi}_2$ be a decreasing function of p_M, i.e.

$$\hat{\chi}_2' < 0 \ . \tag{31}$$

In particular, as p_M approaches 1, i.e. as the excess pore water pressure approaches the confining pressure σ_c, we expect that the positive function $\hat{\chi}_2(p_M)$ takes on small values.

Let us now consider power series expansions for the functions $\hat{\chi}_2(p_M)$ and $\hat{\gamma}_1(\tau_0)$, and write

$$\gamma_M = (a_1\tau_0 + a_3\tau_0^3 + \ldots)/(1 + c_1 p_M + c_2 p_M^2 + \ldots), \tag{32}$$

where the material parameters c_1, c_2, ..., and a_1, a_3, ..., are possibly functions of $e_0 - e_m$. Further, based on our previous requirements we take a_1, a_3, ..., positive and c_1, c_2, ..., negative such that $-\sum_{i=1}^{\infty} c_1 < 1$. We point out that the formulation (32) is valid only for $N \leq N_\ell$, i.e., for $p < 1$ and for initial liquefaction, i.e., when $p = 1$ for the first time. This limitation on relation (32) is a result of the fact that we have separated the function $\hat{\chi}$ into two parts, one only a function of τ and the other only a function of p, as in (27). In order to estimate the response for $N > N_\ell$ and, in particular, to obtain the limiting value of γ_N, we have as a special case of (32) consider

$$\gamma_M = (a_1\tau_0 + a_3\tau_0^3 + \ldots)/(1 - c\, p_M), \quad 0 < c < 1. \tag{33}$$

Note that as the excess pore water pressure p_M approaches 1, γ_M becomes very large, especially if c is assigned a value close to unity. The parameter c as well as the constants a_1, a_3, ... must be fixed by comparison with the experimental results. Note that for the general application the approximation (33) may not be adequate, in which case one must consider the more general representation (32). In the next section however, we shall use (33) and retaining only two terms in the series, compare our results with the experimental data reported by DeAlba et al. (1975).

Estimate of Pore Pressure

To use Eq. (17), we need an explicit expression for p_M. We obtain this from Eq. (28) of Chapter 2,

$$p_M = \{1 - N\tau_0^{1+\alpha}(e_0-e_m)^n/\hat{\nu}e_0\}^{\frac{1}{1-r}} - 1, \quad n,r > 1, \tag{34}$$

where $\hat{\nu} = \nu/h(r-1)$. This equation gives the excess pore water pressure as a function of stress amplitude τ_0 and the number of cycles N. It is an approximation and can be improved if better estimates for the material functions g and f are used, and the calculation of the energy loss is improved. Such a possibility is suggested by Eq. (16), for example. Lacking experimental results, however, we shall be content with the estimate given by (34).

Comparison with Experimental Results

Equation (34) gives the excess pore water pressure in terms of the number of cycles N, the dimensionless shear stress amplitude τ_0, and the initial and the minimum values of the void ratio. In Chapter 2, the results of this equation have been compared with several sets of experimental data reported by DeAlba et al. (1975). These experimental results have been obtained at the University of California at Berkeley with the aid of a large shaking table, and using rather large samples of saturated cohesionless Montery number 0 sand with minimum void ratio $e_m = 0.564$, and maximum void ratio $e_M = 0.852$. The experiments were performed on samples with 54, 68, 82, and 90 relative densities, for confining pressure of about 55.2 kPa (8 psi), and for various fixed shear stress amplitudes. The excess pore water pressure and the shear strain amplitude have been reported in terms of the number of cycles for the above stated values of the initial relative density.

In Chapter 2, first theoretical results based on Eq. $(22)_2$ of Chapter 2, for the densification of dry sand ($p = 0$) have been obtained and compared with the extensive experimental data reported by Youd (1970 and 1972). In this manner it was found that for a first-order approximation, $n = 3.5$ fits nicely all the experimental results reported by Youd. Then liquefaction data of DeAlba et al. (1975) and others (Peacock and Seed, 1968; Yoshimi and Oh-Oka, 1975) were considered in connection with (34), and it was found that $r = 2.5$ with $\alpha = 4$ fits all reported experimental results. In this chapter, therefore we shall use the same values for these parameters, i.e., we shall set $\alpha = 4$, $n = 3.5$, and $r = 2.5$.

The parameter $\hat{\nu}$ in (34) is inversely proportional to parameter h which occurs in the expression for the work in Eq. (15) of Chapter 2. It is reasonable to expect that h should increase with increasing confining pressure σ_c and with increasing relative density D_r (or with decreasing $e_0 - e_m$); this is because under a larger confining pressure or when one starts with a denser sand, more work will be required to rearrange the sand grains in the course of cyclic shearing. Therefore, the parameter $\hat{\nu}$ in (34) is expected to decrease with increasing confining pressure or with increasing relative density.

If we set in (34) $p_M = 1$, and denote by N_ℓ the corresponding number of cycles to liquefaction initiation, we obtain

$$N_\ell \tau_0^{\alpha+1} \frac{(e_0 - e_m)^n}{e_0} = \hat{\nu} (1 - 2^{1-r}) \equiv \eta. \tag{35}$$

It has been observed in Chapter 2 that, experimental results reported by DeAlba et al. (1975) for less than 70% relative densities, correspond to $\eta = 0.87 \times 10^{-6}$, and those for 82% relative density correspond to $\eta = 0.40 \times 10^{-6}$. We shall use these results in connection with the following approximate version of Eq. (33), in order to predict the strain amplitude build-up in

terms of the number of cycles and other relevant parameters:

$$\gamma_M = (a_1\tau_0 + a_3\tau_0^3)/(1 - cp_M) \ . \tag{36}$$

We have used the experimental results for 54% relative density, in order to establish the following form for Eq. (36):

$$\gamma_M = (3/2 \times 10^{-4}\tau_0 + 10^{-1}\tau_0^3)/(1 - 4/5p_M) \tag{37}$$

which is intended for small strain amplitudes. The corresponding results are compared with experimental points in Fig. 1, for 54 and 68, and in Fig. 2 for 82% relative densities, respectively. As is seen, the comparison for 54% and 82% relative densities is quite good, especially since primitive forms for the material functions have been used. For 68% relative density, however, the comparison is not good for a small number of cycles. We feel, however, that in this range the experimental results are not compatible with those reported for 54 and 82% relative densities. As was pointed out above, for the same confining pressure and the same shear stress amplitude, one expects that, initially, say, after one or two cycles, the strain amplitude should be smaller for the denser sand than for the looser one. Some of the experimental points for 68% relative density violate this expectation. For example, experimental points for $\tau_0 = 0.135$ and $D_r = 54\%$, are reported to fall below the corresponding points for $\tau_0 = 0.134$ and $D_r = 68\%$, for the number of cycles from one to twelve. Notwithstanding this, the experimental results reported by DeAlba et al. (1975) seem to be the most extensive ones that the present author has been able to obtain so far. These results certainly confirm the validity of our basic theoretical approach. However, a systematic and coordinated theoretical and experimental work is still required, in order to establish a reliable stress-strain relation for cyclic shearing of saturated drained or undrained sand.

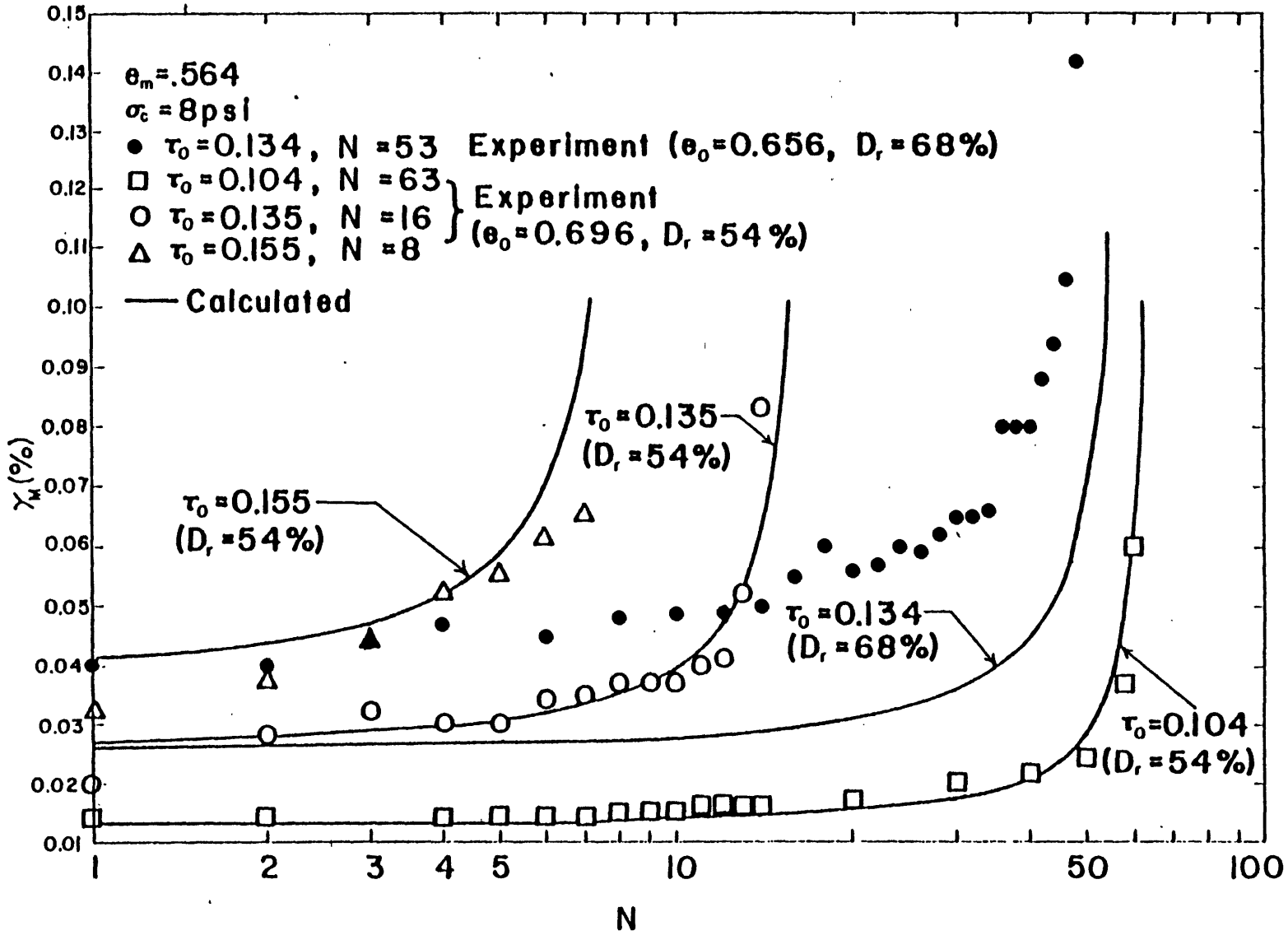

Fig. 1. Strain amplitude vs. number of cycles in cyclic shearing of undrained saturated sand under 55.2 kPa (8 psi) confining pressure (data from DeAlba et al. (1975)).

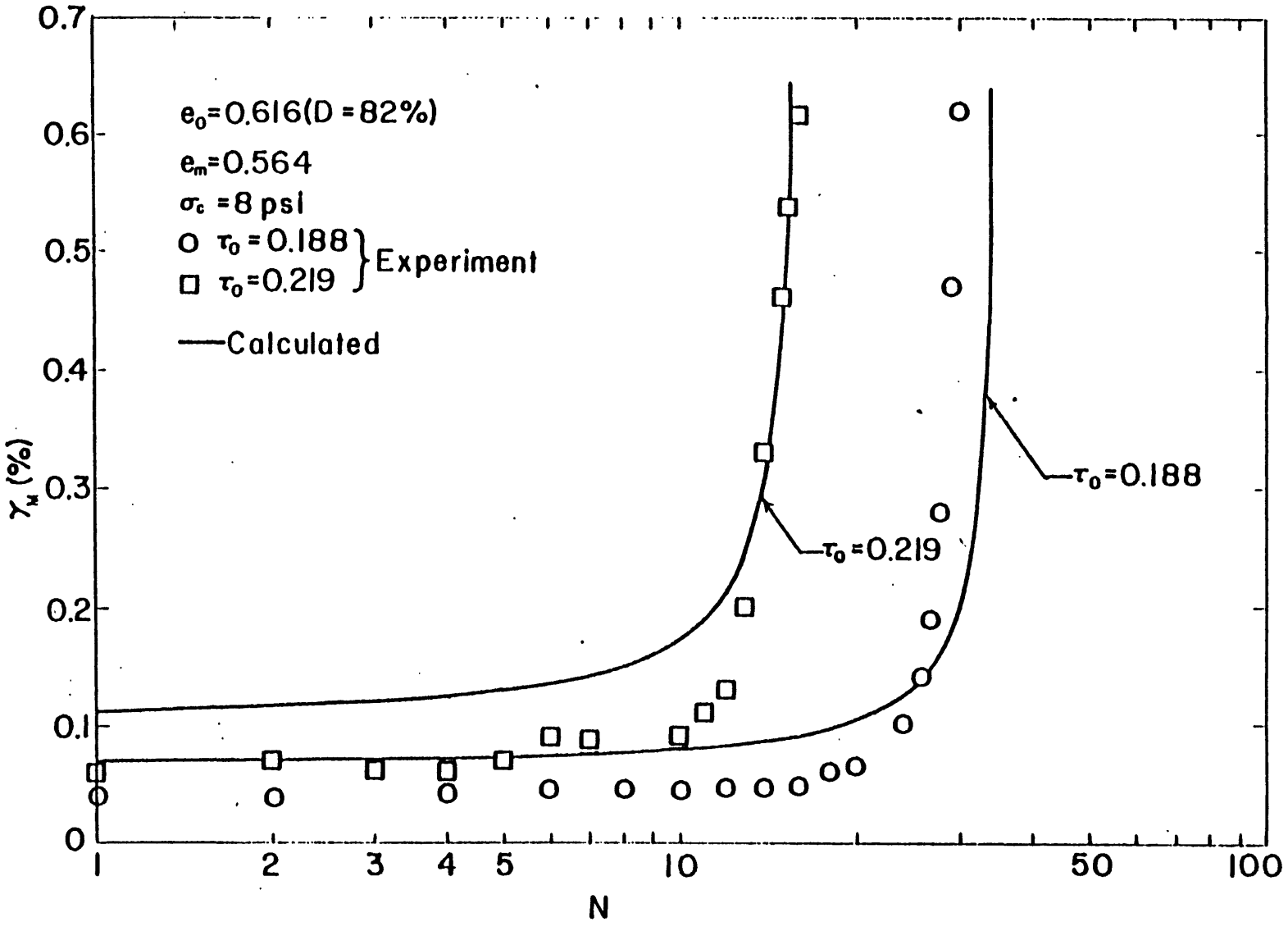

Fig. 2. Strain amplitude vs. number of cycles in cyclic shearing of undrained saturated sand under 55.2 kPa (8psi) confining pressure (data from DeAlba et al. (1975)).

REFERENCES

DeAlba, P. S., Chan, C. K., and Seed, H. B., 1975. Determination of soil liquefaction characteristics by large-scale laboratory tests. NUREG-0027 NRC-6, Shannon and Wilson, Inc., and Agbabian Assoc., Seattle, Washington, Sept. 1976, prepared for the U.S. Nuclear Regulatory Commission under Contract Number AT(04-3)954; manuscript completed May, 1975; see also EERC Report 75-14, Univ. Calif. Berkeley, CA.

Hardin, B. D., and Drnevich, V. P. 1972. Shear modulus and damping in soils: design equations and curves. Journal of the Soil Mechanics and Foundation Div., ASCE 98 #SM7: 667-692.

Nemat-Nasser, S. 1975. On nonequilibrium thermodynamics of continua. In S. Nemat-Nasser (Editor), Mechanics Today, Vol. 2, Pergamon Press, New York, Chapter II: 94-158.

Nemat-Nasser, S. 1977. On nonęquilibrium thermodynamics of coninua: Addendum. In S. Nemat-Nasser (Editor), Mechanics Today, Vol. 4, Pergamon Press, New York, Chapter VI: 391-405.

Nemat-Nasser, S. and Shokooh, A., 1977. A unified approach to densification and liquefaction of cohesionless sand. Earthquake Research and Engineering Laboratory, Technical Report No. 77-10-3, Dept. of Civil Engineering, Northwestern University, Evanston, Ill.

Nemat-Nasser, S. and Shokooh, A., 1978. A new approach for the analysis of liquefaction of sand in cyclic shearing. Proc. of the Second International Conference on Microzonation, 2: 957-969, San Francisco, CA.

Peacock, W. H. and Seed, H. B., 1968. Sand liquefaction under cyclic loading simple shear conditions. Journal of the Soil Mechanics and Foundations Div. ASCE 94 #SM3: 689-708.

Seed, H. B. and Lee, K. L., 1966. Liquefaction of saturated sands during cyclic loading. Journal of the Soil Mechanics and Foundations Div., ASCE 92 #SM6: 105-134.

Seed, H. B. and Peacock, W. H., 1971. Test procedures for measuring soil liquefaction characteristics. Journal of the Soil Mechanics and Foundations Div. ASCE 97 #SM8: 1099-1119.

Silver, M. L. and Seed, H. B., 1971a. Deformation characteristics of sands under cyclic loading. Journal of the Soil Mechanics and Foundations Div., ASCE 97 #SM8: 1081-1098

Silver, M. L. and Seed, H. B., 1971b. Volume changes in sands during cyclic loadings. Journal of the Soil Mechanics and Foundations Div., ASCE 97 #SM9; 1171-1182.

Van Eckelen, H. A. M., 1977. Single-parameter models for progressive weakening of soils by cyclic loading. Geotechnique 27, No. 3: 357-368.

Yoshimi, Y., and Oh-Oka, H., 1975. Influence of degree of shear stress reversal on the liquefaction potential of saturated sand. Soils and Foundations, 15, No. 3: 27-40.

Yoshimi, Y., Richard, Jr., F. E., Prakash, S., Barkan, D. D., and Ilyichev, A. A., 1977. Soil dynamics and its application to foundation engineering. State-of-the-Art Report, IX ICSMFE, Tokyo.

Youd, T. L., 1970. Densification and shear of sand during vibration, Journal of the Soil Mechanics and Foundations Div., ASCE 96 #SM3: 863-880.

Youd, T. L., 1972. Compaction of sands by repeated shear straining. Journal of the Soil Mechanics and Foundations Div., ASCE 98 #SM7: 709-725.

CHAPTER 4

ON BEHAVIOR OF GRANULAR MATERIALS IN SIMPLE SHEAR

1. INTRODUCTION

When a sample of a granular cohesionless material is horizontally sheared under vertical pressure, it is experimentally observed that (see, for example, Reynolds (1885), Taylor (1948), Terzaghi and Peck (1948), Roscoe, Schofield, and Wroth (1958), Rowe (1962), and more recently Youd (1970, 1972), and Silver and Seed (1971); for references to other related works, see Faccioli and Rese'ndiz (1976)):

(1) There is always an initial densification (decrease in void volume), the magnitude of which decreases as the initial void ratio (the ratio of void volume to the volume of the solid) approaches its minimum value;

(2) if the sample is dense (i.e. its initial void ratio is close to the corresponding minimum value), then the initial densification will be followed by dilatancy (increase in void volume) which continues until a critical* void ratio is attained asymptotically;

(3) if at a certain stage during the course of dilatancy, discussed in item (2) above, the shearing is reversed, and the shear strain is gradually decreased to its initial zero value (completing half of a strain cycle), then there is always a net amount of densification, this amount decreasing as the initial void ratio approaches its minimum value;

(4) if the sample is loose, i.e. the initial void ratio is larger than the critical value, then the sample densifies continuously until the critical void ratio is reached asymptotically.

---

* This critical value, in general, depends on the value of the confining pressure, on the size and shape distribution of the grains, and on other relevant parameters.

Although there has been considerable theoretical work devoted to the analysis of the deformation of granular materials (see, for example, Drucker and Prager (1952), de Josselin de Jong (1958, 1971), Sepencer (1964, 1971), Spencer and Kingston (1973), Mandl and Luque (1970), Mehrabadi and Cowin (1978), and Nemat-Nasser and Shokooh (1977, 1978)), there exists no theory which can account for all the above-stated physically observed facts. In recent papers, Nemat-Nasser and Shokooh (1977, 1978) have used an energy consideration in a setting of the classical irreversible thermodynamics, see Nemat-Nasser (1974, 1978), to formulate densification of dry sand and liquefaction of saturated undrained sand in cyclic shearing, focusing attention only on the state of the sample at the end of a given number of cycles. These authors do not consider the detailed processes of dilatancy and densification which take place during the course of each cycle.

It is the purpose of this paper to present a theory for two-dimensional (plane strain) flow of granular material, which introduces no additional kinematical or dynamical parameters than have already been presented by other researchers in the literature, nevertheless, it explains in a simple and convincing manner the phenomena of initial densification, subsequent dilatancy, and the net amount of densification which results in the course of cyclic deformation of a sample. The theory complements the work of Mehrabadi and Cowin (1978) who focused attention on the phenomenon of dilatancy of a very densely packed sample. We shall demonstrate that a simple reinterpretation of Mehrabadi's and Cowin's work in line with the physics of the process, can be used to generalize the theory to include all the previously stated, physically observed phenomena, without the introduction of any new kinematical or dynamical variables.

In Sec. 2 we discuss in detail the consequence of a simple model, and show how it leads to an equation identical to that obtained by Mehrabadi and

Cowin (1978), which relates the rate of change of void ratio to the corresponding rate of distortional work. In Sec. 3 we then explain in terms of the same model, how this equation not only explains the observed dilatancy and densification, but also, because of its inherent nonsymmetry in dilatancy and densification processes, yields a net amount of densification over a cycle of shearing.

2. A MODEL FOR DENSIFICATION AND DILATANCY

In this section we shall introduce a simple model for two-dimensional flow of granular material, which seems to account rather convincingly for the phenomena of densification and dilatancy that accompany the shearing of these materials. Following Mandl and Luque (1970), the model distinguishes between the macroscopic slip planes and the microscopic motion of individual particles which must override each other within a shear band which defines the macroscopic slip region, or within a sample which is macroscopically undergoing a homogeneous shearing. We shall concentrate on the physics of the process, and to this end, examine to a certain extent possible detailed flow of grains within a sample which is (macroscopically) homogeneously sheared; see Fig. 2.1a.

In Fig. 2.1b the macroscopic slip line is denoted by SS, which cuts through the individual grains or families of grains, in a random manner. As has been pointed out by Mandl and Luque (1970), the actual slip may occur along the wavy line S'S'. In Fig. 2.1b the individual grains are identified, but these grains may be interpreted as groups of particles which participate momentarily as a unit in the overall microscopic deformation.*

---

* It has been observed experimentally, see for example, Davis and Deresiewicz (1977), Fig. 4, p. 80, that grains often form individual groups which participate in the overall deformation as individual units.

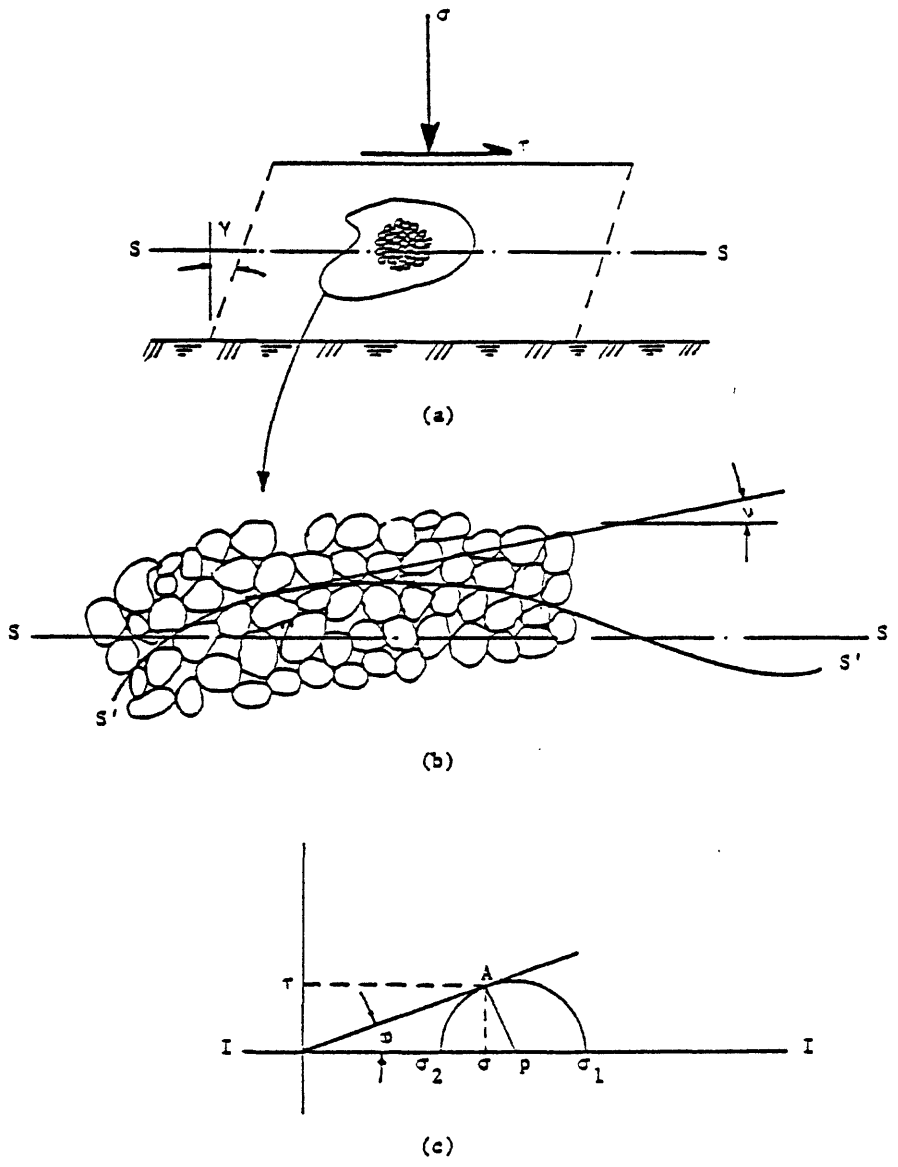

Figure 2.1 : (a) Simple shear under vertical pressure;

(b) Actual slip line S'S', macroscopic slip line SS, and the angle of dilatancy ν.

(c) The Mohr-Coulomb yield condition.

If the macroscopic shear stress and normal stress transmitted across the plane SS are denoted, respectively, by τ and σ, then we may write

$$\tau = \sigma \tan \phi, \tag{2.1}$$

where ϕ is the macroscopic overall angle of friction. This angle of friction is, in general, different from the microscopic local angle of friction, ϕ_μ, which corresponds to the slip of grains over the wavy line S'S'; i.e. for the microscopic slip we must have

$$\tau^* = \sigma^* \tan \phi_\mu, \tag{2.2}$$

where τ^* and σ^* are the shear and normal stresses transmitted across planes tangent to the S'S' at each point. We shall denote by ν the angle that the tangent to S'S' makes with the positive SS-direction (which is in the direction of flow), and note that when ν is positive, the particles tend to rise during the course of flow (dilatancy), and when ν is negative, the particles move down (densification). This is perhaps the most important observation in our development, especially when we note that the normal stress σ (which is compressive) acts in a totally nonsymmetrical way with respect to the upward and downward motions: the normal stress assists particles in their downward motion along the wavy line S'S', whereas it addes to the resistance to the motion, when the particles are forced to override each other upward along S'S'. It is this nonsymmetrical behavior which seems to lie at the basis of the observed initial densification, and the net densification in cyclic shearing, when granular materials are horizontally sheared under vertical pressure, or when they are sheared under confining pressure (simple shear).

We shall refer to the angle ν as the "dilatancy angle."

In the sequel we shall derive the basic equations for the model, using the Mohr-Coulomb yield condition, but we point out that our results can

easily be extended to other suitable yield conditions which involve the first two invariants of stress. Since plane strain is considered, we use a two-dimensional rectangular Cartesian coordinate system with unit base vectors, $\underset{\sim}{e}_i$, and coordinate axes x_i, $i = 1, 2$.

2.1 Governing Equations

To demonstrate the essential features of the model we consider a simple, macroscopically homogeneous, shearing (under a constant vertical pressure) of a sample of granular material which obeys the Mohr-Coulomb failure criterion; see Fig. 2.1. In Fig. 2.1c the state of stress at failure is defined by the corresponding Mohr circle which is tangent to the failure line in the τ, σ-plane at point A. The macroscopic failure plane makes an angle of $\frac{\pi}{4} + \frac{\phi}{2}$ with the major principal II-plane across which the maximum compressive normal stress is transmitted. From the geometry of the Mohr circle we have

$$\tau = \frac{1}{2}(\sigma_1 - \sigma_2)\cos\phi = \tau_{max}\cos\phi,$$

$$\sigma = \frac{1}{2}(\sigma_1 - \sigma_2)\cos\phi\cot\phi = \tau_{max}\cos\phi\cot\phi. \qquad (2.3)$$

Microscopic slip occurs within a slip band which consists of a stack of microscopic slip lines similar to S'S'. We consider a typical microscopic slip line, S'S', which locally makes an angle ν with the macroscopic shear plane SS; see Figs. 2.1. We regard ν positive when the motion of individual particles or groups of particles along the direction defined by ν is against the resultant normal stress transmitted across macroscopic shear plane SS; this results in dilation. With this convention, ν negative, therefore, corresponds to densification. We shall derive all our equations for ν positive, and then allow ν to take on both positive and negative values, as the physics of the situation may dictate.

The slip of particles or groups of particles at a given point on micro-

scopic slip line S'S', may be idealized and defined by a block moving along the S'S'-direction, as shown in Fig. 2.2. The resultant forces on the block consist of a vertical force, N, and a horizontal force, T, which are transmitted across an elementary area A of macroscopic shear plane SS; hence, $\sigma = N/A$ and $\tau = T/A$. The resultant normal force acting on the S'S'-plane is thus given by

$$N^* = N \cos \nu + T \sin \nu \ . \tag{2.4}$$

When sliding occurs, the associated frictional force, F*, against which energy is dissipated, will be given by

$$F^* = N^* \tan \phi_\mu \tag{2.5}$$

which is the counterpart of (2.2). If we multiply both sides of (2.1) by A, we obtain

$$T = N \tan \phi \ . \tag{2.6}$$

We note, for positive ν, ϕ exceeds ϕ_μ.

Substitution from (2.6) into (2.4), and then into (2.5), yields

$$F^* = \frac{T \tan \phi_\mu}{\sin \phi} \cos(\phi - \nu). \tag{2.7}$$

Consider now the motion of the block in Fig. 2.2b, by distance $\Delta\ell$ along the S'S' plane. The vertical upward (for ν positive) motion of the block, denoted by Δh, is given by

$$\Delta h = \Delta\ell \sin \nu, \tag{2.8}$$

and the corresponding energy dissipation is

$$\Delta W = F^* \Delta\ell = F^* \Delta h/\sin \nu. \tag{2.9}$$

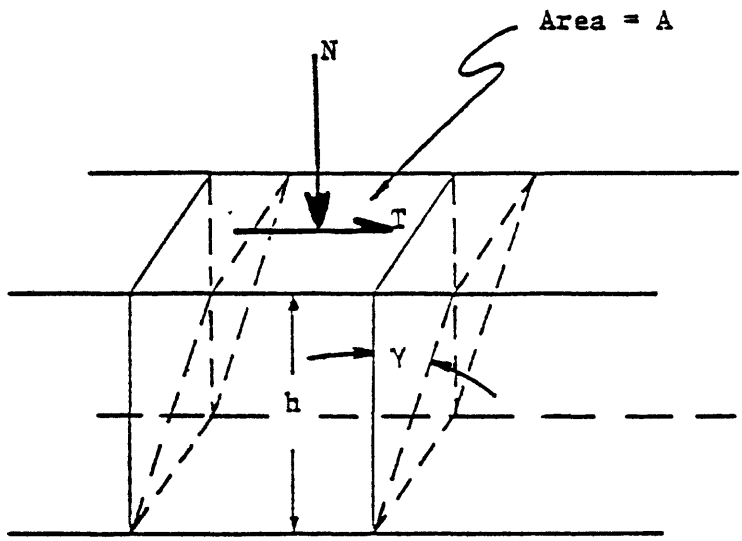

(a)

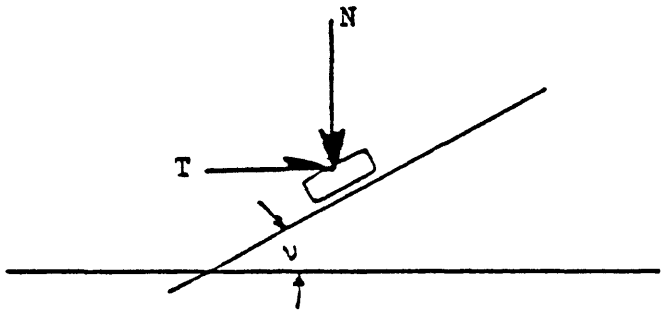

(b)

Figure 2.2 : (a) A macroscopic sample of height h, and area A, subjected to the total shear force T and normal force N;

(b) A block characterizing the slip of groups of particles moving in the S'S'-direction, with dilatancy angle ν.

Substitution for F* then gives

$$\Delta W = \frac{T \tan \phi_\mu \cos(\phi - \nu)}{\sin \phi \sin \nu} \Delta h \ . \qquad (2.10)$$

The microscopic (true) friction angle ϕ_μ, the macroscopic (effective) friction angle ϕ, and the <u>average</u> dilatancy angle ν corresponding to the macroscopic sample shown in Fig. 2.2a, are related by a simple equation. To obtain this, we use the balance of energy, as follows:

$$-N\Delta h + T\Delta x = \Delta W \ , \qquad (2.11)$$

where Δx is the horizontal displacement of the block in Fig. 2.2b. We now substitute from (2.6) and (2.10) into (2.11), note that $\Delta h / \Delta x = \tan \nu$, and arrive at

$$\tan \phi_\mu = \tan(\phi - \nu). \qquad (2.12)$$

Note that in this equation both ϕ and ν are average macroscopic quantities corresponding to the global response of the macroscopic sample whose behavior is symbolically characterized by the block in Fig. 2.2b.

Later on we shall examine statistically the behavior of the macroscopic sample which contains a finite number of families of particles, each having possibly different dilatancy angles. Here however, let us assume that there is only a single dilatancy angle ν associated with the entire macroscopic sample. With this assumption the total work per unit volume of the sample is obtained if (2.10) is divided by $V = hA$, arriving at

$$\Delta w = \frac{\tau \tan \phi_\mu \cos(\phi - \nu)}{\sin \phi \sin \nu} \frac{\Delta h}{h} \ , \qquad (2.13)$$

where $\Delta w = \Delta W/V$ is the incremental work per unit volume. Equation (2.13) can be written in the rate form, by dividing both sides by the increment of

time, Δt, and taking the limit; in this manner we obtain

$$\dot{w} = \frac{\tau \tan \phi_\mu \cos(\phi - \nu)}{\sin \phi \sin \nu} \frac{\dot{V}}{V}, \tag{2.14}$$

where, since A is constant, we have $\dot{h}/h = A\dot{h}/Ah = \dot{V}/V$.

In Sec. 3 we shall exploit Eq. (2.14), in an effort to understand the densification and dilatancy phenomena, by considering in a typical macroscopic sample, a suitable statistical distribution for groups of particles with active ν's. Here, let us continue to assume that ν has a constant value within a given macroscopic sample.

The quantity, $\dot{V}/V$, represents the rate of change of volume per unit current volume, and is given by

$$\frac{\dot{V}}{V} = \text{tr } \underset{\sim}{D} = D_{ii}, \tag{2.15}$$

where $\underset{\sim}{D} = D_{ij}\, \underset{\sim}{e}_i\, \underset{\sim}{e}_j$ is the deformation rate tensor; repeated indices are summed over 1,2.

Equation (2.14) is equivalent to the equation obtained by Mehrabadi and Cowin (1978), using a completely different approach. To see this equivalence, we first observe that $\dot{w}$ in (2.14) is the <u>total</u> rate of work, consisting of the distortional rate of work, $\dot{w}'$, and the dilatational rate of work, $\dot{w}''$, i.e.

$$\dot{w}' = \dot{w} - \dot{w}'' = \sigma_{ij} D_{ij} + p D_{kk},$$

where p is the hydrostatic pressure, $p = \tau/\sin \phi \cos \phi$, as is seen from Fig. 2.1c. Hence, substitution into (2.14) yields

$$\dot{w}' = \left[\frac{\tau \sin(\phi - \nu)}{\sin \phi \sin \nu} + \frac{\tau}{\cos \phi \sin \phi}\right] D_{kk}$$

$$= \frac{\tau \cos(\phi - \nu)}{\cos \phi \sin \nu} D_{kk}. \tag{2.16}$$

If we note that $\tau/\cos\phi = \tau_{max}$, then we obtain the corresponding equation reported by Mehrabadi and Cowin (1968); observe that these authors used τ for the maximum shear stress, which is here denoted by τ_{max}. We note that the theory presented by Mehrabadi and Cowin is in a more general setting and involves another equation pertaining to noncoaxiality of stress and strain rates. However, our development has its own appeal as it provides a simple and intuitive derivation. Observe that the dilatancy angle used in our derivation can be positive or negative, as the situation may dictate. This fact has been also observed in Mehrabadi's doctoral thesis (1979), although the published paper by Mehrabadi and Cowin (1978) considers constant positive ν only.

As was pointed out before, the actual motion of individual grains or groups of grains along the S'S' wavy line, is nonsymmetric, because of the effect of the vertical force transmitted across SS. This is true even if the wavy line S'S' marks a completely symmetrical variation (e.g. a sine wave) along the SS direction. Equation (2.14) contains this and related facts, as we shall discuss below.

3. DENSIFICATION AND DILATANCY

We shall now consider a continuum approximation for granular material. In this approximation we replace the nonhomogeneous material by a locally homogeneous equivalent continuum which is endowed with certain average properties of the actual material. To establish these properties we consider the response of a suitably large sample which is initially statistically homogeneous, and which is subjected to macroscopically homogeneous stress states. On the microscopic level, however, the sample would be highly heterogeneous, as discussed before.

Consider a sample of the kind mentioned above with total volume, V, and total void volume, V_v, the corresponding volume of the solid being $V_s = V - V_v$. The void ratio, therefore, is $e = V_v/V_s$, and it is easily verified that

$$\frac{\dot{V}}{V} = \operatorname{tr} \underset{\sim}{D} = \frac{\dot{e}}{1+e} , \tag{3.1}$$

where it is assumed that the solid constitutent is rigid.

We consider the sample to be a magnified element of the equivalent continuum, the element may be momentarily located in a macroscopic slip band. The element, therefore, will have the properties which are obtained by statistical averaging over the sample. The sample includes a stack of microscopic wavy slip lines similar to S'S' in Fig. 2.1b, over which individual particles or groups of particles may slip. We take the macroscopic shear direction to be in the horizontal SS-direction, assume that the macroscopic traction transmitted across SS consists of a compressive normal stress σ, and a shear stress τ, as shown in Fig. 2.1a. In accordance with the Mohr-Coulomb assumption, a particle (or a group of particles) begins to slide in the SS-direction, when the resultant shear stress in the slip direction reaches a

critical value. Since the normal stress σ assists the particles which tend to slide down (the corresponding ν is negative), and hinders those which tend to move upward (the corresponding ν is positive), we immediately conclude that, as the normal stress is kept fixed and the shear stress, τ, is increased from zero, particles or groups of particles with negative values of ν become active first, starting with those with larger absolute values of ν. As the shear stress is increased, and as the particles with negative ν move on the microscopic slip planes, they become engaged with other particles or groups of particles which have positive values of ν. Moreover, for larger shear stress, particles with positive ν begin to slide. Hence, although initially more particles with negative ν are active (initial densification), the distribution of the active particles changes as the stress is increased, and flow proceeds. In the sequel we shall only include in our statistical averaging the values of ν associated with only the active particles or groups of particles within the sample.

Let the macroscopic shear strain rate be denoted by $\dot{\gamma}$. Then the rate of distortional work per unit volume, $\dot{w}'$, in the present case equals $\tau\dot{\gamma}$. With this, (2.16) becomes

$$\frac{1}{V}\frac{\dot{V}}{\dot{\gamma}} = \frac{\cos(\phi_\mu + \nu)\ \sin\nu}{\cos\phi_\mu} \quad . \tag{3.2}$$

With the aid of this equation we shall now explain the observed initial densification, subsequent dilatancy, asymptotic approach to the critical state, and the net densification in cyclic shearing, which occur when a sample of granular material is sheared horizontally under vertical pressure.

To this end, let

$$p_i = V_i/V,\ i = 1,2,\ldots,n, \tag{3.3}$$

be the volume fraction of the family of particles which at the considered

instant have a dilatancy angle equal to ν_i; V_i is the collective volume of this family, and it is assumed that there are a total of n active families. Hence,

$$\sum_{i=1}^{n} p_i = 1 \ . \tag{3.4}$$

During the shearing of the macroscopic sample, each family makes a contribution to the total rate of dilatation proportional to its own fractional volume. Hence, from Eq. (3.2) we have

$$\frac{1}{V}\frac{\dot{V}}{\dot{\gamma}} = \frac{1}{\cos \phi_\mu} \sum_{i=1}^{n} p_i \cos(\phi_\mu + \nu_i) \sin \nu_i . \tag{3.5}$$

This equation contains all observed behavior of granular materials in simple shear. Although we may puruse the corresponding arguments in terms of a discrete set of values for the dilatancy angle ν, as in (3.5), arriving at the intended conclusions, we shall consider a large number of families and use a continuous distribution for the dilatancy angle ν. To this end, let the range of variation of ν be ν_0^- to ν_0^+, and denote the corresponding distribution density function by $p(\nu)$, so that $p(\nu)\, d\nu$ is the volume fraction of elements with ν in the range ν to $\nu + d\nu$. In this manner, instead of (3.5) we may write

$$\frac{1}{V}\frac{\dot{V}}{\dot{\gamma}} = \frac{1}{\cos \phi_\mu} \int_{\nu_0^-}^{\nu_0^+} p(\nu) \cos(\phi_\mu + \nu) \sin\nu \, d\nu . \tag{3.6}$$

In the sequel we shall use this equivalent form. Note that $\int_{\nu_0^-}^{\nu_0^+} p(\nu)d\nu = 1$.

3.1 Initial Densification

When a sample of granular material is initially sheared under a confining pressure, the initial distribution of ν's is biased toward the negative values of ν, as we discussed before; see Fig. 3.1a. Therefore, the integral in

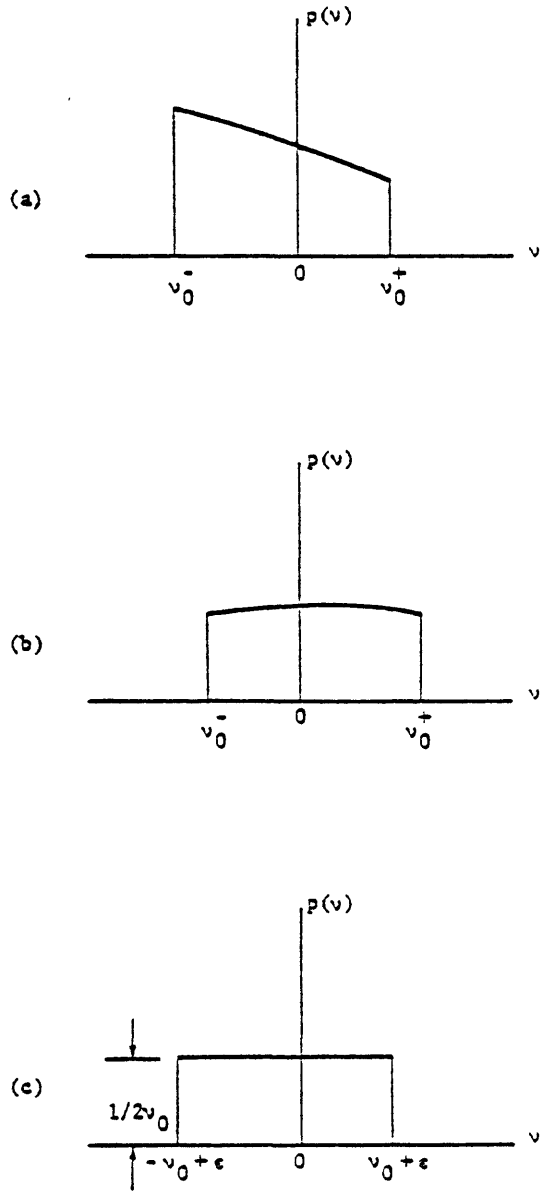

Figure 3.1 : (a) Initial distribution of the dilatancy angle ν;
(b) Distribution of the dilatancy angle ν after monotone shearing;
(c) The simplest distribution.

(3.6) would be negative in this case, i.e. initially the sample must densify. Note that, even for a completely symmetric variation in p, i.e., even if we assume that

$$p(\nu) = -p(-\nu) \text{ for } -\nu_0 \leq \nu \leq \nu_0 ,$$

$$p(\nu) = 0 \quad \text{otherwise,} \tag{3.7}$$

we still have

$$\int_{-\nu_0}^{\nu_0} p(\nu) \cos(\phi_\mu + \nu) \sin\nu \, d\nu < 0 \tag{3.8}$$

for all $p(\nu)$ that satisfy (3.7). Hence we see that $\dot{V}/\dot{\gamma} = dV/d\gamma$ is <u>initially</u> negative. This explains the observed initial densification of loose as well as dense sands.

For illustration, let $p(\nu)$ have a uniform symmetric distribution,

$$p(\nu) = \frac{1}{2\nu_0} \text{ for } -\nu_0 \leq \nu \leq \nu_0 ,$$

$$p(\nu) = 0 \quad \text{for} \quad |\nu| > \nu_0 . \tag{3.9}$$

Then substitution into (3.6) yields

$$\frac{1}{V}\frac{\dot{V}}{\dot{\gamma}} = -\frac{1}{2} \tan\phi_\mu \left[1 - \frac{\sin 2\nu_0}{2\nu_0}\right] . \tag{3.10}$$

This is an interesting equation, as it shows that without internal friction, i.e. if $\phi_\mu = 0$, there is no densification or dilatancy in the present case. Moreover, since the quantity inside the brackets is always positive, the right-hand side is negative, i.e. densification.

3.2 Dilatancy

As the shearing is continued, more families of particles with positive ν's become active. This means that the distribution function $p(\nu)$ (which is

initially biased toward negative ν's), tends to become biased toward positive values of ν's, as shearing is continued. This fact has been observed experimentally by Oda and Konishi (1974) and Matsuoka (1974). However, experimental observations are not conclusive. Therefore, it is impossible to characterize the distribution function $p(\nu)$ with any certainty. Nevertheless, as $p(\nu)$ becomes biased toward the positive values of ν, see Fig. 3.1b, the absolute value of the integral in (3.6) decreases with increasing macroscopic shear strain, becoming zero at a certain value of the strain. The fact that such a state will be reached sooner or later for any granular material that is sheared under confining pressure, can be seen from Eq. (2.10), because for the same energy consumption the particles with negative values of ν can move much more down, than the particles with positive (but equal in magnitude) values of ν can move up. The down-going particles then either become engaged with the up-going ones, or since their ν gradually decreases to zero, they become either up-going particles or inactive. Hence, on the average, the population of the active down-going particles decreases, and the population of the up-going ones increases, with increasing shear strain. With the weighting function $p(\nu)$ becoming biased toward the positive values of ν, the integral in (3.6) may become positive, hence leading to the phenomenon of dilatancy of dense sand. This will continue to the critical state at which the integral again vanishes. On the other hand, for loose sands, although the population of the families with negative ν's decreases with shearing, not enough families with positive ν's become active, since the looseness of the sand provides more freedom for particle movement. In this case also , the distribution function $p(\nu)$ tends to become biased toward positive values of ν, but the integral in (3.6) remains negative, approaching zero asymptotically.

We shall consider the simplest distribution function which yet explains all the above-mentioned experimentally observed facts. To this end we assume that the distribution function $p(\nu)$ is uniform having the constant width $2\nu_0$ and height $1/2\nu_0$, as shown in Fig. 3.1c. Initially the center of this rectangular distribution is located to the left of the p-axis, because, as we discussed before, the distribution function $p(\nu)$ is initially biased toward the negative ν's. As the shearing is continued, we expect that $p(\nu)$ should shift to the right; here it is assumed that the form of this distribution remains invariant but only its location changes with straining (this is an arbitrary but simplifying assumption). Hence, in general, we write

$$p(\nu) = \frac{1}{2\nu_0} \text{ for } -\nu_0 + \varepsilon \leq \nu \leq \nu_0 + \varepsilon,$$

$$p(\nu) = 0 \quad \text{otherwise.} \tag{3.11}$$

We do not suggest that this is the actual manner by which $p(\nu)$ changes, but it is the simplest form and yet yields qualitatively all observed results. Note that in (3.11), ε is regarded to be a function of γ, i.e.

$$\varepsilon = \varepsilon(\gamma) \ , \ \varepsilon(0) \leq 0; \tag{3.12}$$

the equality sign in $(3.12)_2$ corresponds to a symmetric distribution.

We now assume that ε is very small, substitute from (3.11) into (3.6), carry out the integration, expand the resulting expression in a Taylor series with respect to ε, and retaining only the first order terms, arrive at

$$\frac{1}{V}\frac{\dot{V}}{\dot{\gamma}} = -\frac{1}{2}\left[\tan\phi_\mu\left(1 - \frac{\sin 2\nu_0}{2\nu_0}\right) - 2\varepsilon\,\frac{\sin 2\nu_0}{2\nu_0}\right] . \tag{3.13}$$

Initially, $\varepsilon \leq 0$, and if $\varepsilon = 0$, then (3.13) reduces to (3.10). In either case we have initial densification. As ε increases, the rate of densification, i.e. $dV/d\gamma$, decreases, attaining zero value for

$$\varepsilon = \varepsilon_c = \frac{1}{2}\tan\phi_\mu\left[\frac{2\nu_0}{\sin 2\nu_0} - 1\right] . \tag{3.14}$$

If this value is attained asymptotically, for example if the variation of ε with respect to γ is as sketched in Fig. 3.2a by curve (1), then the material densifies monotonically, but at a decreasing rate, attaining the critical density asymptotically. On the other hand, if ε increases beyond the value ε_c given by (3.14), reaching a maximum value and then decreasing asymptotically to the same value, ε_c, as sketched by curve (2) in Fig. 3.2a, then we have a case of initial densification followed by subsequent dilatancy and asymptotic approach to the critical density, i.e. the behavior of dense sand. Note that, in Fig. 3.2a, $\varepsilon(0)$ is assumed to be negative for both curves, having a larger absolute value for loose sand (hence leading to a larger initial densification, in this case). In fact, we expect that $\varepsilon(0)$ should be a function of the initial void ratio, e_0, and should increase with decreasing e_0.

It is possible to correlate the variation of ε with that of τ/σ, in line with the recent work of Nemat-Nasser and Shokooh (1979) who proposed a finite deformation plasticity theory for frictional materials. Consider Eq. (2.12) and note that ν in this equation is to be interpreted as the average value of ν, i.e. $\bar{\nu}$ given by

$$\bar{\nu} = \int_{\nu_0^-}^{\nu_0^+} \nu p(\nu)\, d\nu. \tag{3.15}$$

If we substitute into this equation from (3.11), we obtain $\varepsilon = \bar{\nu}$. Then, in view of (2.1) and (2.12), we have

$$\varepsilon = \bar{\nu} = \tan^{-1}\left(\frac{\tau}{\sigma}\right) - \phi_\mu . \tag{3.16}$$

Hence, for this simple microscopic model, $\varepsilon(\gamma)$ is exactly the average value of ν, and is related to the $\tau/\sigma = \tan\phi$ by (3.16). In Fig. 3.2b we have

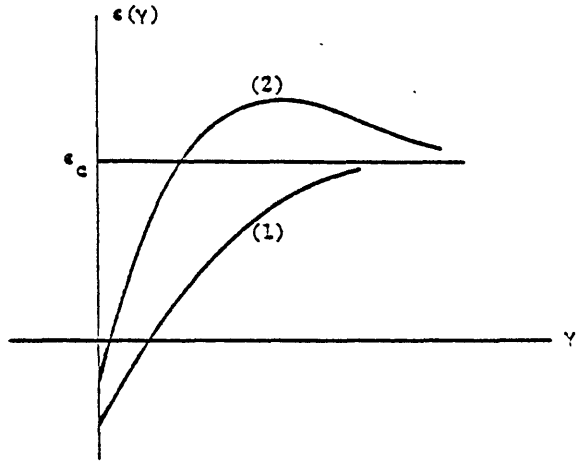

(a)

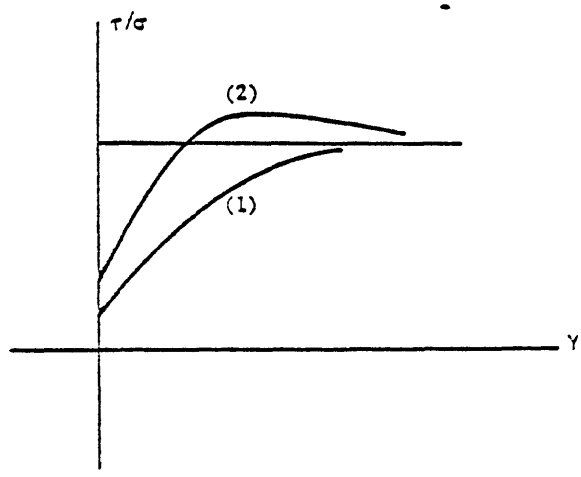

(b)

Figure 3.2 : (a) Possible variation of $\varepsilon(\gamma)$ with strain γ;

(b) Normalized shear stress as function of shear strain; curve (1) is for loose sand, and curve (2) is for dense sand.

sketched possible variations of τ/σ in terms of γ for loose (curve(1)) and dense (curve(2)) sands; at $\gamma = 0$, it is assumed that $\tau/\sigma > 0$, i.e. $\varepsilon(0) + \phi_\mu > 0$ for both curves. If we want to have $\tau = 0$ at $\gamma = 0$, then we must take $\varepsilon(0) = -\phi_\mu$.

With the aid of Eqs. (3.14) and (3.16) we can eliminate the parameter ν_0 in favor of the measurable quantity

$$\bar{M} = \lim_{\gamma \to \infty} \frac{\tau}{\sigma} = \left(\frac{\tau}{\sigma}\right)_{crit.} ; \tag{3.17}$$

here $\bar{M}$ is the asymptotic or critical value of the stress ratio τ/σ which is attained for large values of the shear strain γ. As discussed by Nemat-Nasser and shokooh (1979), $\bar{M}$ is equal to the values of τ/σ at the strain where the void ratio for dense sand attains its minimum value; this provides an easy method of measuring $\bar{M}$. Now from (3.14) and (3.16) we can write

$$\frac{2\nu_0}{\sin 2\nu_0} = 1 + 2(\tan^{-1} \bar{M} - \phi_\mu) \cot \phi_\mu = A . \tag{3.18}$$

Hence, for the present model, Eq. (3.13) can be written as

$$\frac{1}{V}\frac{\dot{V}}{\dot{\gamma}} = -\frac{1}{2}\left[\tan \phi_\mu (1 - A^{-1}) - 2A^{-1}\left\{\tan^{-1}\left(\frac{\tau}{\sigma}\right) - \phi_\mu\right\}\right] , \tag{3.19}$$

in which all the quantities in the right-hand side have fixed values except τ/σ which defines the stress state; note that in (3.18) ϕ_μ and $\bar{M}$ are measurable material parameters, and hence, for a given sand, they can be measured directly.

Let us now consider a special case in which ν_0 is so small that $2\nu_0 = \sin 2\nu_0$. Equation (3.13) then becomes

$$\frac{1}{V}\frac{\dot{V}}{\dot{\gamma}} = \varepsilon = \tan^{-1}\left(\frac{\tau}{\sigma}\right) - \phi_\mu , \tag{3.20}$$

where (3.16) is also used. Assume further that $\tau/\sigma << 1$ (which requires that ϕ be small) so that we can write, for (3.20),

$$\frac{1}{V}\frac{\dot{V}}{\dot{\gamma}} = \frac{\tau}{\sigma} - \phi_\mu . \tag{3.21}$$

This is similar to the equation obtained in critical state soil mechanics; see Schofield and Wroth (1968) and Nemat-Nasser and Shokooh (1979). In our approximation (and for simple shear), $\overline{M} = \phi_\mu$.

3.3 Load Reversal and Cyclic Shearing

The proposed model vividly manifests the observed densification which emerges by load reversal during cyclic shearing. Consider a situation where for a dense sand, for example, continuous shearing has resulted in dilatancy. At this instant, the distribution function $p(\nu)$ must be suitably biased toward positive values of ν, see Fig. 3.1b, in such a manner that the integral in (3.6) is actually positive.

Suppose at this point we consider shear strain reversal. To this end we assume that the vertical stress σ is held fixed, while the shear stress τ is gradually reduced to zero. Although the individual grains are assumed to be rigid, there is always a certain amount of strain recovery during this process, it being essentially caused by the action of the vertical pressure σ. As τ is being reduced, all the families of particles which, prior to the beginning of the process of shear stress reduction, had negative dilatancy angles ν, become inactive, whereas those with large positive dilatancy angles begin to move downward with decreasing shear stress. This is sketched in Fig. 3.3. As the shear stress is reduced further, more families with previously positive dilatancy angles begin to participate in this densification process. Hence a net amount of densification results by the time that the shear stress is reduced to zero. At the instant that the direction of shear stress is then reversed, the distribution function $p(\nu)$ would be biased toward positive ν's. Hence, continuous stressing in the reverse direction leads to further densification.

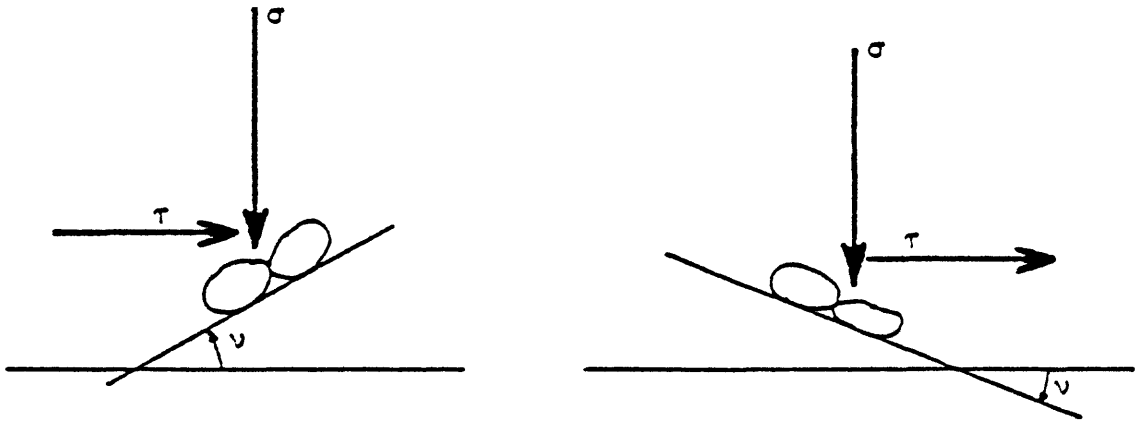

Figure 3.3 : As τ is decreased, particles which prior to this reduction had large positive ν's, may first move down, as those with prior negative ν's become inactive.

The simple example of uniform distribution for $p(\nu)$ further illustrates this point. Suppose that ε has a variation with γ similar to that shown by curve (2) in Fig. 3.2a, and further, suppose that the value of ε exceeds ε_c, so that the quantity within the brackets in (3.13) is actually negative. The reduction of the shear stress from its peak value to zero tends to shift the rectangular distribution slightly to the left, but still remaining biased toward positive ν's. Let at $\tau = 0$, $\varepsilon = \bar{\varepsilon} > 0$. Then the rate of densification as the shear stress is applied in the opposite direction, becomes

$$\frac{1}{V}\frac{\dot{V}}{\dot{\gamma}} = -\frac{1}{2}\left[\tan\phi_\mu\left(1 - \frac{\sin 2\nu_0}{2\nu_0}\right) + 2\bar{\varepsilon}\,\frac{\sin 2\nu_0}{2\nu_0}\right], \tag{3.22}$$

which is negative; here $\bar{\varepsilon} > 0$.

On the basis of the above discussion it is clear that there is always a certain amount of densification associated with the stress reversal imposed during a course of deformation when the material is in the dilatancy regime.

REFERENCES

Davis, R. A. and Deresiewicz, H., (1977). A discrete probabilistic model for mechanical response of a granular medium. Acta Mechanica 27, 69-89.

de Josselin de Jong, G. (1958). The undefiniteness in kinematics for friction materials. Proc. Conf. Earth Pressure Probl., Brussels, 1, 55-70.

de Josselin de Jong, G. (1971). The double sliding, free rotating model for granular assemblies. Geotechnique, 21, 155-163.

Drucker, D. C. and Prager, W. (1952). Soil mechanics and plastic analysis or limit design. Q. Appl. Math. 10, 157-165.

Faccioli, E. and Rese'ndiz, D. (1976). Soil dynamics: behavior including liquefaction. Seismic Risk and Engineering Decisions, C. Lomitz and E. Rosenblueth (eds.), Elsevier Scientific Pub. Co.

Mandl, G. and Luque, R. F. (1970). Fully developed plastic shear flow of granular materials. Geotechnique, 20, 277-307.

Matsuoka, H. (1974). A microscopic study on shear mechanism of granular materials. Soils and Foundations, 14, No. 1, 29-43.

Mehrabadi, M. M. and Cowin, S. C. (1978). Initial planar deformation of dilatant granular materials. J. Mech. Phys. Solids. 26, 269-284.

Mehrabadi, M. M. (1979). Planar deformation of granular materials. Ph.D. Thesis, Tulane University, May 1979.

Nemat-Nasser, S. (1975). On nonequilibrium thermodynamics of continua. In S. Nemat-Nasser (Editor), Mechanics Today, Vol. 2, Pergamon Press, New York, Chapter II: 94-158.

Nemat-Nasser, S. and Shokooh, A. (1977). A unified approach to densification and liquefaction of cohesionless sand. Earthquake Research and Engineering Laboratory, Technical Report No. 77-10-3, Dept. of Civil Engineering, Northwestern University, Evanston, Ill.; a revised version published in Canadian

Geotechnical Journal 16, (1979) 659-678.

Nemat-Nasser, S. (1977). On nonequilibrium thermodynamics of continua: Addendum. In S. Nemat-Nasser (Editor), Mechanics Today, Vol. 4, Pergamon Press, New York, Chapter VI: 391-405.

Nemat-Nasser, S. and Shokooh, A. (1978). A new approach for the analysis of liquefaction of sand in cyclic shearing. Proc. of the Second International Conference on Microzonation, 2, 957-969, San Francisco, Cal.

Nemat-Nasser, S., and Shokooh, A. (1979). On finite plastic flows of compressible materials with internal friction. Earthquake Research and Engineering Laboratory, Technical Report No. 79-5-16, Dept. of Civil Engineering, Northwestern Univ., Evanston, Ill.; Int. J. Solids Struct. 16 (1980) 495-514.

Oda, M. and Konishi, J. (1974). Microscopic deformation mechanism of granular material in simple shear. Soils and Foundations 14, 25-38.

Reynolds, O. (1885). On the dilatancy of media composed of rigid particles in contact. Phil. Mag. (5), 20, 469-481.

Roscoe, K. H., Schofield, A. N., and Wroth, C. P. (1958). On the yielding of soils. Geotechnique, Lond. 8, 22-53.

Rowe, P. W. (1962). The stress-dilatancy relation for static equilibrium of an assembly of particles in contact. Proc. Roy. Soc. A, 269, 500-527.

Schofield, A. N. and Wroth, C. P. (1968). Critical state soil mechanics. London, McGraw-Hill.

Silver, M. L. and Seed, H. B. (1971). Deformation characteristics of sand under cyclic loading. Jnl. Soil Mech. Fdn. Div. Am. Soc. Civ. Engrs. 97 1081-1098.

Spencer, A. J. M. (1964). A theory of the kinematics of ideal soils under plane strain conditions. J. Mech. Phys. Solids 12, 337-351.

Spencer, A. J. M. (1971). Fully developed plastic shear flow of granular materials. Geotechnique 21, 190-192.

Spencer, A. J. M. and Kingston, M. R. (1973). Plane mechanics and kinematics

of compressible ideal granular materials. Rheol. Acta 12, 194-199.

Taylor, D. W. (1948). Fundamentals of soil mechanics. New York, J. Wiley and Sons.

Terzaghi, K. and Peck, R. B. (1948). Soil mechanics in engineering practice. New York, J. Wiley and Sons.

Youd, T. L. (1970). Densification and shear of sand during vibration. Jnl. Soil Mech. Fdn. Div. Am. Soc. Civ. Engrs. 96, SM3, 863-880.

Youd, T. L. (1972). Compaction of sands by repeated shear straining. Jnl. Soil Mech. Fdn. Div. Am. Soc. Civ. Engrs. 98, SM7, 709-725.

CHAPTER 5

ON DYNAMIC AND STATIC BEHAVIOR OF GRANULAR MATERIALS

1. INTRODUCTION

It is reasonable to expect that constitutive relations developed to cover a wide variety of material behavior under diverse loading conditions tend to be either so general that they cannot yield specific needed information, or they become too complicated to be of practical use. Therefore, it is both natural and necessary to attempt to develop for specific classes of materials under specific loading conditions simple constitutive descriptions which capture the essential physical features of the problem, while at the same time involve a minimum number of measurable material parameters, preferably amenable to physically meaningful identifications. On the other hand, while in science as contrasted to religion, old theories are continually disbanded in favor of simpler, more effective new doctrines, no great advantage is gained by abandoning established theories which can still be effective, but require minor modifications to achieve the esthetic appeal of intraconsistency.

In this chapter I shall illustrate this point of view by means of three examples that stem from some recent work at Northwestern University on static and dynamic behavior of granular materials.

The first is the small deformation version of finite deformation plasticity theory with plastic volumetric change and internal friction, that has been formulated for application to finite plastic flows of granular

materials, as well as porous metals (Nemat-Nasser and Shokooh, 1980). This theory provides a systematic and consistent basis for critical state soil mechanics (Schofield and Wroth, 1968) which has been criticized for some of its inconsistencies. For example, the concepts of normality and associative flow rule used in the theory do not accord with the notion of internal friction and plastic compressibility. The introduction of the nonassociative flow rule in the manner developed by Nemat-Nasser and Shokooh (1980) removes this inconsistency and at the same time provides a theory which contains parameters with clear physical definitions. The present kinematically linearized version of this theory is presented in notation common in soil mechanics in order to reach as wide an audience as possible.

The second example involves the phenomena of densification of granular masses and their possible liquefaction (when saturated and undrained) under cyclic shearing. Here, first by means of a simple dimensional analysis the essential features of the problem are brought into focus. Then several physically motivated assumptions are used in line with the work of Nemat-Nasser and Shokooh (1977, 1979), in order to obtain explicit expressions for the changes of the void ratio and the pore water pressure as functions of the number of cycles and other relevant parameters.

The final example concerns the methodology for a fundamental statistical approach to the description of the macroscopic response of granular masses on the basis of an examination of microstructural changes. This part is essentially a progress report on work that is being continued, although already some specific encouraging results have been obtained

(Christoffersen et al., 1980; Mehrabadi et al., 1980; Nemat-Nasser, 1980; Oda et al., 1980b).

No attempt will be made to give extensive references, as the cited few list a large number of relevant papers.

2. A PLASTICITY THEORY

2.1 Notation

A fixed rectangular Cartesian coordinate system with coordinate axes x_i, $i = 1, 2, 3$, is used. The macroscopic stress tensor (linearized), elastic strain tensor (linearized), and the plastic part of the strain tensor (linearized) are respectively denoted by, σ_{ij}, e_{ij}, and ε_{ij}, where the stress denotes only the effective part (i.e., the normal stresses are reduced by the pressure pore) of the stress, if the material is saturated with nonzero pore pressure; note that for simplicity, we do not use prime for this effective stress, nor superposed p for the plastic part of the strain. Henceforth we do not consider the elastic part of the strain and, therefore, all kinematical quantities will refer to the plastic part of the deformation. Also, all stresses refer to the effective part of the stress.

2.2 General Theory

The stress tensor is split into deviatoric (denoted by S_{ij}) and

spherical parts, as

$$\sigma_{ij} = S_{ij} + p\delta_{ij}, \quad p = \frac{1}{3}\sigma_{kk}, \quad i,j,k = 1,2,3 , \tag{2.1}$$

where repeated indices are summed and, as commonly used in soil mechanics, compression is viewed positive, p being the mean pressure.

We now introduce a yield function and a flow potential which are obtained by a minor but significant amendment to the commonly used J_2 flow potential:

$$f \equiv \bar{\sigma} - F(p,\theta,\bar{\varepsilon}), \text{ yield function;}$$

$$g \equiv \bar{\sigma} + G(p,\theta, \bar{\varepsilon}), \text{ flow potential,} \tag{2.2}$$

where

$$\bar{\sigma} = (\tfrac{1}{2} S_{ij} S_{ij})^{1/2}, \quad \theta = \varepsilon_{kk}, \quad \bar{\varepsilon} = \int_0^t (2\dot{\varepsilon}'_{ij}\dot{\varepsilon}'_{ij})^{1/2} dt; \tag{2.3}$$

here, θ is plastic volumetric strain, $\dot{\theta} = \dot{v}/v$ is the rate of volumetric strain per unit current volume, $\bar{\varepsilon}$ represents the effective* distortional plastic strain,

---

* In plasticity theory, $\bar{\sigma}$ and $\bar{\varepsilon}$ as defined by Eqs. $(2.3)_{1,3}$ are called the "effective" stress and strain, respectively; see Hill (1950). The term effective is also used in soil mechanics to denote stresses when the pore water pressure is subtracted from the normal stresses. The context should make it clear which usage is being implied in the present paper.

$\dot{\varepsilon}'_{ij}$ is the deviatoric part of the plastic strain, and t is a monotone increasing load parameter; superposed dot stands for the rate. The rate of plastic strain is

$$\dot{\varepsilon}_{ij} = \dot{\lambda} \frac{\partial g}{\partial \sigma_{ij}} = \dot{\lambda} \{\frac{S_{ij}}{2\bar{\sigma}} + \frac{1}{3} \frac{\partial G}{\partial p} \delta_{ij}\} \quad . \tag{2.4}$$

This and the consistency relation for the yield function, i.e. $\dot{f} = 0$, now give

$$\dot{\varepsilon}_{ij} = \frac{1}{H} \{\frac{S_{ij}}{2\bar{\sigma}} + \frac{1}{3} \frac{\partial G}{\partial p} \delta_{ij}\}\{ \frac{S_{k\ell}}{2\bar{\sigma}} - \frac{1}{3} \frac{\partial F}{\partial p} \delta_{k\ell}\} \dot{\sigma}_{k\ell} \tag{2.5}$$

which defines the plastic strain rate in terms of the corresponding stress rate. In (2.5) H is the workhardening parameter,

$$H = \frac{\partial G}{\partial p} \frac{\partial F}{\partial \theta} + \frac{\partial F}{\partial \bar{\varepsilon}} \tag{2.6}$$

which consists of two parts: (1) workhardening associated with volumetric strain,

$$h_1 = \frac{\partial G}{\partial p} \frac{\partial F}{\partial \theta} \tag{2.7}$$

which may be positive or negative and which will be referred to as <u>density-hardening</u>; and (2) workhardening associated with plastic distortion,

$$h = \frac{\partial F}{\partial \bar{\varepsilon}} \tag{2.8}$$

which is nonnegative. To gain insight into the implication of the density-hardening parameter, h_1, observe from (2.4) that

$$\frac{\partial G}{\partial p} = \left\{\frac{\bar{\sigma}}{S_{ij}\,\dot{\varepsilon}_{ij}}\right\}\dot{\theta} = \frac{\dot{\theta}}{\dot{\bar{\varepsilon}}} = \frac{d\theta}{d\bar{\varepsilon}}\,, \tag{2.9}$$

where the fact that $\bar{\sigma}\,\dot{\bar{\varepsilon}} = S_{ij}\,\dot{\varepsilon}_{ij}$ is used. Hence, the sign of $\partial G/\partial p$ follows the sign of $\dot{\theta}$, because $\bar{\sigma}$ and the rate of distortional plastic work, $S_{ij}\,\dot{\varepsilon}_{ij}$, are both positive.

We refer to $\partial G/\partial p$ as the dilatancy factor, and observe that since $\partial F/\partial\theta$ is always positive (hardening due to compaction), h_1 has the same sign as $\dot{\theta}$: hardening during densification, softening during dilatancy, and being zero at the critical state.

The quantity $\partial F/\partial p$ in (2.5) represents the overall macroscopic friction factor, and is always positive. This can be seen by keeping instantaneously θ and $\bar{\varepsilon}$ fixed in the yield function which, in view of the consistency relation $\dot{f} = 0$, then gives

$$\frac{d\bar{\sigma}}{dp} = \frac{\partial F}{\partial p} > 0, \tag{2.10}$$

where $\bar{\sigma}$ can be viewed as the octahedral effective shear stress. Note that, in this theory, the overall friction factor, $\partial F/\partial p$, need not be a constant, as it probably is not, especially under large hydrostatic pressures (Byerlee, 1975).

Equations (2.9) and (2.10) bring into focus the need for a nonassociative flow rule for consistent plasticity theories of dilatant frictional granular materials. An associative flow rule demands $F \equiv G$, which then results in $\partial G/\partial p = \partial F/\partial p$, which is a contradiction, as the dilatancy factor $\partial G/\partial p$, is essentially a geometrical quantity, being positive, negative, or zero, depending on the rate of volumetric strain per unit rate of distortional strain,

whereas the friction coefficient, $\partial F/\partial p$, is a strictly positive quantity. The two quantities are, however, related because of the condition of energy requirement: for rigid granules the total rate of plastic work must equal the total rate of frictional loss, both measured per unit volume.

The total rate of plastic work per unit volume is

$$\sigma_{ij}\,\dot{\varepsilon}_{ij} = S_{ij}\,\dot{\varepsilon}_{ij} + p\dot{\theta} \ , \tag{2.11}$$

whereas the rate of frictional loss may be taken to be proportional to the coefficient of friction, the pressure, and the rate of effective distortional strain, i.e.

$$\dot{w}_f \simeq \alpha \frac{\partial F}{\partial p}\, p\, \dot{\bar{\varepsilon}} \ , \tag{2.12}$$

where α is a parameter depending on the state of stress, e.g. $\alpha = 1$ for simple shear, and $\alpha \simeq \sqrt{3}$ in the triaxial case; this last choice of α is consistent with Eq. (4.25) of Nemat-Nasser and Shokooh (1980). From (2.1) and (2.12) it now follows

$$\frac{\partial G}{\partial p} = \alpha \frac{\partial F}{\partial p} - \frac{\bar{\sigma}}{p} \ , \tag{2.13}$$

where (2.9) is used.

The critical state is defined by $\dot{\theta} = \partial G/\partial p = 0$. Hence, $(2.13)_1$ yields for $\dot{\theta} = 0$,

$$\alpha \frac{\partial F}{\partial p} - \frac{\bar{\sigma}}{p} = 0 \tag{2.14}$$

which is a curve in the $\bar{\sigma}$,p-plane, characterizing the critical states; see Fig. 2.1. Points above this curve correspond to states with a negative dilatancy factor (dilatation), and points below this curve are associated with positive $\dot{\theta}$ (compaction).

From the definition of the void ratio, $e = v_v/v_s$, $v = v_v + v_s$, it follows that

$$\dot{\theta} = -\frac{\dot{e}}{1+e} \quad , \tag{2.15}$$

where the minus sign is because the void ratio decreases in compaction for which $\dot{\theta}$ is regarded positive. Substitution from (2.9) and integration with respect to $\bar{\varepsilon}$, now results in

$$\begin{aligned} e &= (1 + e_0) \exp \{-\int_0^{\bar{\varepsilon}} \frac{\partial G}{\partial p} \, d\bar{\varepsilon}\} - 1 \\ &= (1 + e_0) \exp \{-\int_0^{\bar{\varepsilon}} [\alpha \frac{\partial F}{\partial p} - \frac{\bar{\sigma}}{p}] \, d\bar{\varepsilon}\} - 1 \quad , \end{aligned} \tag{2.16}$$

where e_0 is the initial void ratio; this equation is consistent with Eq. (4.19) of Nemat-Nasser and Shokooh (1980).

2.3 General Qualitative Results

The theory presented above includes the general behavior of loose as well as dense sand in simple shearing as well as in triaxial tests (monotonic loading only). Both cases can be discussed simultaneously in terms of the effective stress, $\bar{\sigma}$, and the effective distortional strain, $\bar{\varepsilon}$, which, however, will have a different meaning in each case.

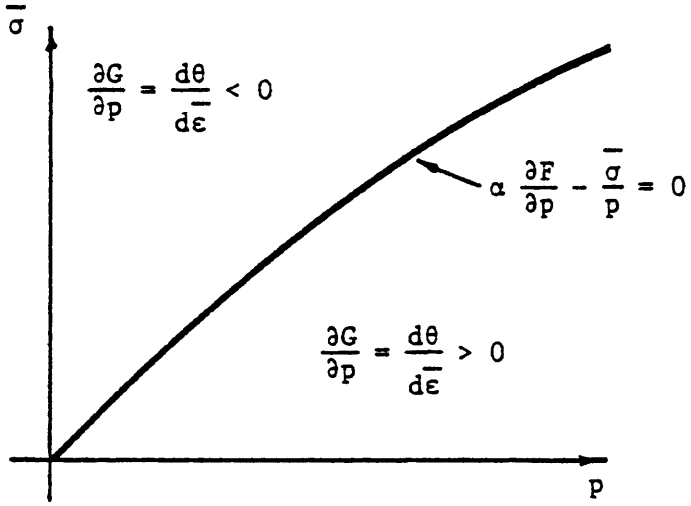

Fig. 2.1. The critical curve in the $\bar{\sigma}$,p-plane.

For pure shear, the state of stress is defined by

$$\sigma_{11} = \sigma_{22} = \sigma_{33} = p \ ,$$

$$\sigma_{12} = \sigma_{21} = \tau \ , \quad \sigma_{23} = \sigma_{31} = 0 \ . \tag{2.17}$$

Hence $\bar{\sigma} = \tau$. The strain rates, moreover, are defined by volumetric strain rate, $\dot{\theta}$, and by the only nonzero shear strain rate, $\dot{\varepsilon}_{12}$. Hence, $\dot{\bar{\varepsilon}} = 2\dot{\varepsilon}_{12}$, which is the rate of engineering shear strain.

For the triaxial state of stress, on the other hand,

$$\sigma_{11} = \sigma_1 \ , \quad \sigma_{22} = \sigma_{33} = \sigma_2 \ , \tag{2.18}$$

with all other stress components being zero. The corresponding strain rates are,

$$\dot{\varepsilon}_{11} = \dot{\varepsilon}_1 , \quad \dot{\varepsilon}_{22} = \dot{\varepsilon}_{33} = \dot{\varepsilon}_2 \ , \tag{2.19}$$

with all other strain rate components being zero. In this case, therefore, $\bar{\sigma} = \frac{\sqrt{3}}{3}(\sigma_1 - \sigma_2)$, and $\dot{\bar{\varepsilon}} = \frac{2\sqrt{3}}{3}(\dot{\varepsilon}_1 - \dot{\varepsilon}_2)$.

Since $\bar{\varepsilon}$ is a monotone increasing parameter, it is used as the "time parameter" and therefore, all superposed dots denote differentiation with respect to $\bar{\varepsilon}$. In particular, it follows that $\dot{\lambda} = \dot{\bar{\varepsilon}} = 1$.

Consider the yield function and note from $\dot{f} = 0$,

$$\frac{d\bar{\sigma}}{d\bar{\varepsilon}} - \frac{\partial F}{\partial p}\frac{dp}{d\bar{\varepsilon}} = H = \frac{\partial G}{\partial p}\frac{\partial F}{\partial \theta} + \frac{\partial F}{\partial \bar{\varepsilon}} = \left(\alpha \frac{\partial F}{\partial p} - \frac{\bar{\sigma}}{p}\right)\frac{\partial F}{\partial \theta} + \frac{\partial F}{\partial \bar{\varepsilon}} \tag{2.20}$$

which is a general differential equation giving the variation of stress in terms of the effective strain $\bar{\varepsilon}$. This equation together with Eq. (2.16), models very nicely the behavior of loose, as well as densely packed, granular materials, both in pure shear and in triaxial tests.

To illustrate this fact, consider the case of constant pressure test; the other cases can easily be studied in a similar manner. Then, $dp/d\bar{\varepsilon} = 0$, and Eq. (2.20) can be written as

$$\frac{d\bar{\sigma}}{d\bar{\varepsilon}} = (aM + h) - \frac{a}{p}\bar{\sigma} \ , \tag{2.21}$$

where the following notation is used:

$$a = \frac{\partial F}{\partial \theta} > 0, \quad M = \alpha \frac{\partial F}{\partial p} > 0 \ , \tag{2.22}$$

and where h is defined by (2.8).

Since h denotes distortional hardening, it may be assumed to depend only on the distortional strain $\bar{\varepsilon}$,

$$h = \hat{h}(\bar{\varepsilon}) \ . \tag{2.23}$$

Then, depending on how fast the function $\hat{h}$ decays to zero with increasing $\bar{\varepsilon}$, differential Eq. (2.21) displays in the $\bar{\sigma}$, $\bar{\varepsilon}$-plane the loosely or densely packed granular material behavior. Figure 2.2a illustrates two possible cases for the variation of $\hat{h}$, and Fig. 2.2b gives the corresponding stress-strain relations.

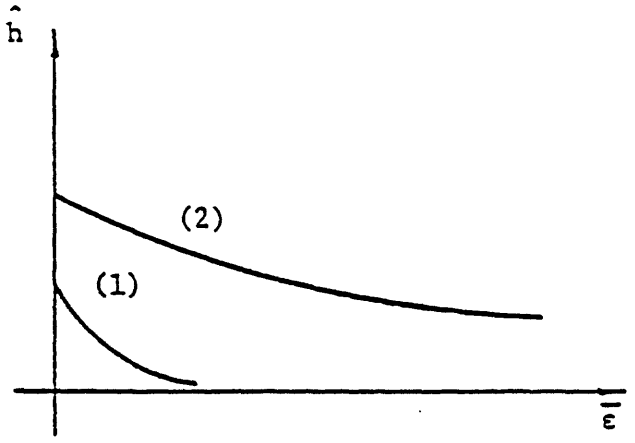

(a) Possible variations of the distortional hardening parameter, $\hat{h}$

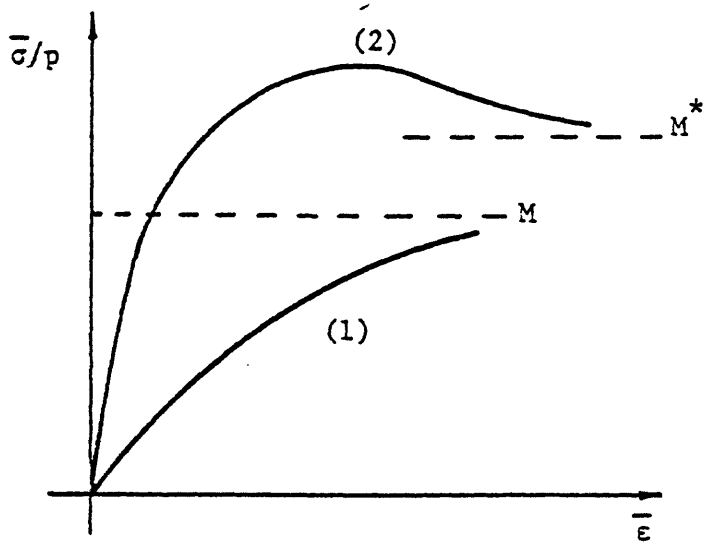

(b) Stress-strain relations

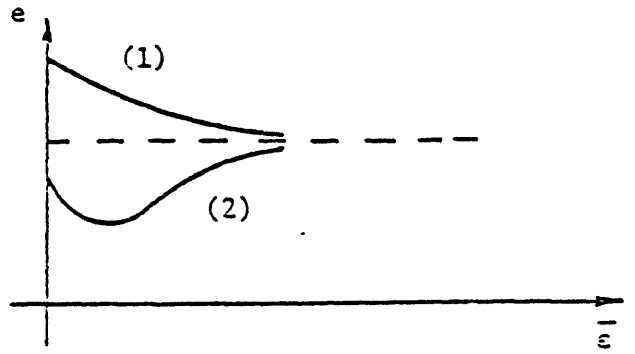

(c) Variation of void ratio with distortional strain

Fig. 2.2.

Note: Curves marked (1) are for loose sands;
Curves marked (2) are for dense sands.

It is seen that when the material is very loose, little distortional hardening exists, as the particles have more freedom to move relative to each other. In this case the distortional hardening is insignificant as compared with the density hardening. This results in Curve 1 of Fig. 2.2b. From Eq. (2.16) the corresponding variation of the void ratio is easily seen to be as shown by Curve 1 in Fig. 2.2c.

When the material is densely packed, on the other hand, the distortional hardening remains a dominant factor. Its variation with $\bar{\varepsilon}$ may take on a form schematically shown by Curve 2 of Fig. 2.2a. In this case, the critical state is first reached when $\bar{\sigma}/p = M$, at which point the right-hand side of (2.21) is still positive, and therefore, $\bar{\sigma}$ continues to increase to a peak value, and then decreases as the right-hand side of (2.21) becomes negative. This continues, and the curve approaches asymptotically the limiting value,

$$\lim_{\bar{\varepsilon}\to\infty} \{M + \frac{h}{a}\} = M^* \ ; \tag{2.24}$$

see Curve 2 of Fig. 2.2b. The corresponding variation of the void ratio is shown by Curve 2 of Fig. 2.2c.

The model can easily be modified to include the effect of cohesion, as discussed by Nemat-Nasser and Shokooh (1980). Also, it is well known that the strain rate tensor, in general, is noncoaxial with the stress tensor, for dilatant frictional materials. This fact is examined from a more fundamental basis in Section 4. Here, however, it should be noted that one may modify Eq. (2.5) to read

$$\dot{\varepsilon}_{ij} = \frac{1}{H} \{\frac{\sigma'_{ij}}{2\bar{\sigma}} + \frac{1}{3}\frac{\partial G}{\partial p}\delta_{ij}\} \{\frac{\sigma'_{k\ell}}{2\bar{\sigma}} - \frac{1}{3}\frac{\partial F}{\partial p}\delta_{k\ell}\} \dot{\sigma}_{k\ell} + D_{ijk\ell}(\bar{\varepsilon}, \theta)\dot{\sigma}_{k\ell} \ , \tag{2.25}$$

where $D_{ijk\ell}$ may be viewed as an "effective secant compliance" tensor depending on the effective distortional strain, as well as on the volumetric strain. For example, if it is required that this additional term should not affect the definition of dilatancy, (2.9), and have no contribution to the rate of distortional work, then it may be taken as

$$D_{ijk\ell} = A[\delta_{ij}\,\delta_{k\ell} - \frac{1}{2\bar{\sigma}^2}\,\sigma'_{ij}\,\sigma'_{k\ell}]\overset{\nabla}{\sigma}'_{k\ell} \tag{2.26}$$

where A is a function of $\bar{\epsilon}$ and θ, and $\overset{\nabla}{\sigma}_{k\ell}$ is the co-rotational stress rate; see $(4.17)_1$. It has been argued in the literature (Rice, 1977; Rudnicki and Rice, 1975), that modifications of this kind represent the vertex yield function.

2.4 Unloading and Change of Fabric

In the above discussion, no unloading has been considered. It is an experimental fact that there is always some strain recovery during unloading. This strain recovery may be partly elastic unloading and partly inelastic unloading due to (dissipative) rearrangement of grains, when cohesionless elastic granules are involved. Even if the granules are assumed to be rigid, so that there is no elasticity involved, a small incremental load reduction (unloading) is accompanied by some strain recovery. Traditionally, it has been convenient to regard this as elastic unloading; however, in reality, it stems from microstructural changes due to the changes of the "fabric", and in fact, it involves a dissipative, thermodynamically irreversible process. In fact, for a collection of rigid granules, any deformation is plastic, be it during continuous loading, or as a result of strain recovery in unloading.

This is a fundamental question relating to the basic micromechanical behavior of granular masses. It has been recently examined by this writer and coworkers in the context of a statistical approach, where the notion of fabric tensor has been introduced and has been related to the macroscopic stress tensor, see Mehrabadi et al. (1980) and Oda et al. (1980b).

3. LIQUEFACTION AND DENSIFICATION OF COHESIONLESS SAND

3.1 Notation

Attention is focused on cyclic shearing at constant confining pressure. Therefore, the state of stress is as defined by Eq. (2.17). Hence, for simplicity, the applied stress and the (constant) confining pressure are denoted by $\hat{\tau}$ and σ_c, respectively, and the corresponding sheer strain (engineering) is denoted by γ. The pore water pressure is designated by $\hat{p}_w$, and the following dimensionless quantities are used:

$$\tau = \hat{\tau}/\sigma_c, \quad p_w = \hat{p}_w/\sigma_c \ . \tag{3.1}$$

3.2 General Discussion

When a sample of cohesionless sand is subjected to cyclic shearing under a fixed confining pressure, the grains are moved relative to each other, and because of the action of confining pressure, the sample tends to densify after each cycle. If the sample is saturated and is undrained, the tendency toward densification causes an increase in pore water pressure, and therefore a decrease in the interparticular contact forces. When the pore water pressure

increases to a value close to that of the confining pressure, the interparticular contact forces become very small, and therefore, the corresponding frictional resistance is rendered small: the overall shear resistance of the material tends to become negligibly small, i.e. the sample tends to liquefy.

If, on the other hand, drainage is provided, and the cyclic shearing is performed at low frequencies, the sample densifies with the increase in the number of cycles, resulting in an increase in its shear resistance.

Here we shall illustrate how a simple model can be generated, which would encompass the basic physical features of the phenomenon, and therefore can have effective predictive value.

3.3 Dimensional Analysis

Let e_0 and e_m be, respectively, the initial and the minimum values of the void ratio for the considered sample. It is clear that, as the relative void ratio, $e_0 - e_m$, increases, the potential for liquefaction increases. In fact, if the grains are assumed to be rigid, no liquefaction can take place, if $e_0 = e_m$.

With this in mind, we observe that the basic dimensionless parameters relevant for a first-order of approximation theory of liquefaction in cyclic shearing, are: dimensionless applied shear stress amplitude, τ_0; pore pressure (measured at the end of each cycle), p_w; the relative void ratio, $e_0 - e_m$; and the number of cycles, N. Therefore, it is reasonable to expect that

$$F(\tau_0, p_w, e_0 - e_m, N) = C \tag{3.2}$$

should define the relation between the stated dimensionless parameters, where the constant C may, however, depend on the initial void ratio e_0. The simplest form for this equation would be

$$\tau_0^a (e_0 - e_m)^c N = A_0 P(1 + p_w), \quad a,b > 1, \tag{3.3}$$

where positive exponents a and b must exceed 1, so that if a larger shear stress amplitude is used, or when initially looser sand is involved, then a fewer number of cycles would be required to attain the same pore pressure under the same confining pressure. A_0 on the right-hand side is a parameter which could only depend on the initial void ratio e_0. The function $P(1 + p_w)$ must be such that

$$P(1) = 1 , \quad P' \geq 0, \quad P'' \leq 0 . \tag{3.4}$$

The first condition corresponds to the initial state $p_w = 0$ at $N = 0$, and the second two conditions guarantee that positive work is required to increase the pore pressure and that this increase results in less resistive materials (this is discussed further in the sequel). Note that, since A_0 is an as yet unspecified parameter, without a loss in generality, the exponent of N in (3.3) is chosen to be 1.

When a drained condition is involved, then the densification can be characterized by the following modified version of (3.3):

$$\tau_0^a (e - e_m)^b N = A_0 , \tag{3.5}$$

where e now is the void ratio after N cycles of cyclic shearing at constant

dimensionless shear stress amplitude τ_0.

From (3.3), liquefaction occurs when $p_w = 1$, so that $P(2) = P_\ell$ at $N = N_\ell$. From (3.5), on the other hand, the change in void ratio e can be calculated in response to a given number of cyclic shearings. In this case, most experiments are performed for cyclic shearing at constant strain amplitude, γ_0, rather than at constant stress amplitude. If we assume that

$$\tau_0 = A_1\gamma_0^{a1} + A_2\gamma_0^{a2} + \ldots, \tag{3.6}$$

then we can substitute for τ_0 into (3.5). We note that the exponents a_1 and a_2, ..., must all be positive and odd fractions so that the shear stress amplitude versus the shear strain amplitude will be a centrally symmetric curve in the τ_0,γ_0-plane.

The above approach, although quite straight-forward, does not bring the physics of the process to heavily bear on the mathematical model. In the sequel a physical approach is presented, from which equations similar to (3.3) and (3.4) emerge in a natural manner.

3.4 An Energy Approach

Based on an energy consideration, a unified densification and liquefaction theory for cohesionless sand in cyclic shearing has been developed by Nemat-Nasser and Shokooh (1977, 1978, 1979). Here, a brief summary of the theory is presented and results are compared with the above development.

To this end we first make the following physically obvious observations:

1. To change the void ratio from its current value e to e + de, an increment of energy dW is required for rearranging the sand

grains (microstructural rearrangement);

2. This increment of energy dW increases as the void ratio approaches e_m;
3. Since an increase in the excess pore water pressure p_w results in a decrease in the intergranular forces, the required incremental energy dW decreases with increasing p_w.

Based on these we may write

$$dW = - \tilde{\nu} \frac{de}{f(1 + p_w)g(e - e_m)} \quad , \tag{3.7}$$

where $\tilde{\nu}$ is a positive parameter, and the functions f and g are such that

$$f(1) = 1, \quad f' \geq 0, \quad g(0) = 0, \quad g' \geq 0 \ . \tag{3.8}$$

Since

$$de = - \frac{e\sigma_c}{\kappa_w} dp_w \quad , \tag{3.9}$$

where κ_w is the bulk modulus of water, (3.7) can also be expressed as

$$dW = \frac{\nu}{\kappa_w} \frac{e\, dp_w}{f(1 + p_w)g(e - e_m)} \quad , \tag{3.10}$$

where $\nu = \tilde{\nu}\, \sigma_c = \nu(\sigma_c)$, i.e. a parameter which depends on the confining pressure.

For densification of drained sample $p_w = 0$, and (3.7) becomes

$$dW = -\tilde{\nu} \frac{de}{g(e - e_m)} \tag{3.11}$$

which upon integration yields

$$\Delta W = -\tilde{\nu} \int_{e_0}^{e} \frac{dx}{g(x - e_m)} \quad , \tag{3.12}$$

where ΔW is the total energy required to change the void ratio from e_0 to its current value e.

For liquefaction, we first integrate (3.9) to obtain

$$e = e_0 \exp \{- \frac{\sigma_c}{\kappa_w} p_w\} \quad , \tag{3.13}$$

where it is assumed that initially $p_w = 0$. With the aid of (3.13), Eq. (3.10) can now be integrated. But since σ_c/κ_w for pressures of several bars, is so small that $e \simeq e_0$ in (3.13), we may simplify the calculations considerably (but without a loss in accuracy) by using e_0 instead of e in Eq. (3.10). Then upon integration, it follows that

$$\Delta W = \frac{\nu e_0}{g(e_0 - e_m)} \int_0^{p_w} \frac{dx}{f(1 + x)} \quad . \tag{3.14}$$

To obtain explicit results, we use approximate expressions for functions g and f in such a manner that (3.8) is satisfied. Simplest functions of this kind are

$$g(e - e_m) \equiv (e - e_m)^n \quad , \qquad n > 1 \quad ,$$

$$f(1 + p_w) \equiv (1 + p_w)^r \quad , \qquad r > 1 \quad . \tag{3.15}$$

With these expressions, Eqs. (3.12) and (3.14) upon integration respectively yield

$$e = e_m + [(e_0 - e_m)^{1-n} + \bar{\nu}\,\Delta W]^{\frac{1}{1-n}}, \qquad n > 1, \tag{3.16}$$

and

$$\Delta W = \frac{\hat{\nu} e_0}{(e_0 - e_m)^n}\left[1 - (1 + p_w)^{1-r}\right], \qquad r > 1, \tag{3.17}$$

where we have set $\bar{\nu} = (n - 1)/\tilde{\nu}$, and $\hat{\nu} = \nu/(r - 1)\kappa_w$, respectively.

To complete the solution, we must now estimate the energy loss ΔW. In a cyclic shearing, ΔW can be related to the area of hysteretic loop and the number of cycles (Nemat-Nasser and Shokooh, 1979). Here two cases may be distinguished: (1) large amplitude shearing; and (2) small amplitude shearing, each either stress- or strain-controlled tests.

When the amplitude of shearing is large enough, all the particles are mobilized during each cycle, and hence the energy loss in each cycle is not very much dependent on the previous cycles. In this case we may assume that ΔW is proportional to the number of cycles, N. For very small amplitude shearing, on the other hand, the particles are only partially mobilized in each cycle, and hence the energy loss changes from cycle to cycle as the particles gradually take on new (more stable) positions relative to each other.

A series of experimental results on cyclic shearing of cohesionless sands, has been carefully examined by Nemat-Nasser and Shokooh (1979), and because of the observed symmetry of the hysteretic loop, it has been concluded that the area of hysteretic loop in the i^{th} cycle may be approximated by $A_i = h_i \tau_0^{1+\alpha}$,

where α must be an even positive integer (because of the symmetry), and h_i is an increasing function of the number of cycles. Hence, for stress-controlled tests, it follows that

$$\Delta W = \sum_{i=1}^{N} \lambda_i \, h_i \, \tau_0^{1+\alpha} = \tau_0^{1+\alpha} \sum_{i=1}^{N} \lambda_i \, h_i$$

$$= \hat{h}(N) \, \tau_0^{1+\alpha} \, . \tag{3.18}$$

Moreover, for large stress amplitudes, we may assume

$$\Delta W \simeq h \, N \, \tau_0^{1+\alpha} \, . \tag{3.19}$$

From (3.19) and (3.17) it now follows that

$$\tau_0^{1+\alpha} \, (e_0 - e_m)^n \, N = \hat{\nu} \, e_0 [1 - (1 + p_w)^{1-r}] \, , \tag{3.20}$$

where $\hat{\nu} = \nu/h$. Since α is even, it can easily be fixed by inspection of experimental results. For cohesionless samples considered by De Alba et al. (1975), it is immediately seen that $\alpha = 4$. Moreover, this result is not very sensitive to small variations in the other parameters. For example for De Alba et al.'s (1975) experiments, n and r in (3.20) may be chosen in the ranges of 3 to 4 and 2 to 3, respectively, and hence $n = 3.5$ and $r = 2.5$ were selected for comparison with the considered experimental results. The parameter $\hat{\nu}$ then turned out to be a constant which did not vary much from test to test over a wide range of sample densities (Nemat-Nasser and Shokooh, 1979).

A loss of total bearing capacity occurs momentarily, when the pore pressure equals the confining pressure, so that $p_w = 1$ in (3.20). If the number

of cycles to this liquefaction is denoted by N_ℓ, then (3.20) yields

$$\tau_0^{1+\alpha} = \frac{\eta\, e_0}{N_\ell (e_0 - e_m)^n} \quad , \tag{3.21}$$

where η is a constant. This equation has been compared with experimental results (Nemat-Nasser and Shokooh; 1977, 1979), and it has been verified that over a wide range of densities, η indeed appears to be a constant which, of course, would depend on the material, the grain distribution, and the confining pressure. Figure 3.1 is a typical result (Nemat-Nasser and Shokooh; 1977, 1979).

If α is taken to equal 4 (or any other positive even number), and since $n > 1$, it follows from (3.21) that,, for the same number of cycles to liquefaction, the dimensionless shear stress amplitude increases, as the initial void ratio approaches its minimum value; in fact, for void ratios close to the minimum (very dense send) a very large shear stress amplitude (approaching infinity as e_0 approaches e_m) is required. Moreover, since τ_0 is normalized with respect to the confining pressure, (3.21) again shows that, for the same number of cycles to liquefaction, the dimensional shear stress amplitude is proportional to the confining pressure. These are results which are confirmed both experimentally and by field investigations.

It is possible to relate the shear strain amplitude to the number of cycles and the shear stress amplitude during liquefaction of undrained sand. This is discussed by Nemat-Nasser and Shokooh (1978), where comparisons with experimental results are also made.

For strain-controlled tests, one may use Eq. (3.6) in (3.19). However, as a first-order-approximation, it has been found adequate to take

$$\tau_0 = K\, \gamma_0^{1/\beta}, \tag{3.22}$$

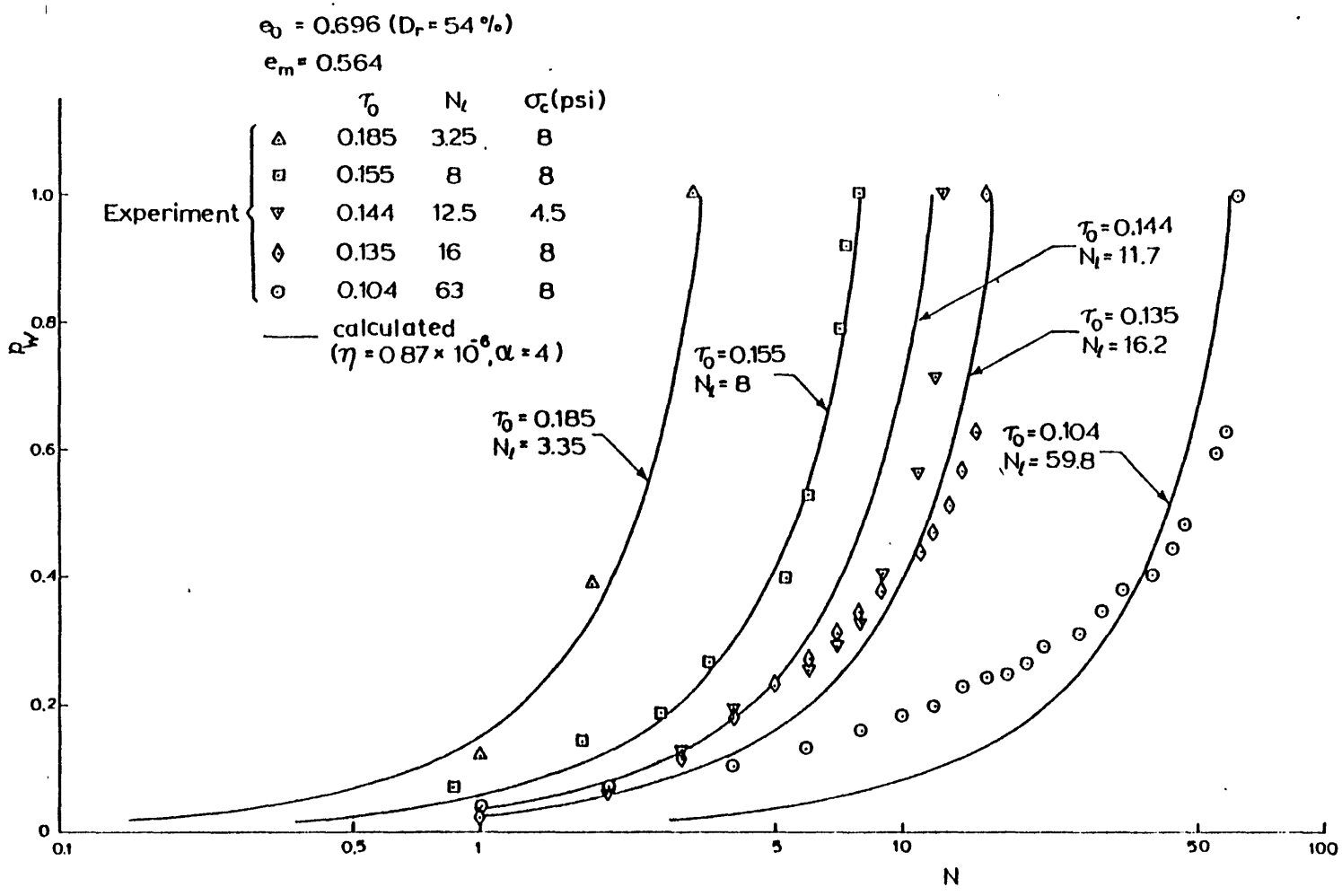

Fig. 3.1. Normalized pore water pressure, p_w, in terms of the number of cycles, N, for indicated values of the normalized shear stress amplitude.

where β must be an odd positive integer. This then gives

$$\Delta W \sim \hat{k}(N)\ \gamma_0^{\frac{1+\alpha}{\beta}} \quad . \tag{3.23}$$

Extensive comparison with experimental results for densification has been made (Nemat-Nasser and Shokooh; 1977, 1979), employing (3.23) with $\hat{k}(N) = k_0 N$ for large strain amplitudes ($\gamma_0 > 0.1\%$), and $\hat{k}(N) = k_0\sqrt{N}$ for small strain amplitudes ($\gamma_0 < 0.1\%$), where $n = 3.5$, $\alpha = 4$, and $\beta = 5$ have been used.

4. MICROMECHANICAL APPROACH

If one assumes that individual grains are rigid and their mutual interaction involve only friction over the contacting regions, then it is reasonable to expect that the overall macroscopic quantities, such as stress, strain, and their rates should be expressible in terms of the relevant microscopic quantities by means of a systematic averaging process. A fundamental program of this kind has been recently initiated by the writer and his associates, where several preliminary but significant results have been obtained (Christoffersen et al., 1980; Mehrabadi et al., 1980; Nemat-Nasser, 1980; Oda et al., 1980a,b). In particular, explicit results for the overall stress tensor, the strain rate and spin tensors, and the macroscopic equations for the dilatancy phenomenon and the noncoaxiality of the stress and strain rates have been developed. In the sequel some of the results are briefly summarized, where attention is focused on the two-dimensional (plane strain) case; for simplicity, two-dimensional, rod-like granules may be envisaged.

4.1 Overall Stress Tensor

To develop overall stresses in terms of contact forces, the principle of virtual work can be used as an effective tool. To this end, let there be N

contacts in a typical, suitably large volume, V, of sample (chosen as unit volume), denote the contact forces at a typical contact α by f_i^α, let the vector which connects the centroid of, say, grain A to the centroid of grain B that are contacting at α, be denoted by $\underset{\sim}{\ell}^\alpha$. Then, following the development outlined by Christoffersen et al. (1980), it is easy to show that the average stress tensor is describable as

$$\bar{\sigma}_{ij} \equiv \int_V \sigma_{ij}\, dV = \sum_{\alpha=1}^{N} f_i^\alpha \ell_j^\alpha \,. \tag{4.1}$$

If, moreover, it is assumed that the rotation of individual grains coincides with the overall macroscopic rotation field evaluated at the corresponding contact point, then the stress tensor becomes symmetric and one has

$$\bar{\sigma}_{ij} = \frac{1}{2} N \, \langle f_i \ell_j + f_j \ell_i \rangle \,,$$

$$\langle f_i \ell_j - f_j \ell_i \rangle = 0 \,, \tag{4.2}$$

where the notation

$$\frac{1}{N} \sum_{\alpha=1}^{N} f_i^\alpha \ell_j^\alpha \equiv \langle f_i \ell_j \rangle \tag{4.3}$$

is used.

In the work by Mehrabadi et al. (1980), the implications of Eqs. (4.2) and their relation with average tractions defined in terms of the resultant contact forces transmitted across an imagined plane, are examined in detail. In particular, it is shown that the definition of overall stress in terms of the virtual work method

coincides with that developed with the aid of average tractions transmitted across imagined planes. Moreover, the stress tensor is related to the fabric tensor which characterizes the microstructure of the grain configuration (Christoffersen et al., 1980; Mehrabadi et al., 1980; Oda et al., 1980b).

At each contact, introduce the unit contact normal, $\underset{\sim}{n}$, the unit vector, $\underset{\sim}{s}$, normal to $\underset{\sim}{n}$, as shown in Fig. 4.1, and consider the following notation:

$$\mu = \tan \phi, \quad b = \tan \theta, \quad t = f \ell \cos \phi \sin \theta, \tag{4.4}$$

where f and ℓ are the magnitudes of the contact force and the vector $\underset{\sim}{\ell}$, respectively; the superscript α is dropped for simplicity. Then, it is easy to show that

$$\bar{\sigma}_{ij} = N \langle t[\mu b \delta_{ij} + (1 - \mu b) n_i n_j + \tfrac{1}{2}(\mu + b)(n_i s_j + n_j s_i)] \rangle \ . \tag{4.5}$$

Moreover, the symmetry of the stress tensor results in

$$\langle f \ell \sin(\phi - \theta) \rangle = 0 \ . \tag{4.6}$$

From (4.5) it follows that

$$\bar{\sigma}_{kk} = N \langle f \ell \cos(\theta - \phi) \rangle \ . \tag{4.7}$$

4.2 Overall Kinematics

To obtain the overall kinematics, we observe that the rate of change of vector $\underset{\sim}{\ell}$ corresponding to a typical contact α (the superscript α is dropped for

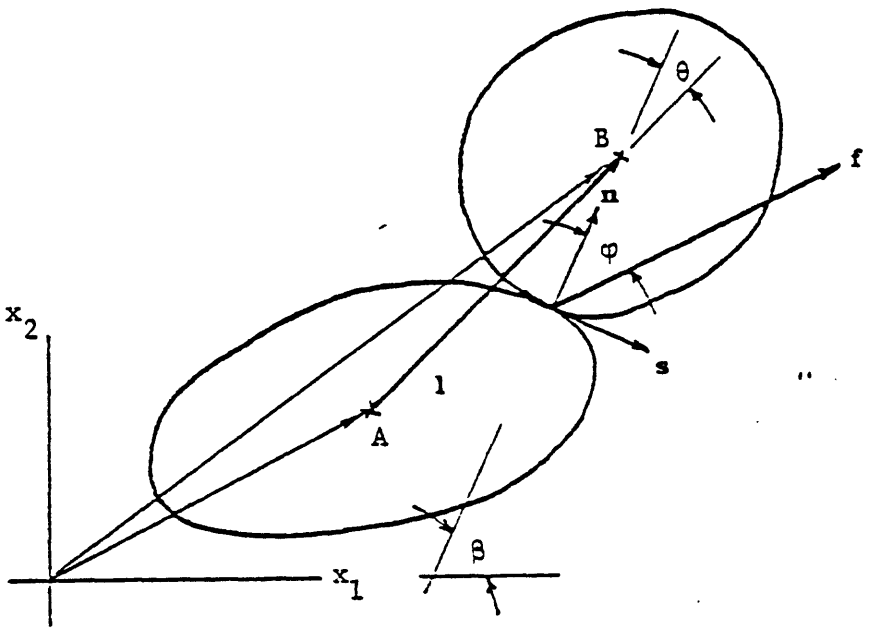

Fig. 4.1. Two contacting granules (A and B).

simplicity) can be written as

$$\dot{\ell}_i = \left(\frac{\dot{\ell}}{\ell}\,\delta_{ij} + r_{ij}\right)\ell_j \ , \tag{4.8}$$

where the rotation matrix, r_{ij}, may be expressed as

$$r_{ij} = \dot{\Omega}(s_i n_j - s_j n_i), \quad \dot{\Omega} = \dot{\nu} + \dot{\theta} \ , \tag{4.9}$$

where ν is the angle formed by the contact unit normal, $\underset{\sim}{n}$, with the x_1-axis. Equation (4.8) can be interpreted as $\dot{\ell}_i = L_{ij}\,\ell_j$, where L_{ij} is the local deformation rate tensor. To solve this expression for L_{ij}, we note that this quantity can be defined only to within a vector perpendicular to the vector $\underset{\sim}{\ell}$. This is an important observation, since the additional undefined quantity is exactly needed in order to provide a compatible overall deformation rate. Hence, we obtain for, say, the contact α,

$$L_{ij} = \frac{\dot{\ell}}{\ell}\,\delta_{ij} + r_{ij} + \dot{\gamma}k_i(\cos\theta\ s_j - \sin\theta\, n_j), \tag{4.10}$$

where $\underset{\sim}{k}$ is any unit vector, and $\dot{\gamma}$ is a yet unspecified angular rate.

The overall deformation rate tensor (the velocity gradient) is then obtained by averaging, i.e.

$$\overline{L}_{ij} = \langle L_{ij} \rangle \ , \tag{4.11}$$

so that the macroscopic overall strain rate and the spin tensors are given by

$$\dot{\bar{\varepsilon}}_{ij} = \frac{1}{2}(\bar{L}_{ij} + \bar{L}_{ji}), \quad \dot{\bar{\omega}}_{ij} = \frac{1}{2}(\bar{L}_{ij} - \bar{L}_{ji}) \ ; \tag{4.12}$$

the detailed results are given in the work by Christoffersen et al. (1980) and will not be presented here.

4.3 Energy Balance

Since the only source of dissipation is friction, the rate of stress-work, $\bar{\sigma}_{ij}\,\dot{\bar{\varepsilon}}_{ij}$, can be expressed by

$$\bar{\sigma}_{ij}\,\dot{\bar{\varepsilon}}_{ij} = N\,\langle(\underset{\sim}{f}\cdot\underset{\sim}{s})(\underset{\sim}{\ell}^{*}\cdot\underset{\sim}{s})\rangle \ , \tag{4.13}$$

where $\underset{\sim}{\ell}^{*}$ is the rate of change of $\underset{\sim}{\ell}$ observed in a coordinate system corotational with it, i.e.

$$\underset{\sim}{\ell}^{*} = \frac{\dot{\ell}}{\ell}\,\underset{\sim}{\ell} \ . \tag{4.14}$$

In terms of notation introduced in previous subsections, the rate of dissipation becomes

$$\bar{\sigma}_{ij}\,\dot{\bar{\varepsilon}}_{ij} = N\,\langle f\,\dot{\ell}\,\sin\theta\,\sin\phi\rangle \ . \tag{4.15}$$

It has been observed experimentally that, as granular masses deform, they momentarily form clusters consisting of instantaneously mutually immobile granules. This is true even for granular masses consisting of, say, spherical granules. In general, clusters are not spherical, and therefore, even for spherical granules anisotropic behavior exists. Equation (4.15) shows this fact, because, if the clusters were spherical, then $\dot{\ell}$ would be zero, and there

would be no energy dissipation. Note that, when clusters of mutually immobile grains constitute a unit granule, then $\underset{\sim}{\ell}$ is the vector connecting the centroid of two adjacent contacting clusters.

4.4 Dilatancy and Noncoaxiality

The plasticity theory presented in Section 2 gives a dilatancy equation which is in good accord with observation. However, it yields a strain rate coaxial with stress unless this is excluded by the additional term in the manner given in Eq. (2.25). The microscopic development, however, provides us not only with a dilatancy equation, but also with another equation which clearly shows noncoaxiality of the stress and the strain rate. These are obtained from the observation that the quantities $\langle n_i n_j \rangle$ and $\langle n_i s_j + n_j s_i \rangle$ are not independent. The detailed development is presented in the work by Christoffersen et al. (1980). The final equations are:

$$(\sin^2\phi - R^2)\,\frac{\bar{\sigma}_{ij}\,\dot{\bar{\varepsilon}}'_{ij}}{\tau} = R\cos^2\phi\,\dot{\bar{\varepsilon}}_{kk},$$

$$\bar{\sigma}_{ik}\,\overset{\nabla}{\bar{\sigma}}_{kj} - \overset{\nabla}{\bar{\sigma}}_{ik}\,\bar{\sigma}_{kj} = \frac{2\tau}{R}\,(\bar{\sigma}_{ik}\,\dot{\bar{\varepsilon}}_{kj} - \dot{\bar{\varepsilon}}_{ik}\,\bar{\sigma}_{kj}), \tag{4.16}$$

where

$$\overset{\nabla}{\bar{\sigma}}_{ij} = \dot{\bar{\sigma}}_{ij} - \Omega_{ik}\bar{\sigma}_{kj} - \Omega_{jk}\,\bar{\sigma}_{ki}\,,$$

$$\Omega_{12} = -\,\Omega_{21} = \dot{\bar{\omega}}_{12} - \langle\dot{\beta} + \dot{\theta}\rangle - \dot{\psi}\,,$$

$$R = \tau/p\,, \quad \tan 2\psi = \frac{2\,\bar{\sigma}_{12}}{\bar{\sigma}_{11} - \bar{\sigma}_{22}}\,, \tag{4.17}$$

and where τ is the maximum shear stress; see Fig. 4.1 for definition of β and θ.

4.5 Concluding Comments

It is clear that the development summarized in this section is fundamental and should provide guidance for the formulation of constitutive relations for granular materials. It can be generalized to include the elasticity of the granules, the cohesive forces that may exist between the grains, the possibility of rate dependent inelastic deformations of clusters of granules (e.g. in clay), and other relevant physical features. The author and his associates are pursuing these questions at this time. However, one of the most important outstanding problems that requires careful attention is the calculation of the stress rate in terms of the strain rate. This requires a knowledge of the manner by which new contacts are formed and some existing contacts are lost, as the deformation proceeds. In other words, we need to know the evolution of the distribution of contacts and their unit normals. While some theoretical conclusions can be obtained on the basis of reasonable simple assumptions, experiments must provide general guidance. The main problem is to identify the manner by which the "fabric" changes in the course of deformation (Christoffersen et al., 1980; Mehrabadi et al., 1980; Oda et al., 1980a,b).

REFERENCES

Byerlee, J. D. (1975). The fracture strength and frictional strength of Weber sandstone. Int. J. Rock Mech. Min. Sci. & Geomech. Abstr. 12, 1-4.

Christoffersen, J., Mehrabadi, M. M., and Nemat-Nasser, S. (1980). A micromechanical description of granular material behavior. Earthquake Research and Engineering Laboratory, Technical Report No. 80-1-22, Dept. of Civil Engineering, Northwestern University, Evanston, Ill., January 1980; J. Appl. Mech., in press.

De Alba, P. S., Chan, C. K., and Seed, H. B. (1975). Determination of soil liquefaction characteristics by large-scale laboratory tests. NUREG-0027, NRC-6, Shannon and Wilson, Inc., and Agbabian Assoc., Seattle, Wash., September 1976, prepared for the U. S. Nuclear Regulatory Commission under Contract No. AT(04-3)-954; see also EERC Report 75-14, University of California, Berkeley, Calif.

Hill, R. (1950). The Mathematical Theory of Plasticity. Oxford University Press.

Mehrabadi, M. M., Nemat-Nasser, S., and Oda, M. (1980). On statistical description of stress and fabric in granular materials. Earthquake Research and Engineering Laboratory, Technical Report No. 80-4-29, Dept. of Civil Engineering, Northwestern University, Evanston, Ill., April 1980; Int. J. Numerical & Analytical Methods in Geomechanics, submitted.

Nemat-Nasser, S. (1980). On behavior of granular materials in simple shear. Earthquake Research and Engineering Laboratory, Technical Report No. 79-6-19, Dept. of Civil Engineering, Northwestern University, Evanston, Ill., June 1979; Soils and Foundations 20, 59-73.

Nemat-Nasser, S. and Shokooh, A. (1977). A unified approach to densification and liquefaction of cohesionless sand. Earthquake Research and Engineering Laboratory, Technical Report No. 77-10-3, Dept. of Civil Engineering, Northwestern University, Evanston, Ill., October 1977.

Nemat-Nasser, S. and Shokooh, A. (1978). A new approach for the analysis of liquefaction of sand in cyclic shearing. Proc. of the Second International Conference on Microzonation, 2, 957-969, San Francisco, Calif.

Nemat-Nasser, S. and Shokooh, A. (1979). A unified approach to densification and liquefaction of cohesionless sand in cyclic shearing. Canadian Geotechnical J. 16, 659-678.

Nemat-Nasser, S. and Shokooh, A. (1980). On finite plastic flows of compressible materials with internal friction. Earthquake Research and Engineering Laboratory, Technical Report No. 79-5-16, Dept. of Civil Engineering, Northwestern University, Evanston, Ill., May 1979; Int. J. Solids & Struct. 16, 495-514.

Oda, M., Konishi, J., and Nemat-Nasser, S. (1980). Index measures for granular materials. Earthquake Research and Engineering Laboratory, Technical Report No. 80-3-26, Dept. of Civil Engineering, Northwestern University, Evanston, Ill., March 1980; revised version in Géotechnique, in press.

Oda, M., Nemat-Nasser, S., and Mehrabadi, M. M. (1980). A statistical study of fabric in a random assembly of spherical granules. Earthquake Research and Engineering Laboratory, Technical Report No. 80-4-28, Dept. of Civil Engineering, Northwestern University, Evanston, Ill., April 1980; Int. J. Numerical & Analytical Methods in Geomechanics, submitted.

Rice, J. R. (1977). The localization of plastic deformation. In Theoretical and Applied Mechanics, W. T. Koiter (ed.), North-Holland Pub. Co., 207-220.

Rudnicki, J. W. and Rice, J. R. (1975). Conditions for the localization of deformation in pressure-sensitive dilatant materials. J. Mech. Phys. Solids 23, 371-394.

Schofield, A. and Wroth, P. (1968). Critical State Soil Mechanics. McGraw-Hill, London.

CHAPTER 6

EXPERIMENTAL RESULTS ON DENSIFICATION AND LIQUEFACTION OF COHESIONLESS SAND

1. INTRODUCTION

The response of granular materials is critically affected by the granular fabric which evolves in the course of deformation. The fabric and its influence on mechanical behavior has been discussed extensively in the literature. A summary of the basic results is presented by Oda, Konishi, and Nemat-Nasser (1980). The influence of fabric on the resistance of sand to liquefaction has been demonstrated experimentally by Finn et al. (1970) and Ishihara and Okada (1978), where it has been shown that two samples of sand with essentially the same void ratio can liquefy in cyclic shearing under the same stress amplitude, but after the number of cycles which can differ by one or even two orders of magnitude, if one sample is virgin and the other is subjected to relatively large prestraining; for example, the virgin sample may liquefy after 100 to 200 cycles, whereas the prestrained sample (with the same or even smaller void ratio) may liquefy within one or two cycles.

We have made a systematic study in simple shear of the effect of prestraining (change in fabric) on the densification and liquefaction potential of cohesionless sands. We have observed that strong anisotropy develops upon prestraining, resulting in strong directional dependency of densification and hence, liquefaction. These results are in support of the theory discussed in Chapter 5. In the present chapter, the experimental results are summarized.

2. TEST PROCEDURE AND MATERIALS

Monterey No. 0 sand has been used in this study. The specific gravity is 2.65. The maximum and minimum void ratios are 0.83 and 0.53, respectively.

Maximum void ratio has been determined by pouring sand into the mould through a funnel as gently as possible. Minimum void ratio has been determined by pouring sand into the mould in five layers, each time tamping the sample 1000 times by a light hammer.

The tests have been performed in the dynamic simple shear device shown in Fig. 1. On the average, diameter and height of samples were 7.10 and 3.10 cm, respectively.

Sand which has been mixed with 1.5% water by weight is poured into the mould by spoon and then tamped by specially designed rod through the plane plastic plate in order to obtain the desired height. Sample is poured in three layers, each 1.03 cm thick.

Sand or water protected sand paper is attached to the surface of top and base platens in order to prevent sliding between these platens and the specimen.

Carbon dioxide (CO_2) is percolated for half an hour through the specimen to obtain a satisfactory degree of saturation, and then deaired water is circulated through the specimen for one hour. A back pressure of 100 kN/m^2 is applied to achieve saturation with a B-value exceeding 0.95.

All tests have been performed on isotropically consolidated samples, with effective confining pressure 100 kN/m^2.

Horizontal force is applied by pneumatic loader through a load cell which monitors the intensity of load transmitted to the specimen. Also the vertical load is monitored by a load cell on the top platen.

Linear variable differential transformer (LVDT) is connected on one side of the loading ram to measure the horizontal displacement at the top of the specimen. Vertical displacement is also monitored by LVDT. Drainage lines are provided through both the top and base platens. The pressure transducer is installed

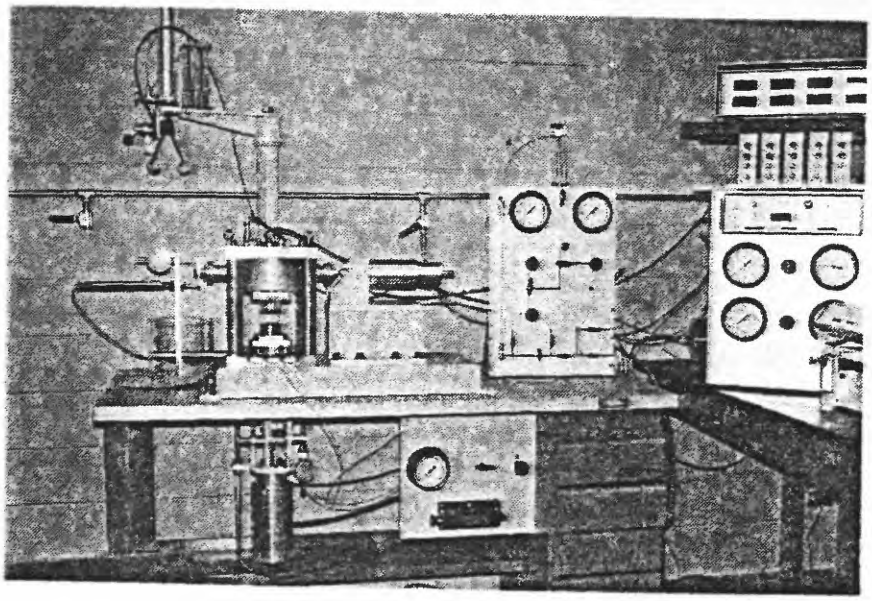

Laboratory simple shear test equipment able to apply confining pressure to specimen and with capability of following random stress paths.

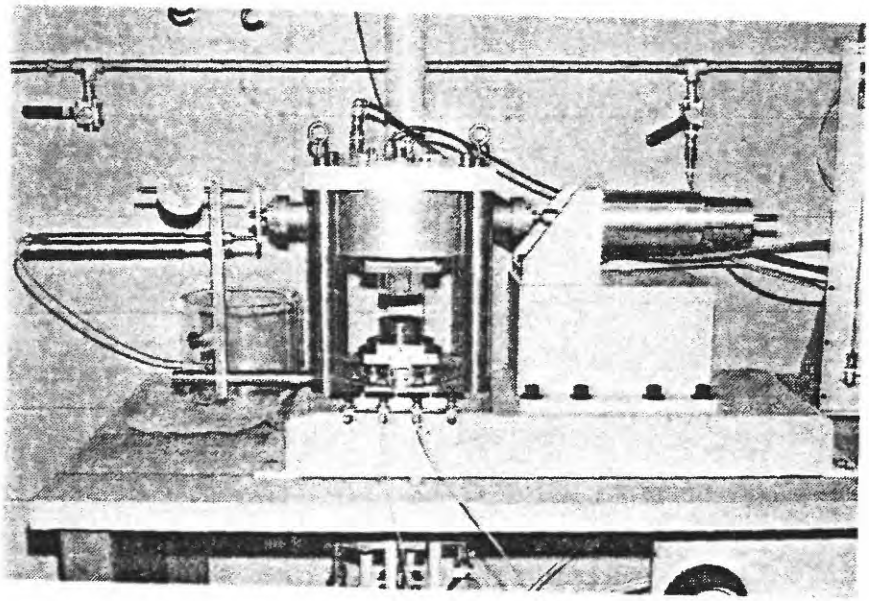

Detail of simple shear test equipment showing measurement transducers, pressure chamber and loading mechanism.

Fig. 1

in the drainage line and pore pressure is measured by preventing drainage through the specimen.

Output from load cells and transducers is recorded by a twelve-channel Honeywell Visirecorder and load-deformation relation is recorded by an X-Y plotter.

3. BASIC RESULTS

In order to classify the effect of prestraining on the subsequent response of granular materials, three stages in a monotonic loading of the drained sample are considered in Fig. 2. Stage I begins with the deformation and continues until the point of maximum density (minimum void ratio). Stage II begins with the initiation of positive dilatancy and continues until the point of maximum load (peak stress). Stage III corresponds to the post peak-stress response to the critical state, and is associated with a strain-softening behavior.

3.1 Cyclic Loading of Drained Samples

The densification in cyclic loading under the drained condition, depends on the stress amplitude, corresponding to the three stages mentioned above. These are discussed below.

Stage I

As shown in Fig. 3a, hysteresis curve of saturated drained sand, subjected to quasi-static loading with a constant shear stress amplitude, shows a slight hardening effect. The net volume reduction per cycle, decreases with increasing number of cycles, as shown in Fig. 3b. The pattern of volume change is almost the same for either direction of loading. In other words, the volume change at the end of a half-cycle in one direction of loading is independent of the preceding half-cycle of loading in the opposite direction. This result agrees with that reported by Tatsuoka and Ishihara (1974).

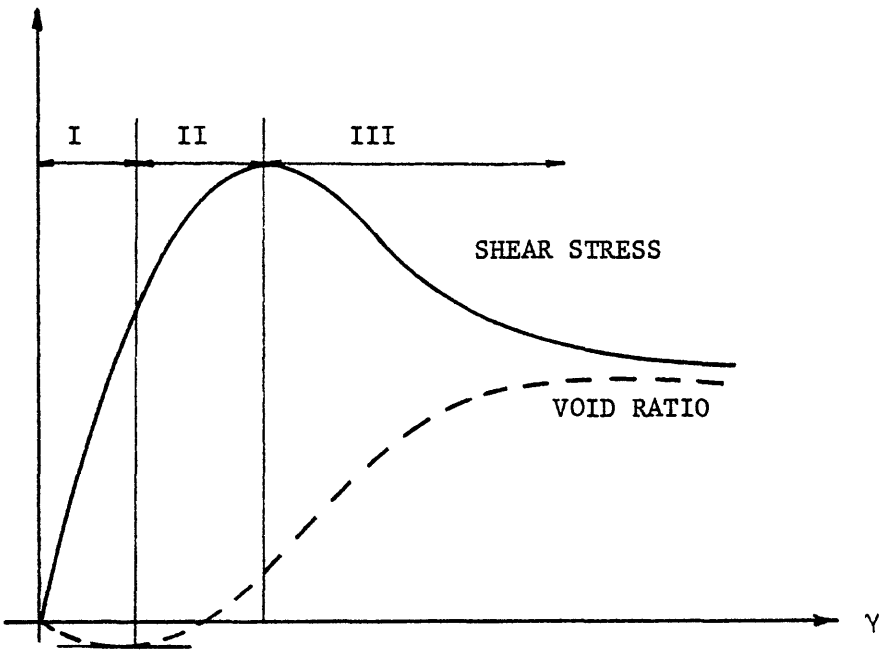

Fig. 2

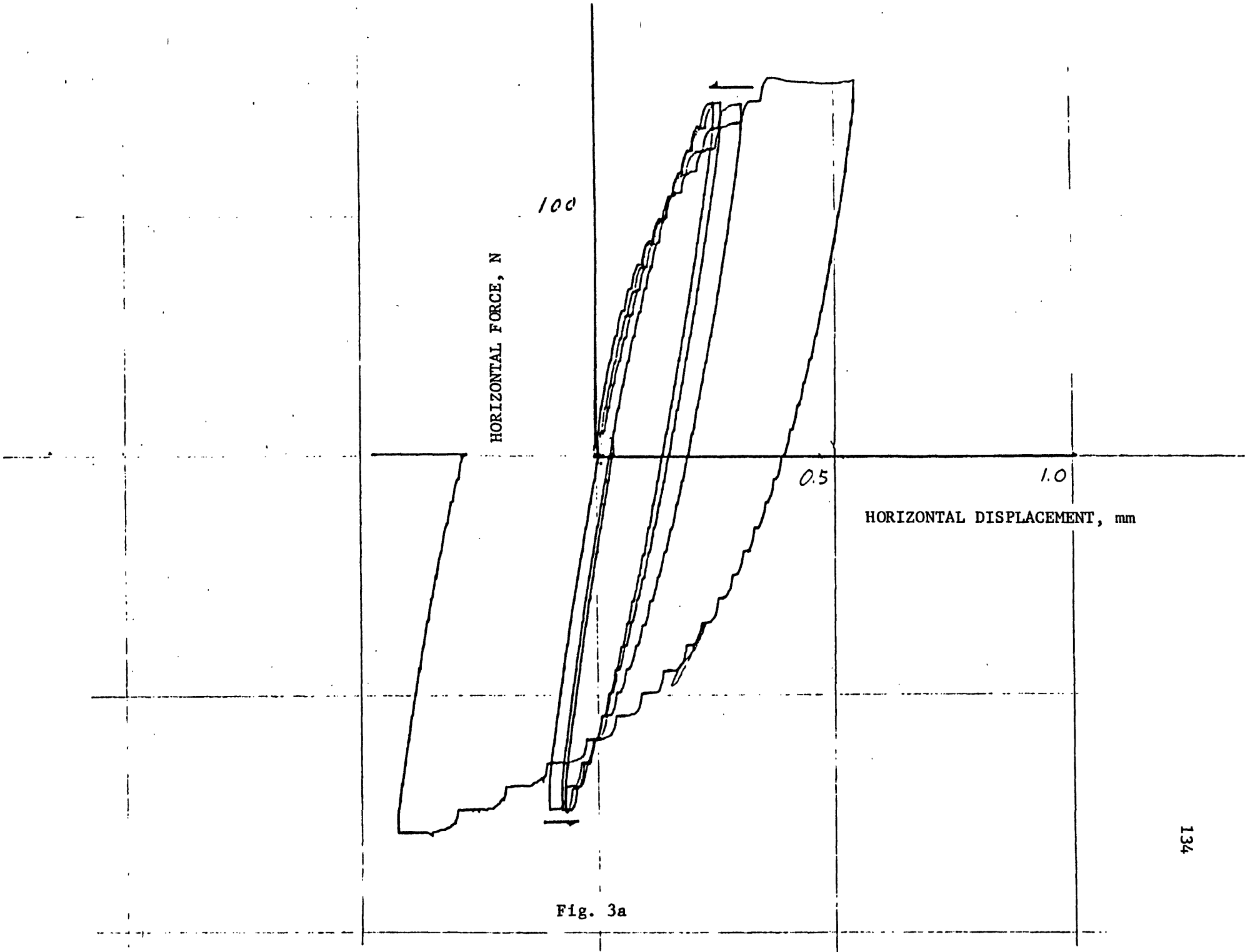

Fig. 3a

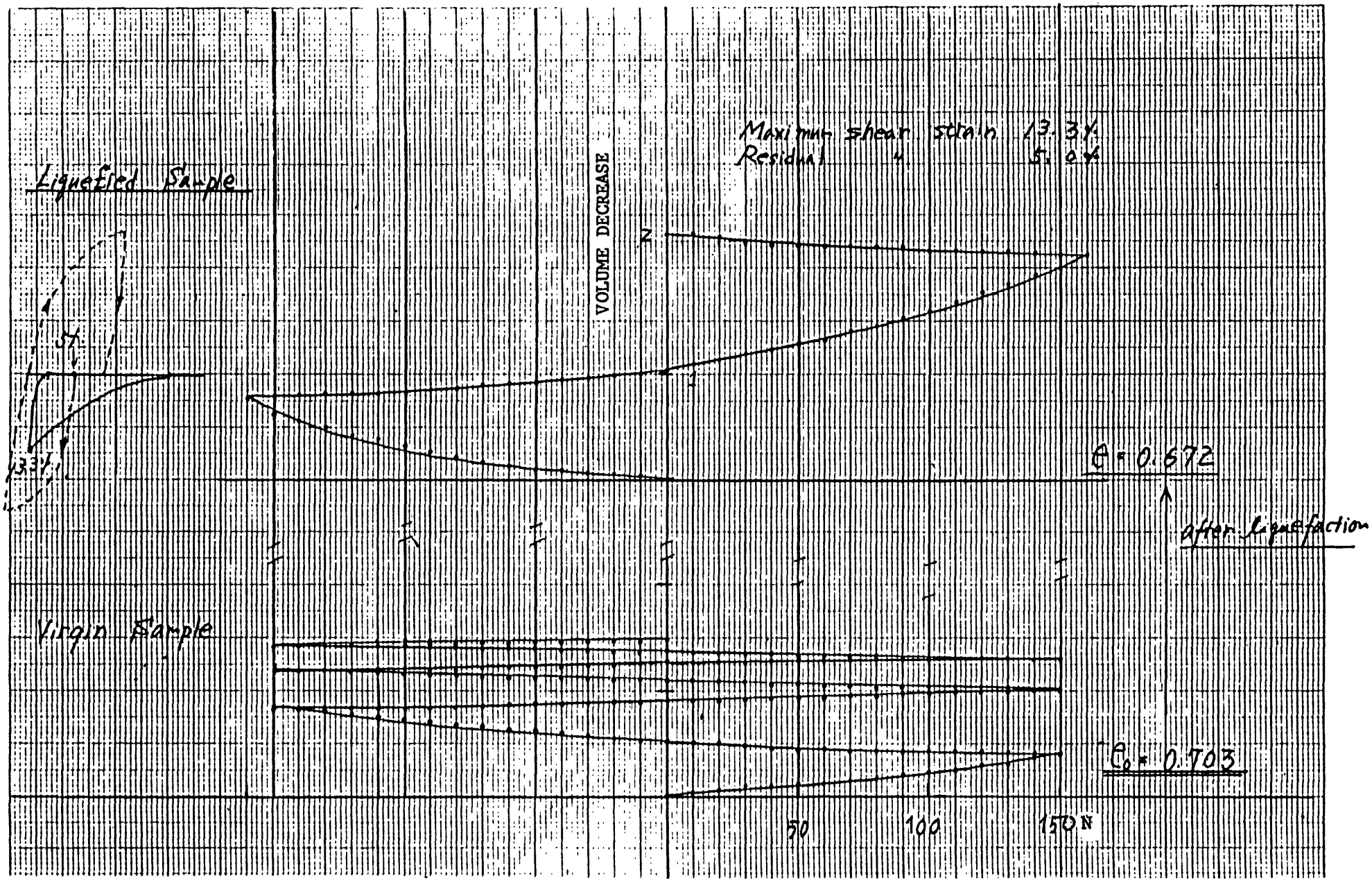
Liquefied Sample
5%
13.3%
Virgin Sample
VOLUME DECREASE
N
Maximum shear strain 13.3%
Residual " 5.0%
e = 0.672
after Liquefaction
e₀ = 0.703
50
100
150 N

135

Fig. 3b

Stage II

Hysteresis curve does not show a hardening effect in Stage II. Almost the same characteristic is observed in each cycle irrespective of the number of cycles. The volume reduction in unloading is first small and then very large as the isotropic stress state is approached. A large volume reduction is observed as soon as the direction of shear stress is changed; see Fig. 4. The remarkable volume reduction upon load reversal plays a key role in liquefaction of saturated undrained sand.

In the case of one-directional cyclic loading (i.e., when the shear stress is increased and then decreased to zero, without load reversal), dilatancy (volume increase) is observed with the start of the second cycle of loading. According to Konishi's (1978) experimental observation on simple shearing of cylindrical granules (rods), the fabric created during the loading in one direction, is essentially preserved upon unloading. A similar idea has been presented by Nemat-Nasser (1980) in terms of the distribution of the dilatancy angles in simple shearing; see Chapter 5.

Stage III

It is easily seen that cyclic loading into the Stage III is impractical. The adoptation of Stage III is mainly for the explanation of prestressing effect on the subsequent behavior of sand.

As has been already pointed out by Ishihara and Okada (1978), the key features of deformation of sand in drained condition for the explanation of liquefaction can be considered as follows:

1) Initial densification and subsequent dilatancy;
2) Independent behavior in each test cycle with small stress amplitude (Stage I);
3) Large volume reduction upon load reversal, and negligible volume reduction (or small volume expansion) in the same direction of loading with large stress amplitude (Stage II).

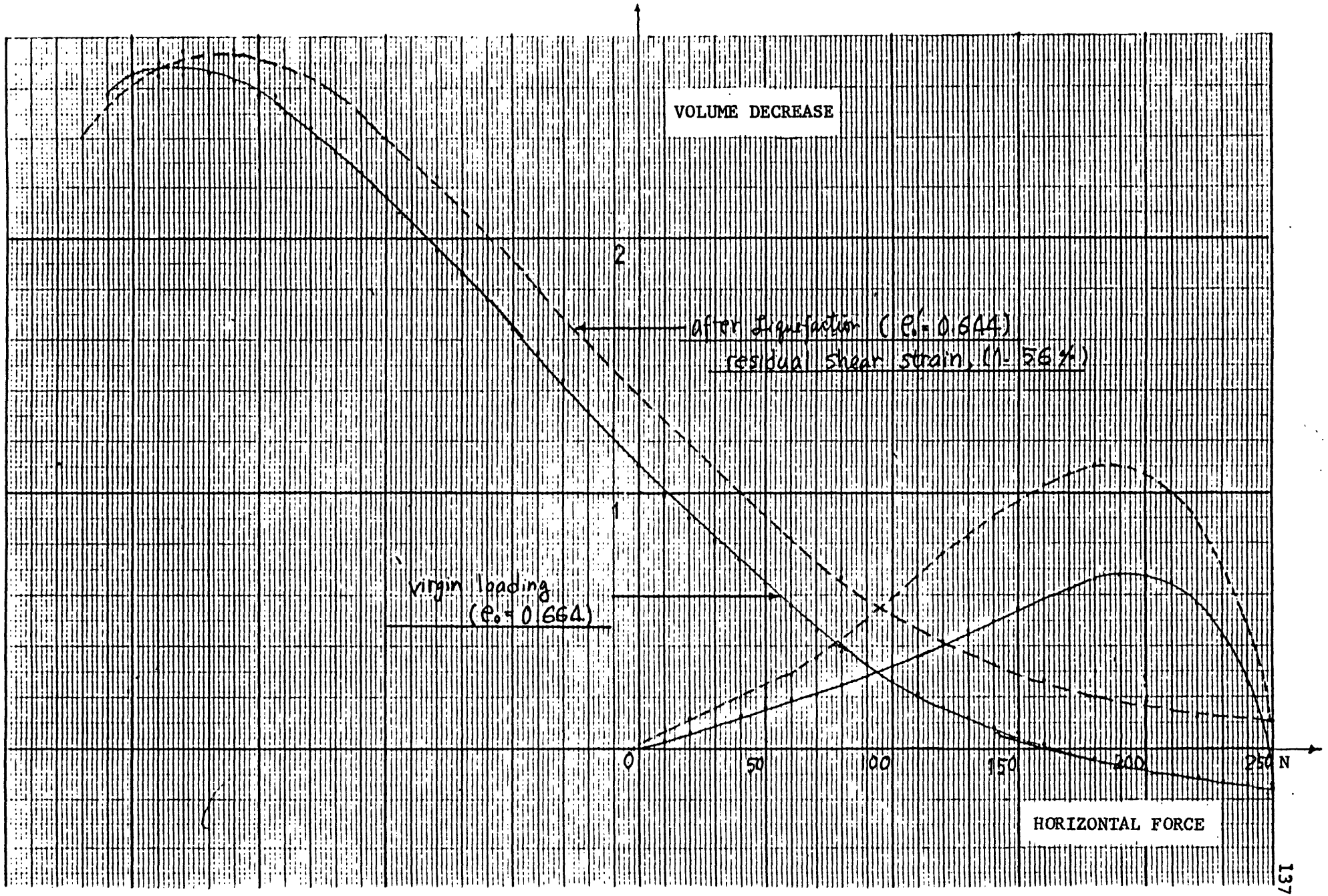
VOLUME DECREASE
2
after liquefaction (e.= 0.644)
residual shear strain, (h= 56%)
1
virgin loading
(e.= 0.664)
0
50
100
150
200
250 N
HORIZONTAL FORCE

137

Fig. 4

3.2 Cyclic Loading of Undrained Sample

A typical result of cyclic loading of an undrained saturated sample is shown in Fig. 5. The general characteristics of this type of experimental results may be summarized as follows:

1) Pore pressure increases gradually up to some critical pressure, and then rises rapidly to the value of the initial confining pressure within one or a few cycles;
2) Shear strain is very small (negligible) up to some critical number of cycles irrespective of the increase of pore pressure. The dramatic increase in shear strain depends on the rapid increase of pore pressure;
3) The looser samples undergo larger shear strain after the initial liquefaction;
4) The effective pressure in the specimen equals zero when shear stress goes to zero;
5) When dynamic shear stress attains its maximum value, the pore pressure attains its minimum value.

It is known that within a certain freqency range, the resistance to liquefaction of saturated sand is almost independent of the frequency of the applied dynamic stress. It is therefore expected that some significant characteristics of liquefaction behavior of sand can be obtained by means of a quasi-static loading.

It seems reasonable that the undrained behavior of saturated sand in dynamic loading be considered as the accumulated effect of undrained behavior of sand in quasi-static loading. Furthermore, undrained behavior of saturated sand can be explained in terms of its drained behavior.

We seek to explain the general characteristics of undrained saturated sand, subjected to the dynamic loading, on the basis of the volume changes observed

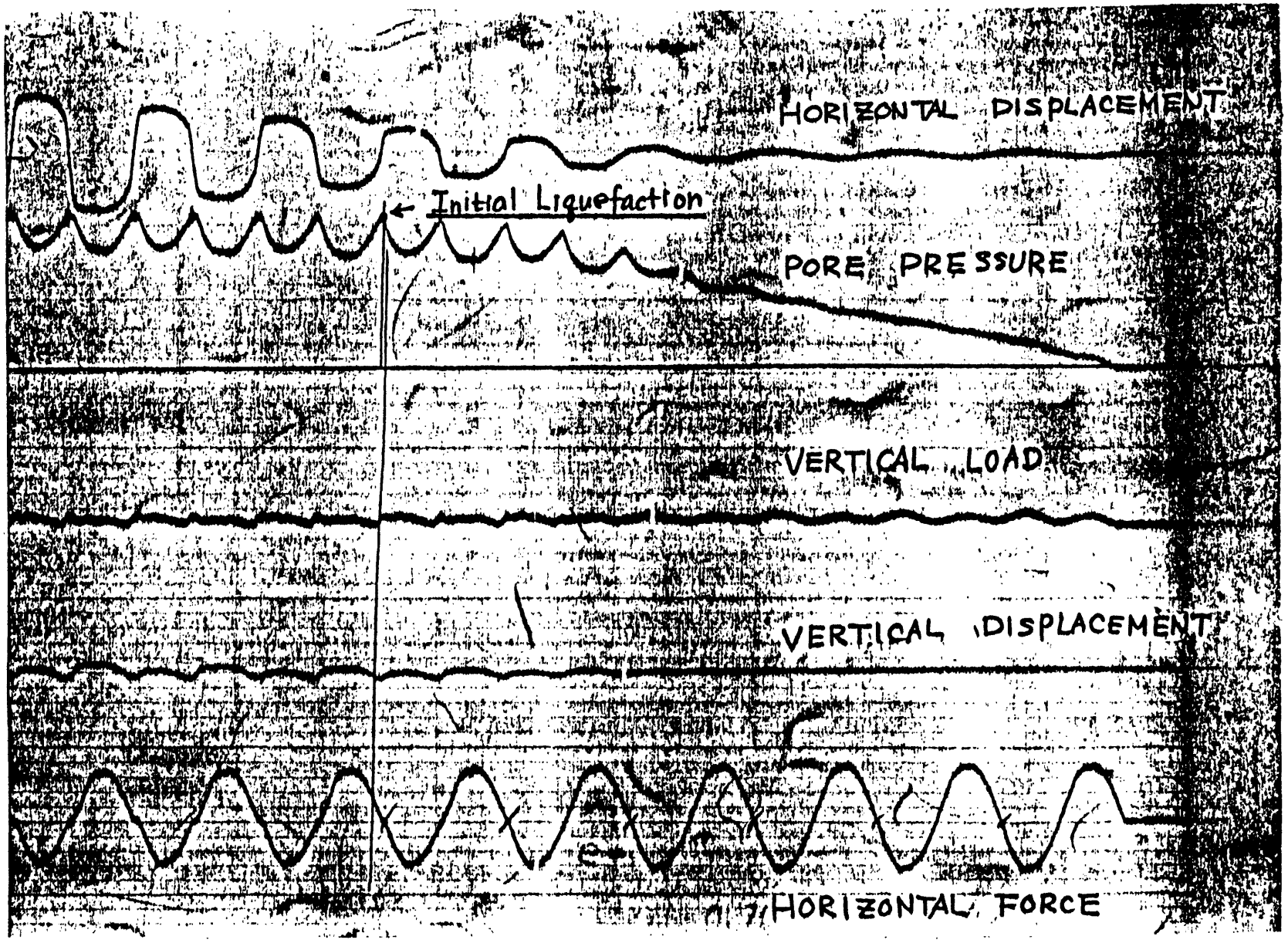
HORIZONTAL DISPLACEMENT
Initial Liquefaction
PORE PRESSURE
VERTICAL LOAD
VERTICAL DISPLACEMENT
HORIZONTAL FORCE

Fig. 5

in the drained condition. To this end, it is convenient to use the effective stress path. A typical effective stress path is schematically shown in Fig. 6.

As described before, the volume reduces in Stage I, resulting in an increase in the pore pressure, and this is almost independent of the direction of loading. The generation of pore pressure results in the loss of effective confining pressure, so that the ratio of the applied shear stress to the effective confining pressure increases, resulting in an additional volume change and further generation of pore pressure. The magnitude of the shear strain remains negligibly small as long as the stress path remains within Stage I.

As the stress ratio increases with the gradual pore pressure generation, the stress path enters Stage II, resulting in an initial dilatancy which is followed by a large amount of densification upon unloading and load reversal. A rapid increase in pore pressure occurs as the stress path approaches the isotropic state. Initial liquefaction occurs when pore pressure equals the confining pressure.

3.3 Effect of Stress History

As described before, the liquefaction behavior of saturated sand in undrained dynamic loading can be explained by the tendency of the volume change in drained condition. It is therefore believed that the effects of prestress can be explained in the same manner. We therefore consider the three stages of loading as before.

Stage I

The sample subjected to a small amplitude prestressing in drained condition shows higher resistance to liquefaction, as shown in Fig. 7. Before liquefaction test, three cycles of shear stress of 38.0 kN/m^2 amplitude are applied. The specimen then liquefies after 10 cycles of the shear stress of 28.0 kN/m^2

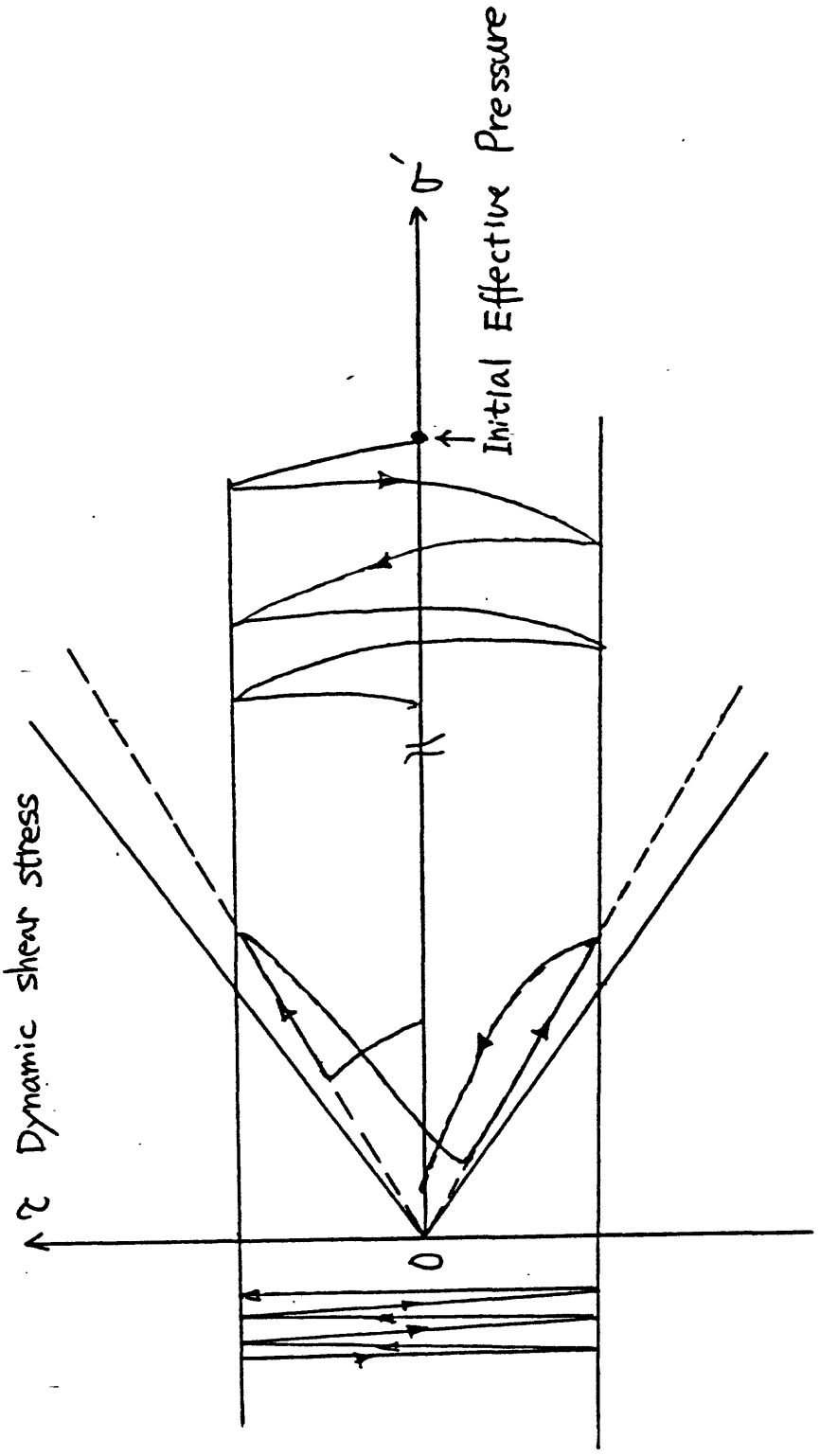

Fig. 6. Effective stress path in undrained cyclic loading.

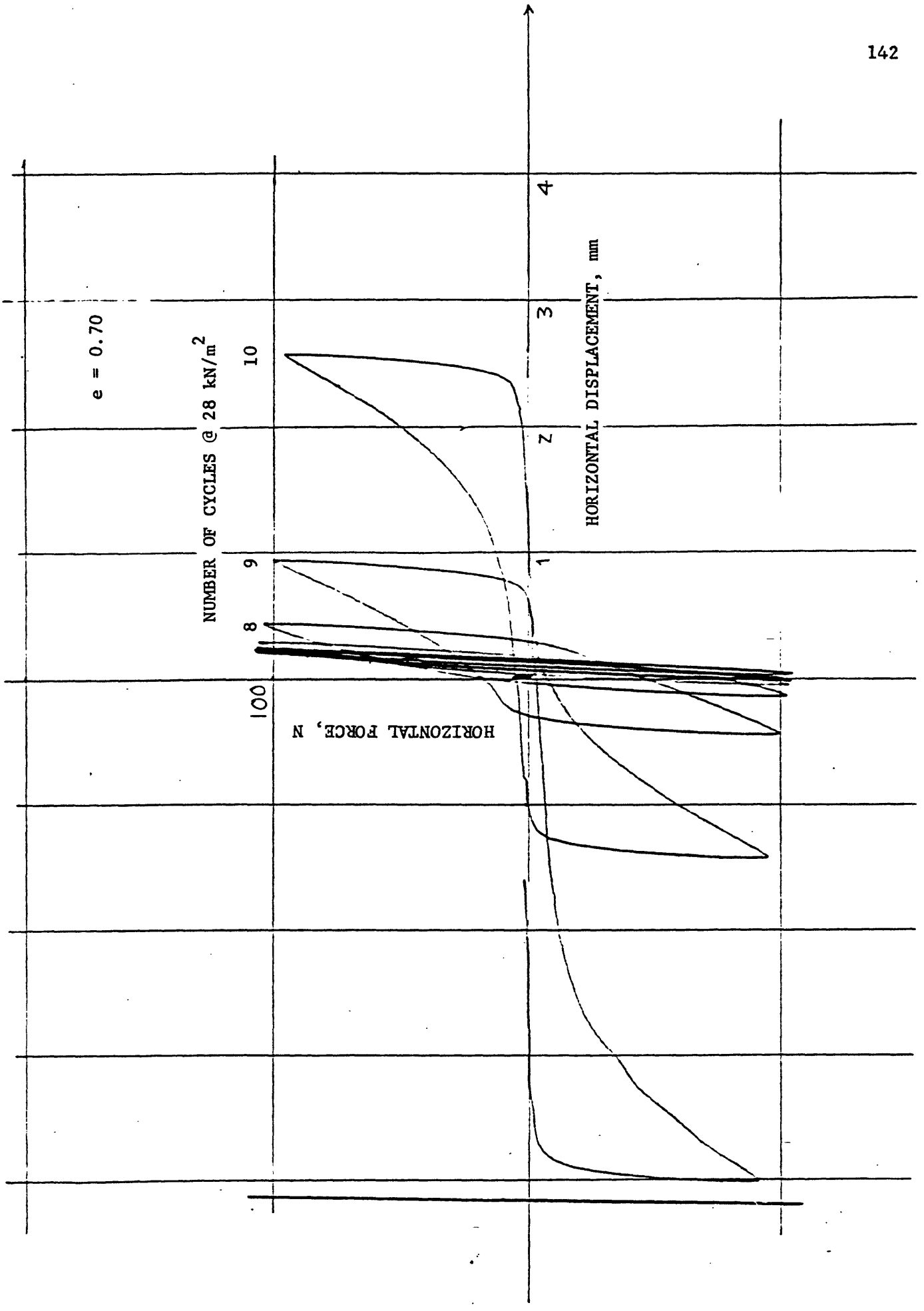
e = 0.70
NUMBER OF CYCLES @ 28 kN/m^2
10
9
8
100
HORIZONTAL FORCE, N
1
2
3
4
HORIZONTAL DISPLACEMENT, mm

Fig. 7

amplitude. The number of cycles of the same stress amplitude required for initial liquefaction for the virgin sample is one or two.

Stage II

Figure 8 shows the undrained behavior of saturated sand subjected to a cyclic quasi-static stress. The sample is reconsolidated to initial effective stress after liquefaction. The sample once liquefied shows large displacement around shear stress of 15 kN/m^2 irrespective of the number of previous liquefactions. It is interesting to note that shear strain developed in the undrained test becomes smaller as the number of previous liquefactions increases.

It can be expected that the densification due to reconsolidation after liquefaction has little effect on the subsequent undrained behavior up to the initial liquefaction. The sample once liquefied shows more densification than the virgin sample. Figure 4 also shows the volume change of liquefied sample. It is clearly shown that the succeeding loading in the same direction as the last loading in undrained test, results in a considerably smaller densification than in the opposite direction. The behavior described is the same as that of the sample subjected to large preshearing. Effective stress path of saturated sand subjected to large prestress in drained condition clearly shows this trend. The succeeding cyclic loading in the same direction as the last loading in the drained condition, results in a slightly negative pore pressure and leads to drastic generation of pore pressure in the opposite direction of loading.

Stage III

Our experimental apparatus does not allow large enough prestraining to enter this stage of loading.

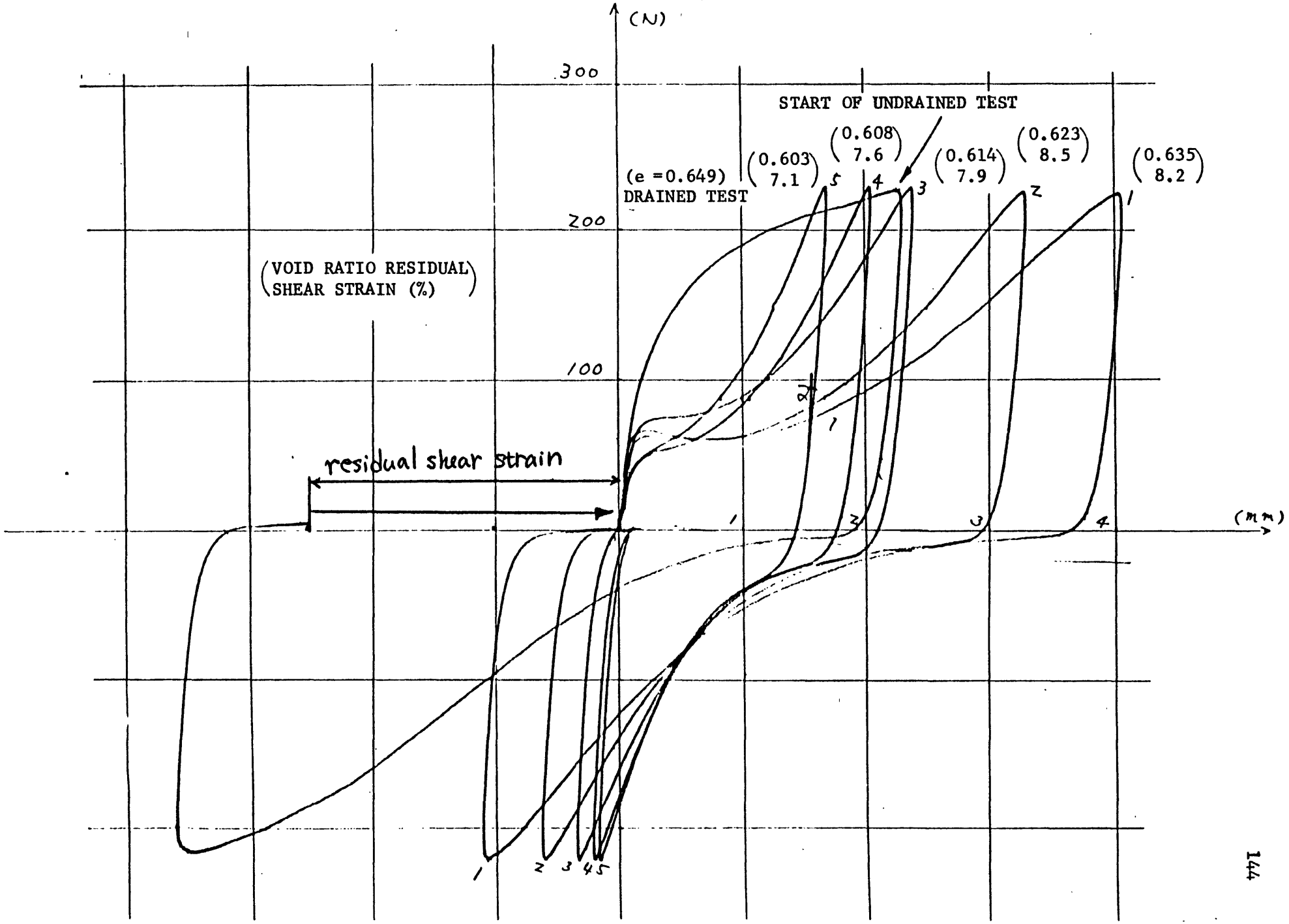
(N)
300
200
100
START OF UNDRAINED TEST
(0.608
7.6)
(0.603
7.1)
(0.614
7.9)
(0.623
8.5)
(0.635
8.2)
(e =0.649)
DRAINED TEST
(VOID RATIO RESIDUAL
SHEAR STRAIN (%)
residual shear strain
(mm)
1
2
3
4
5

Fig. 8

REFERENCES

Finn, W. D., Bransby, P. L., and Pickering, D. J. (1970). Effect of strain history on liquefaction of sand. J. Soil Mech. Found. Div., ASCE, 96, SM6, 1917-1933.

Ishihara, K. and Okada, S. (1978). Effects of stress history on cyclic behavior of sand. Soils and Foundations 18, 31-45.

Konishi, J. (1978). Microscopic studies on the mechanical behavior of granular materials. Proc. U.S.-Japan Seminar on Continuum-Mechanical and Statistical Approaches in the Mechanics of Granular Materials, S. C. Cowin and M. Satake (eds.). Gakujutsu Bunken Fukyukai, Tokyo, Japan, 27-45.

Nemat-Nasser, S. (1980). On behavior of granular materials in simple shear. Earthquake Research and Engineering Laboratory, Technical Report No. 79-6-19, Dept. of Civil Engineering, Northwestern University, Evanston, Ill., June 1979; Soils and Foundations 20, 59-73.

Oda, M., Konishi, J., and Nemat-Nasser, S. (1980). Some experimentally based fundamental results on the mechanical behavior of granular materials. Géotechnique 30, in press.

Tatsuoka, F. and Ishihara, K. (1974). Drained Deformation of sand under cyclic stresses reversing direction. Soils and Foundations 14, 51-65.

PUBLICATIONS COMPLETED UNDER

USGS Contract No. 14-08-0001-17770

to Northwestern University

Papers

Nemat-Nasser, S., "Finite Deformation Plasticity and Plastic Instability" (Invited Address), Transactions of the 25th Conference of Army Mathematicians, ARO Report 80-1, U. S. Army Research Office (1979) 715-731.

Nemat-Nasser, S. and Shokooh, A., "A Framework for Prediction of Densification and Liquefaction of Sand in Cyclic Shearing," Ingenieur-Archiv 49 (1980) No. 5/6.

Nemat-Nasser, S., "On Behavior of Granular Materials in Simple Shear," Soils and Foundations 20 (1980) 59-73.

Nemat-Nasser, S., "On Dynamic and Static Behavior of Granular Materials" (Keynote Lecture), Proceedings of the International Symposium on Soils under Cyclic and Transient Loading, Swansea, U.K., Jan. 7-11, 1980, Wiley and Sons; to appear.

Nemat-Nasser, S., "Liquefaction of Soil During Earthquakes," Proceedings of the ASCE-EMD Specialty Conference on Dynamic Response of Structures, Atlanta, Georgia, Jan. 15-16, 1981, American Soc. of Civil Engineers; to appear.

Abstracts or Summaries of Presented Papers

Nemat-Nasser, S., "A Statistical Approach for Predicting the Response of Cohesionless Soils in Simple Shear," in Abstracts, 16th Annual Meeting of the Society of Engineering Science, Inc., Northwestern University, Evanston, Illinois (1979) 106.

Nemat-Nasser, S., "On Dynamic and Static Behavior of Granular Materials," in Soils under Cyclic and Transient Loading, G. N. Pande and O. C. Zienkiewicz (eds.), A. A. Balkema, Rotterdam (1980) 435-436.

RESEARCH PERSONNEL WHO PARTICIPATED IN THE PROJECT

Principal Investigator: S. Nemat-Nasser

Postdoctoral Research Associates:

A. Shokooh (no support)

M. M. Mehrabadi (supported 9/1/79 - 6/30/80)

Visiting Scholars:

M. Shahinpoor (no support)

M. Oda (supported 9/1/79 - 9/30/79)

Graduate Students:

A. Hedayati (supported Fall Quarter 1979)

H. Horii (supported 7/21/80 - 9/30/80)

Y. Tobita (supported 3/21/80 - 9/30/80)